

Optical and infrared observations of the Type IIP SN 2002hh from day 3 to 397

M. Pozzo¹, W.P.S. Meikle¹, J.T. Rayner², R.D. Joseph², A.V. Filippenko³,
R.J. Foley³, W. Li³, S. Mattila⁴, J. Sollerman^{4,5}

¹ *Imperial College London, Blackett Laboratory, Prince Consort Road, London, SW7 2BW, U.K.*

² *Institute for Astronomy, University of Hawaii, 2680 Woodlawn Drive, Honolulu, HI 96822*

³ *Department of Astronomy, 601 Campbell Hall, University of California, Berkeley, CA 94720-3411 USA*

⁴ *Stockholm Observatory, AlbaNova, Dept. of Astronomy, Stockholm SE 106 91, Sweden*

⁵ *DARK cosmology center, NBI, Copenhagen University, Denmark*

Accepted Received ; in original form 2004 ...

ABSTRACT

We present optical and infrared (IR) observations of the type II SN 2002hh from 3 to 397 days after explosion. The optical spectroscopic (4–397 d) and photometric (3–278 d) data are complemented by spectroscopic (137–381 d) and photometric (137–314 d) data acquired at IR wavelengths. This is the first time *L*-band spectra have ever been successfully obtained for a supernova at a distance beyond the Local Group. The *VRI* light curves in the first 40 days reveal SN 2002hh to be a SN IIP (plateau) – the most common of all core-collapse supernovae. SN 2002hh is one of the most highly extinguished supernovae ever investigated. To provide a match between its early-time spectrum and a coeval spectrum of the Type IIP SN 1999em, as well as maintaining consistency with K I interstellar absorption, we invoke a 2-component extinction model. One component is due to the combined effect of the interstellar medium of our Milky Way Galaxy and the SN host galaxy, while the other component is due to a “dust pocket” where the grains have a mean size smaller than in the interstellar medium. The early-time optical light curves of SNe 1999em and 2002hh are generally well-matched, as are the radioactive tails of these two SNe and SN 1987A. The late-time similarity of the SN 2002hh optical light curves to those of SN 1987A, together with measurements of the optical/IR luminosity and [Fe II] 1.257 μm emission indicate that $0.07 \pm 0.02 M_{\odot}$ of ^{56}Ni was ejected by SN 2002hh. However, during the nebular phase the *HKL'* luminosities of SN 2002hh exhibit a growing excess with respect to those of SN 1987A. We attribute much of this excess to an IR echo from a pre-existing, dusty circumstellar medium. Based on an IR-echo interpretation of the near-IR excess, we deduce that the progenitor of SN 2002hh underwent recent mass loss of $\sim 0.3 M_{\odot}$. A detailed comparison of the late-time optical and near-IR spectra of SNe 1987A and 2002hh is presented. While the overall impression is one of similarity between the spectra of the two events, there are notable differences. The Mg I 1.503 μm luminosity of SN 2002hh is a factor of 2.5 greater than in SN 1987A at similar epochs, yet coeval silicon and calcium lines in SN 2002hh are fainter. Interpreting these differences as being due to abundance variations, the overall abundance trend between SN 1987A and SN 2002hh is not consistent with explosion model predictions. It appears that during the burning to intermediate-mass elements, the nucleosynthesis did not progress as far as might have been expected given the mass of iron ejected. Evidence for mixing in the ejecta is presented. Pronounced blueshifts seen in the more isolated lines are attributed to asymmetry in the ejecta. However, during the timespan of these observations (~ 1 year post-explosion) we find no evidence of dust condensation in the ejecta such as might have been revealed by an increasing blueshift and/or attenuation of the red wings of the emission lines. Nevertheless, the clear detection of first overtone CO emission by 200 days and the reddening trend in $(K - L')_0$ suggest that dust formation in the ejecta may occur at later epochs. From the [O I] $\lambda\lambda 6300, 6364 \text{ \AA}$ doublet luminosity we infer a 16–18 M_{\odot} main-sequence progenitor star. The progenitor of SN 2002hh was probably a red supergiant with a substantial, dusty wind.

Figure 1. *R*-band image of the SN 2002hh field taken with KAIT on 2002 December 2 UT, when the SN was about one month post-explosion. The nucleus of the host galaxy, NGC 6946, is visible at the top-left corner. Also shown are the local standards used for the photometric calibration (see Table 1).

1 INTRODUCTION

An important goal of astrophysics is to deepen our understanding of the progenitors and explosion mechanisms of core-collapse supernovae (CCSNe). What kind of stars explode? What drives the explosion? Do CCSNe or their progenitors contribute significant quantities of dust to the interstellar medium (ISM)? Observations of CCSNe at late times have a unique potential for helping us to answer these questions since by these epochs, in the *nebular phase* ($t > 150$ d), we can view directly most of the ejecta. This allows measurements of element/molecule abundances and distributions such as those achieved for SN 1987A (e.g., Meikle et al. 1989, 1993; Varani et al. 1990; Spyromilio, Meikle & Allen 1990; Spyromilio et al. 1991). The drawback is that by the time the nebular phase is reached the supernova has become faint. Consequently, only the very nearest events can be effectively studied in this way.

An excellent opportunity for the study of the nebular phase came with the discovery of SN 2002hh, one of the nearest type II SNe in the past 50 years. Type II supernovae make up the most common subgroup of CCSNe. SN 2002hh was very highly reddened, with a *V*-band extinction which reduced its flux by a factor of over 100. However, the effect of the extinction is much reduced in the infrared (IR), and indeed it can be argued (see below) that this wavelength region is at least as important as the optical region for late-time studies.

IR observations can test the nature of CCSNe in ways not available in other wavelength regions. Constraints on the CCSN progenitor can be obtained with a combination of IR/optical photometry and IR spectroscopy. For example, the presence of first overtone CO emission (*K* band)

in CCSNe is increasingly regarded as ubiquitous, having been detected in all seven CCSNe which have been observed in the *K* band at 3–6 months post-explosion (see Gerardy et al. 2002; Meikle et al. 2003, and references therein). By modelling the first overtone CO spectrum of the Type II In SN 1998S, Fassia et al. (2001) deduced a CO mass of $10^{-3} M_{\odot}$, while from the bolometric light curve they deduced a ^{56}Ni mass of $0.15 M_{\odot}$. Combining these two results they inferred a core mass exceeding $4 M_{\odot}$, implying a massive progenitor. In addition, the detection of CO is important since it is probably an essential precursor to dust condensation in the ejecta.

Infrared spectroscopy during the photospheric phase can probe ejecta mixing and hence the explosion mechanism. Graham (1988) showed how the strong He I $1.083 \mu\text{m}$ line at early times could be used to infer the upward mixing of radioactive iron-group elements in the ejecta of the peculiar Type II SN 1987A. Fassia et al. (1998) and Fassia & Meikle (1999) further developed this technique and applied it, respectively, to the Type IIP SN 1995V and to SN 1987A.

In spite of the high extinction toward SN 2002hh, optical spectra are also of value. The prominent, high signal-to-noise ratio (S/N) H α and Ca II lines allow investigation of ejecta asymmetry. The O I 8446 Å fluorescence line provides confirmation of the identification of the O I $1.1287 \mu\text{m}$ line, and the cascade pair together may allow us to study the conditions under which such lines are formed (Spyromilio et al. 1991).

A major goal in the study of CCSNe is to provide a significant test of the proposal that they are, or have been, a significant source of dust in the universe. While this hypothesis is over 30 years old (Cernuschi, Marsicano & Codina, 1967; Hoyle & Wickramasinghe 1970) and is still popular (Gehrz, 1989; Tielens 1990; Dwek 1998; Todini & Ferrara 2001; Nozawa et al. 2003) *direct evidence that SNe are major dust sources is still very sparse*. Indeed, it is not known if ordinary Type II SNe or their progenitors produce large amounts of dust at all.

Dust condensation in CCSN ejecta can be detected in two ways. In one method, we can make use of the IR emission from the hot dust grains. 13 CCSNe (cf. Gerardy et al. 2002, and references therein), plus 1 peculiar Type Ia event (SN 2002ic: Kotak et al. 2004), have shown a strong, late-time near-IR (NIR) excess implying the presence of hot dust. However, it is difficult to establish whether this dust was newly condensed in the metal-rich SN ejecta or existed previously in the progenitor’s wind and was detected via an IR echo. Even the comprehensive multi-epoch NIR study of the Type II In SN 1998S by Pozzo et al. (2004) could not completely resolve this ambiguity. While their favoured interpretation was that at least $10^{-3} M_{\odot}$ of dust formed in the cool dense shell at the interface between the ejecta and the circumstellar medium (CSM), the alternative IR-echo interpretation was not ruled out. Dunne et al. (2003) claimed that their sub-mm observations of the SN remnant Cassiopeia A indicates that $>1 M_{\odot}$ of dust formed in the ejecta, but this has been recently disproved by Krause et al. (2004) as being instead due to interstellar dust in a molecular cloud complex

located along the line of sight between the Earth and Cas A.

The other way of detecting newly condensed dust is via its attenuating effect on the red wings of the broad ejecta lines during the nebular phase. This technique has the advantage of being relatively unambiguous in its ability to demonstrate the presence of new dust, although it may be more difficult to extract quantitative information about the quantity and nature of the grains. However, owing to the difficulty of acquiring high-quality spectra at late times, this method has demonstrated ejecta dust in just three cases so far: the type II-pec SN 1987A (Danziger et al. 1991; Lucy et al. 1991), the type IIP SN 1999em (Elmhamdi et al. 2003), and the type IIn SN 1998S (Pozzo et al. 2004). Thus, the close proximity of SN 2002hh offers us only the second-ever opportunity for the study of dust condensation in the most common type of CCSN.

SN 2002hh was discovered (Li 2002) on 2002 October 31.1 (UT dates are used throughout this paper) during the course of the Lick Observatory Supernova Search (LOSS; Li et al. 2000; Filippenko et al. 2001; Filippenko 2005) with the 0.76-m Katzman Automatic Imaging Telescope (KAIT) at Lick Observatory. It was discovered at about 16.5 mag (see Fig. 1) and peaked at $V \approx 15$ mag in mid-November 2002. SN 2002hh was not detected in a previous KAIT image taken on October 26.1 at a limiting magnitude of ~ 19.0 . We shall therefore adopt 2002 October 29 as the explosion epoch, the uncertainty being about ± 2 d. SN 2002hh occurred in NGC 6946, an Scd galaxy which has produced 7 other known SNe, five of which were classified [SNe 1917A (II), 1948B (IIP), 1968D (II), 1980K (IIL), and 2004et (IIP)] and two were not [SNe 1939C and 1969P]. SN 2002hh is located at R.A. = 20h34m44s.29, Decl. = $+60^\circ 07' 19''.0$ (2000.0), which is $60''.9$ west and $114''.1$ south of the nucleus (Li 2002). We adopt a host galaxy distance of 5.9 ± 0.4 Mpc (Karachentsev, Sharina & Huchtmeier 2000).

Spectra taken by Filippenko, Foley & Swift (2002) on 2002 November 2 revealed broad, low-contrast H α emission and absorption lines, but with a nearly featureless and very red continuum (cf. Fig. 6). Strong, narrow (interstellar) Na I D absorption is also present. Filippenko et al. inferred a very young, highly reddened Type II supernova. The high reddening was confirmed and measured by Meikle et al. (2002) on Nov. 18.86 from IR images. Adopting a phase of 21 days, comparison of the $J - K_s$ colour with the infrared-temple light curves of Mattila & Meikle (2001) indicated $E(J - K_s) = 1.0$. From the reddening law of Cardelli, Clayton & Mathis (1989), this yields $A_V \approx 6.1$ mag. Subtracting the Galactic extinction (Schlegel, Finkbeiner & Davis 1998) leads to a host-galaxy extinction of $A_V \approx 5.0$ mag. For a distance of 5.9 Mpc, Meikle et al. (2002) derived dereddened absolute IR magnitudes of $M(J) = -18.3$ and $M(K_s) = -18.5$ (but see our revised values in Section 3), which are close to the values given by the templates of Mattila & Meikle (2001) for normal type II SNe. We note that SN 2004et occurred in the same galaxy as SN 2002hh, but was not highly reddened (Li et al. 2005). We attribute this to the fact that SN 2004et was in a “clean” region at the edge of the galaxy while SN 2002hh is located on a spiral arm. SN 1917A also

occurred in NGC 6946, just $\sim 22''.0$ from SN 2002hh, but it has no measured extinction.

Stockdale et al. (2002) reported detection of radio emission from SN 2002hh with the VLA at 17 d (Nov. 15.25 UT) and confirmed the previously reported optical position. They measured fluxes of 0.60 ± 0.10 mJy at 22.485 GHz and 0.81 ± 0.08 mJy at 8.435 GHz. From the apparently optically thin character of the radio emission, they suggested that the CSM/ejecta shock interaction was weak at this epoch, and was evolving unusually rapidly. Pooley & Lewin (2002) reported the detection of X-ray emission from SN 2002hh with the Chandra X-ray observatory at 27 d, confirming the previously reported optical and radio positions. The low X-ray luminosity detected is consistent with the weak circumstellar interaction indicated by the radio observations. Preliminary spectral fits to the X-ray data indicate a column density of $N_H = 10^{22}$ cm $^{-2}$. SN 2002hh was also detected at 1396.75 MHz with the Giant Meterwave Radio Telescope at 59 d (undetected at 32 d) (Chandra, Ray & Bhatnagar 2003). More recently, Beswick et al. (2005) reported VLA measurements of 0.35 ± 0.1 mJy at 4.860 GHz on day 381 and 1.6 ± 0.2 mJy at 1.425 GHz on day 899.

Barlow et al. (2005) reported the detection of SN 2002hh in archival *Spitzer Space Telescope* images (obtained in the SINGS Legacy Program) covering 3.6–24 μ m, in June and November 2004, as well as in an 11.2 μ m Gemini/Michelle image taken in September 2004. They reported a 25% decline in the total 8 μ m flux between days 590 and 758, and suggested that most of the mid-IR emission originates in a massive (10–15 M_\odot), dusty circumstellar shell ejected by the progenitor and heated by the supernova luminosity. They also proposed that a large fraction of the extinction is due to this circumstellar dust. However, they did not rule out the possibility that a small fraction of the mid-IR emission may have originated in newly formed dust in the ejecta.

In contrast, Meikle et al. (2005a,b, and in prep.) found a decline of only $\sim 10\%$ in the 8 μ m flux between days 590 and 994. They concluded that to produce such a large and slowly declining flux with an IR echo would require a CSM mass of about 80 M_\odot assuming a normal dust/gas ratio. They also found that only a small amount of the extinction should be attributed to this dust. They concluded that the total mid-IR emission could *not* have arisen from an IR echo within a dusty CSM ejected by the progenitor. However, the possibility is not ruled out that the supernova occurred within a dense, dusty ISM and that this was responsible for a powerful IR echo. Alternatively, most of the mid-IR flux could simply be due to steady background sources in the beam. The *Spitzer* images show that the region around the supernova is rich in cool, mid-IR emission structures. The apparent disagreement between the two sets of authors is not yet resolved.

In this paper we describe our IR and optical photometry and spectroscopy of SN 2002hh from day 3 to 397. The paper is organized as follows. Optical/IR imaging and spectroscopic observations and data reduction are discussed in Section II; we present *VRI* light curves together with IR light

Table 1. Photometry of the comparison stars for SN 2002hh.

ID	V	R	I
1	15.47(1) ^a	14.98(1)	14.46(1)
2	13.57(0)	13.14(2)	12.79(3)
3	16.86(2)	16.30(1)	15.74(2)
4	13.78(1)	13.34(1)	12.95(3)
5	16.97(3)	16.45(1)	15.94(2)
6	15.80(2)	15.32(1)	14.83(2)
7	16.67(2)	16.14(1)	15.56(2)
8	15.94(2)	15.28(1)	14.64(1)
9	16.16(2)	15.59(1)	15.05(1)
10	16.75(2)	16.18(1)	15.60(1)
11 ^b	12.32(3)	11.84(2)	11.88(3)
12	15.82(2)	15.37(2)	14.88(2)
13	16.41(2)	15.75(1)	15.12(1)
14	16.38(1)	15.83(1)	15.28(1)
15	15.06(1)	14.17(1)	13.36(1)
16	14.74(2)	14.27(2)	13.81(3)
17	16.90(3)	16.45(3)	15.96(2)
18	14.81(1)	14.14(1)	13.48(2)
19	14.85(2)	14.35(2)	13.88(2)
20	16.85(2)	16.00(1)	15.32(1)
21	15.48(2)	15.00(0)	14.53(1)
22	15.67(2)	15.22(1)	14.75(0)
23	13.84(1)	13.36(1)	12.93(3)
24	15.63(2)	14.93(1)	14.36(1)
25	14.46(1)	14.02(1)	13.59(1)
26	14.38(2)	13.70(0)	13.10(2)

^a Figures in brackets give the internal error, in units of the magnitude's least significant digit.

^b This local field star was saturated in many frames and therefore was not used for the final photometric calibration.

curves and colour curves. Section III deals with the redshift and extinction. In particular, we show that the high extinction toward the SN is best described with a 2-component extinction model with different grain sizes. We also derive the optical/IR luminosity of SN 2002hh and the mass of ejected ⁵⁶Ni. Section IV is devoted to the analysis of the spectroscopic behaviour and the main elements detected in the optical and IR spectra. In Section V we compare SN 2002hh with the well-studied core-collapse SN 1987A. Their optical and IR spectra at coeval epochs, although similar, show some interesting differences. The evolution of the CO emission and the unidentified 2.265 μ m feature originally detected in SN 1987A are also discussed. Finally, the late-time near-IR continuum of SN 2002hh and the temporal evolution of the extinction-corrected $(K - L')_0$ colour are analyzed. Conclusions follow in Section VI.

2 OBSERVATIONS

2.1 Optical photometry

We obtained *VRI* images of SN 2002hh during the first ~ 300 days post-explosion with KAIT. An Apogee AP7 512 \times 512 SITE CCD camera was used, covering a total field-of-view of 6.7' \times 6.7' at 0.8'' pixel⁻¹. The images were reduced using

Table 2. *VRI* photometry of SN 2002hh.

JD-2,450,000	Epoch ^a	V	R	I
2580.60	3	17.30(7) ^b	15.64(7)	14.31(6)
2581.62	4	17.28(4)	15.60(3)	14.27(3)
2583.60	6	17.18(5)	15.53(5)	14.19(5)
2590.62	13	17.29(3)	15.60(3)	14.29(6)
2594.65	17	17.20(6)	15.57(3)	14.24(3)
2596.61	19	17.29(6)	15.60(6)	14.26(6)
2605.62	28	17.32(5)	15.55(3)	14.26(4)
2610.59	33	17.48(4)	15.65(4)	14.31(4)
2620.62	43	17.45(4)	15.67(3)	14.23(4)
2744.01	166	19.53(16)	17.40(7)	16.01(8)
2757.01	180	19.71(13)	17.53(6)	16.09(7)
2765.97	188	19.52(10)	17.56(5)	16.18(6)
2774.89	197	–	17.45(8)	15.96(7)
2783.98	206	19.85(16)	17.53(5)	16.08(5)
2792.96	216	19.78(13)	17.85(6)	16.33(6)
2801.94	224	20.16(16)	17.89(5)	16.52(5)
2819.91	242	20.36(19)	18.08(5)	16.61(4)
2828.88	250	20.09(21)	17.91(6)	16.62(5)
2837.92	260	20.74(35)	18.17(6)	16.85(3)
2846.80	269	20.25(25)	18.25(7)	17.01(7)
2855.81	278	–	18.64(5)	16.93(5)

^a Days after explosion, assumed to be 2002 October 29 UT (JD 2452577.5).

^b Figures in brackets give the photometric error (see text), in units of the magnitude's least significant one or two digits.

Figure 2. *VRI* light curves of SN 2002hh.

standard IRAF^{*} routines.

^{*} IRAF (Image Reduction and Analysis Facility) is distributed by the National Optical Astronomy Observatory (NOAO), which is operated by the Association of Universities for Research in Astronomy (AURA), Inc. under cooperative agreement with the National Science Foundation.

Figure 3. *K*-band image of SN 2002hh taken with the SpeX imager on 2003 July 22, when the SN was about nine months post-explosion.

Point-spread function (PSF) fitting photometry was performed after galaxy subtraction using *VRI* template images of the SN field acquired on 2004 Aug 19 after the supernova had faded away. Local stars in the field of the host galaxy (see Fig. 1 and Table 1) were measured on three different dates (2002 Nov 5, 2003 May 31, and 2003 Jun 1), calibrated against 10–15 fields of Landolt standard stars observed at different airmasses at each night (for a final root-mean-square [RMS] solution of about 0.01 mag in all the filters), and finally used for the photometric calibration of the SN magnitudes. The uncertainty in the photometry was estimated by adding in quadrature the RMS of the transformed magnitude of the SN from the observed local standard stars and the error in the IRAF PSF fitting. The photometry may be affected by a systematic error (up to 0.02 – 0.05 mag in *V* and *I*, 0.07 mag in *R*) due to the fact that, although colour terms have been applied to derive standard photometry for the KAIT *V*, *R*, and *I* filters (see Li et al. 2001), none of the local standard stars used for the photometric calibration has the extreme red colour of SN 2002hh. However, in our use of the photometry to flux calibrate the spectra, allowance for the colour term effect was achieved through the use of effective wavelengths (see discussion in section 2.3).

Final optical *VRI* magnitudes and associated uncertainties are listed in Table 2, while the corresponding light curves are shown in Fig. 2. The temporal evolution of the *VRI* magnitudes during the first 40 d shows a typical plateau phase, which indicates that SN 2002hh is a type IIP (plateau) supernova, the most common kind (see also Fig. 13). The late-time decline rates in the *VRI* bands were roughly linear at about 0.007, 0.011 and 0.008 mag day⁻¹ (respectively), and of the same order as those found in the IR bands (see below).

Figure 4. *JHKL'* light curves of SN 2002hh. Also plotted are the the early (+21 d) *J* and *K* points. Only the statistical errors are shown (see text).

Figure 5. Post-100 d IR colour evolution of SN 2002hh. Only the statistical errors are shown (see text).

2.2 Near-infrared photometry

The SpeX imager at IRTF (see Section 2.4) was used to obtain *JHKL'* images of SN 2002hh at four epochs between days 137 and 314. These epochs correspond to four of the five epochs when NIR spectroscopy was also obtained (see below). The imager employs an Aladdin-2 512×512 pixel InSb array covering a $60''.0 \times 60''.0$ field-of-view at $0''.12$ pixel⁻¹. A standard imaging procedure was performed, using 5- to 10-point jitter patterns. The images were reduced using standard IRAF routines. The jittered on-source exposures were median-combined to form sky frames in the *JHK* bands for both the supernova and the standard stars. (By median-combine, we mean that a median value was calculated for each pixel over the sequence of on-source images observed in each band.) In the *L'* band, where the sky varies

rapidly, sky subtraction was performed by subtracting consecutive pairs of on-source offset exposures from each other. In each band, the sky-subtracted frames were then median-combined. Fig. 3 shows the *K*-band image of SN 2002hh taken with the SpeX imager on 2003 July 22, when the SN was about nine months post-explosion.

Aperture photometry was carried out within the Starlink package GAIA[†] (Draper, Gray & Berry 2002) using an aperture radius of 18 pixels (equivalent to 2''.16) corresponding to 2.5 times the full width at half-maximum (FWHM) of the standard star PSF. The sky background was measured using a concentric annular aperture, with inner and outer radii respectively of 1.5 and 2.5 times that of the aperture. The sky variance with 2 sigma clipping was used to determine the photometric statistical uncertainty.

Table 3 lists the details of the IR imaging observations, including the standard stars used. On most nights the magnitudes were determined directly by comparison with the standards observed on the same nights. However, the 200 d epoch was clearly non-photometric and so on this occasion calibration was carried out via relative photometry of SN 2002hh field stars.

The resulting IR magnitudes and colours of SN 2002hh are listed in Table 4 and plotted in Figs. 4 and 5. Associated statistical errors are shown in parentheses and as error bars. The late-time decline rates in the *JHKL'* bands were roughly linear at, respectively, about 0.012, 0.013, 0.013 and 0.011 mag d⁻¹. The *J - H* and *H - K* colours remained roughly constant at ~0.5 and ~0.7, respectively, during the 137–314 d period. The *K - L'* colour reddened between days 137 and 314 from about 1.6 to about 2.0 mag.

2.3 Optical spectroscopy

Optical spectra were obtained at 8 epochs spanning 4–397 days post-explosion. We used (a) the Kast double spectrograph (Miller & Stone 1993) mounted on the Lick Observatory 3.0 m Shane telescope on Mt. Hamilton, (b) the Echelle Spectrograph and Imager (ESI; Sheinis et al. 2002) mounted on the 10.0 m Keck II telescope on Mauna Kea, (c) the ISIS spectrograph at the 4.2 m William Herschel Telescope (WHT) on La Palma, (d) the ALFOSC spectrograph at the 2.56 m Nordic Optical Telescope (NOT) on La Palma, and (e) the Low Resolution Imaging Spectrometer (LRIS; Oke et al. 1995) mounted on the 10.0 m Keck I telescope on Mauna Kea.

With Lick/Kast we used the 452/3306 grism and the 300/7500 grating, together with 180 × 1200 and 210 × 1200 pixel CCD arrays, each having a 0''.798 pixel⁻¹ scale. With Keck/ESI we used the 175 lines mm⁻¹ grating and 32.3° blaze grisms, with a 2048 × 4096 CCD array having a 0''.12–0''.17 pixel⁻¹ scale. With WHT/ISIS we used the R316R grating and the EEV4290 MARCONI2 detector with a 0''.20 pixel⁻¹ scale. With NOT/ALFOSC we used Grism 5 (0.5–1.025 μm) and the Loral 2048 × 2048 pixel array (CCD7, now retired) with a 0''.19 pixel⁻¹ scale. With Keck/LRIS we

used the 400/3400 grism and the 400/8500 grating equipped with the 4620 × 4096 and 1000 × 2245 pixel CCD arrays, respectively, having scales of 0''.211 and 0''.135 pixel⁻¹. For the Kast, ESI, ISIS and LRIS spectra the position angle of the slit was generally aligned along the parallactic angle to reduce differential light losses (Filippenko 1982). For the NOT spectrum, the slit was positioned at PA 181° in order to minimise contamination from the bright nearby star (2MASS J20344320+6007234) lying about 9''.0 WNW from the supernova. Table 5 gives details of the optical spectroscopic observations. Standard stars used are also listed, together with slit widths and position angles.

The spectra from Kast, ESI and LRIS were reduced using standard techniques as described by Li et al. (2001) and references therein. Flatfields for the red CCD were taken at the position of the object to reduce NIR fringing effects. The spectra were corrected for atmospheric extinction and telluric bands (Bessell 1999; Matheson et al. 2000a), and then flux-calibrated using standard stars observed at similar airmass on the same night as the SN (see Table 5). Approximate spectral resolutions were derived from the widths of night-sky lines. The wavelength calibration is accurate to about ±0.2 Å for Kast, from about ±0.02 Å to ±0.06 Å (depending on the order) for ESI, and about ±0.08 Å for LRIS. The ISIS spectra were reduced using standard procedures within FIGARO (Shortridge 1991). The wavelength calibration is accurate to about ±1 Å. The ALFOSC spectrum was reduced using standard procedures within IRAF; the wavelength calibration is accurate to ±3 Å.

Final fluxing of all except the 397 d spectrum was achieved using near-contemporary *VRI* photometry taken with KAIT at Lick Observatory (see Table 2). *VRI* transmission functions were formed taking into account the atmospheric transmission function for Lick Observatory, the KAIT imaging filters, and the CCD quantum efficiency. These were then applied to the SN 2002hh spectra and to a model spectrum of Vega. The resulting optical spectra were integrated and the total fluxes compared with those of Vega for each *VRI* band to derive spectra-based *VRI* magnitudes. These were then compared with contemporary *VRI* photometric magnitudes derived by interpolation of the light curves. Corrections ranged from a factor of ~0.6 to ~2.

It was found that the variation with wavelength could be reasonably described with linear functions. Linear fits were therefore made to the set of *VRI* correction factors for each epoch. For each waveband point the effective wavelength was first determined from $\int \lambda F_\lambda d\lambda / \int F_\lambda d\lambda$. The resulting linear function was then used to scale and tilt the corresponding supernova spectrum. The blue limit of the ALFOSC spectrum (250 d) is 5020 Å and consequently does not encompass the full width of the *V*-band transmission function. Therefore only the *R* and *I* transmission functions were used to derive the flux correction function for this epoch. The wavelength coverage of the ISIS spectra is such that on days +227 and +262 only the *V* band and *I* band (respectively) are fully spanned by the spectra. Therefore, in these cases only single correction factors were applied (0.97 for the +227 d spectrum, and 0.7 for the +262 d spectrum). We judge the accuracy of the final fluxing of the flux-corrected

[†] Graphical Astronomy and Image Analysis Tool, version 2.6-9

Table 3. Log of IR photometric observations taken at IRTF with SpeX.

JD-2,450,000	Date (2003)	Epoch ^a	Photometric standard	Observers
2714.5	Mar 15	137	FS150 (<i>JHK</i>), HD203856 (<i>L'</i>)	R.D. Joseph, J.T. Rayner
2777.5	May 17	200 ^b	HD201941 (<i>JHKL'</i>) ^c	J.T. Rayner
2843.5	Jul 22	266	FS150 (<i>JHK</i>), HD201941 (<i>L'</i>)	R.D. Joseph, J.T. Rayner
2891.5	Sep 8	314	FS150 (<i>JHK</i>), HD201941 (<i>L'</i>)	J.T. Rayner

^a Days after explosion.

^b Mostly cloudy, this night was non-photometric.

^c Due to the non-photometric night, this standard star was not used for calibration; see text for details.

Table 4. IR photometry and colours of SN 2002hh.

JD(2450000+)	Epoch ^a	<i>J</i>	<i>H</i>	<i>K</i>	<i>L'</i>	<i>J</i> - <i>H</i>	<i>H</i> - <i>K</i>	<i>K</i> - <i>L'</i>
2714.5	137	13.383(1) ^b	12.788(1)	12.265(1)	10.631(54)	0.595(1)	0.523(1)	1.634(54)
2777.5	200	14.166(3)	13.691(4)	12.914(6)	11.376(94)	0.475(5)	0.777(7)	1.538(94)
2843.5	266	15.104(6)	14.614(7)	13.901(6)	12.038(71)	0.490(9)	0.713(9)	1.863(71)
2891.5	314	15.562(7)	15.088(10)	14.498(4)	12.501(77)	0.474(12)	0.590(11)	1.997(77)

^a Days after explosion.

^b Figures in brackets give the internal error, in units of the magnitude's least significant one or two digits.

Table 5. Log of optical spectroscopic observations.

JD ^a	Date	Epoch ^b	Telescope/ Instrument	Range (μm)	Resol. ($\lambda/\Delta\lambda$)	Slit width/ pos. angle	Spectroscopic standard ^c	Observers
2581.8	2002 Nov 2	4	Lick/Kast ^d	0.31-1.04	600	2''/166°	BD+28°4211, BD+17°4708	A. Filippenko, R. Foley, B. Swift
2585.9	2002 Nov 6	8	Keck/ESI	0.39-1.04	4000	1''/164°	BD+28°4211	A. Filippenko, S. Jha, R. Chornock
2621.8	2002 Dec 12	44	Lick/Kast	0.31-1.04	550	2''/270°	BD+28°4211, HD 19445	R. Foley, M. Papenkova
2738.8	2003 Apr 8	162	Lick/Kast	0.32-1.04	500	2''/79°	Feige 34, HD 84937	R. Foley, M. Papenkova, D. Weisz
2804.7	2003 Jun 14	227	WHT/ISIS	0.47-0.78	1800	1''5/176°	BD+17°4798	C. Benn
2828.4	2003 Jul 7	250 ^e	NOT/ALFOSC	0.50-0.96	900	1''3/181°	BD+28°4211	J. Sollerman et al.
2839.7	2003 Jul 19	262	WHT/ISIS	0.64-1.03	2050	1''/139°	HD 340611	I. Soechting
2973.9	2003 Nov 29	397	Keck/LRIS ^f	0.31-0.94	1050	1''/127°	BD+28°4211, BD+17°4708	A. Filippenko

^a JD-2,450,000.

^b Days after explosion.

^c For Kast and LRIS observations, we give the standard stars used (respectively) for the blue and red part of the combined spectrum.

^d Lick observations used a D550 dichroic.

^e High temperature and lots of dust reported, very high sky brightness.

^f LRIS observations used a D560 dichroic.

Table 6. Log of IR spectroscopic observations.

JD ^a	Date	Epoch ^b	Telescope/ Instrument	Range (μm)	Resol. ($\lambda/\Delta\lambda$)	Slit width (arcsec)	Spectroscopic standard	Observers
2714.5	2003 Mar 15	137	IRTF/SpeX	0.81-2.42	1200	0.5	HD 199217	R.D. Joseph, J.T. Rayner
2777.5	2003 May 17	200	IRTF/SpeX	0.80-2.42	2000	0.3	HD 205314	J.T. Rayner
				2.84-4.20	1500	0.5	"	
2843.5	2003 Jul 22	266	IRTF/SpeX	0.80-2.42	2000	0.3	HD 194354	R.D. Joseph, J.T. Rayner
				2.86-4.14	1500	0.5	"	
2891.5	2003 Sep 8	314	IRTF/SpeX	0.80-2.42	2000	0.3	HD 194354	J.T. Rayner
2958.5	2003 Nov 14	381 ^c	IRTF/SpeX	0.93-2.42	750	0.8	HD 194354	R.D. Joseph, J.T. Rayner

^a JD (245 0000+).

^b Days after explosion.

^c Bad seeing: thick cirrus most of the night, A_K extinction ranging from ~ 1 mag (when spectrum taken) to opaque.

Figure 6. Evolution of the optical spectra of SN 2002hh during the photospheric phase. The left and right panels show the spectra (respectively) before and after dereddening (see Section 3.2). The spectra have been displaced vertically for clarity (the zero-flux levels are indicated by the dashed lines). No correction has been made for redshift. The narrow emission spikes in the $H\alpha$ (6563 Å) and $H\beta$ (4861 Å) line profiles are discussed in Section 3. Line identifications are discussed in Section 4. The dereddened spectra have been truncated to remove very low S/N regions toward the blue. Residuals from removal of telluric lines are marked.

Figure 7. As in Fig. 6, but showing the evolution of the optical spectra of SN 2002hh during the nebular phase.

Figure 8. Panel (a): Evolution of the *IJK*-band IR spectra of SN 2002hh taken at IRTF during the period 137 to 381 days post-explosion. The spectra have been displaced vertically for clarity (the zero-flux levels are indicated by the dotted lines). No correction has been applied for redshift or reddening. Panels (b-d): Detailed subsections of Panel (a) showing, respectively, spectral ranges 0.8–1.36 μm , 1.36–1.85 μm and 1.85–2.45 μm . The detailed evolution of the Pa α 1.875 μm line is shown separately in Fig. 9.

Figure 9. Evolution of the Pa α line from the IR spectra shown in Fig. 8. The spectra have been displaced vertically for clarity (the zero-flux levels are indicated by the dotted lines). The spectra have not been corrected for redshift or reddening.

optical spectra to be $\sim \pm 10\%$. For the 397 d spectrum, no contemporary photometry was available and so no flux correction was attempted. The fluxing error in this case could be as much as 30%.

The optical spectra are shown in Figs. 6 (photospheric phase) and 7 (nebular phase). Each figure comprises 2 panels. The left and right panels show the spectra respectively before and after dereddening. The dereddening is discussed in subsection 3.2. Optical line identification is discussed in Section 4.

2.4 IR spectroscopy

IR spectra were obtained using the 3.0 m NASA Infrared Telescope Facility (IRTF) on Mauna Kea (Hawaii), equipped with SpeX, a medium-resolution 0.8–5.5 μm cryogenic spectrograph and imager (Rayner et al. 2003). We used both the 0.8–2.4 μm cross-dispersed (SXD) and the 1.9–4.1 μm cross-dispersed (LXD) grating modes which provide resolution of up to $R = \lambda/\Delta\lambda = 2500$. The spectrograph contains an Aladdin-3 1024 \times 1024 pixel InSb array, with a 0'15 pixel $^{-1}$ scale. *JHK*-band spectra were acquired at five epochs, spanning 137–381 days post-explosion. In addition, *I*-band spectra were obtained at 4 epochs (137–314 d), and *L'*-band spectra were obtained at 200 d and 266 d. See Table 6 for the log of IR spectroscopic observations.

The spectra were reduced using FIGARO (Shortridge 1991). Most of the sky emission was removed by subtraction of successive pairs of exposures taken at two nod positions. The pairs were then coadded. The spectral orders were individually straightened, and residual sky emission lines removed. The spectra were optimally extracted (Horne 1986) and the effects of cosmic rays and bad pixels removed. Wavelength calibration was by means of Argon arc spectra and is

Figure 10. *L*-band IR spectra of SN 2002hh taken, respectively, at 200 d and 266 d post-explosion. The 200 d spectrum has been displaced vertically for clarity (the zero-flux level is indicated by the dotted line). No correction has been applied for redshift or reddening.

accurate to better than $\pm 0.0010 \mu\text{m}$. The telluric standards are listed in Table 6.

Final fluxing of the spectra was by means of the contemporary IR photometry (see Table 4). Transmission functions were formed to represent the combined transmission of the Mauna Kea atmosphere and the SpeX imaging filters. A model atmosphere (IRTRANS) for a water vapour column of 1.6 mm and an airmass of 1.5 was used to provide the atmospheric transmission. The filters are the Mauna Kea filter set. Each filter function was multiplied by the atmospheric transmission function to provide net transmission functions in each band. These were then applied to the SN 2002hh spectra and to a model spectrum of Vega. The resulting spectra were integrated and the total fluxes compared with those of Vega for each band to derive spectra-based magnitudes. These were then compared with contemporary photometric magnitudes. For the SXD spectra the dispersion over all epochs in the differences between the spectroscopic and photometric values was about 0.3 mag. This is a respectable value, given the narrowness of the slit and the differences in conditions between the measurements of the supernova and standards.

It was also found that at any given epoch a systematic difference existed between the spectroscopic and photometrically derived magnitudes. We therefore applied corrections to the SXD spectra to match them to the contemporary photometry. The corrections applied were as follows: day 137 ($\times 1.43$), day 200 ($\times 0.8$), day 266 ($\times 1.03$), and day 314 ($\times 1.11$). In the *L* band the required corrections were day 200 ($\times 0.51$) and day 266 ($\times 0.71$). We judge the accuracy of the final fluxing to be $\sim \pm 10\%$ for the *IJK* band spectra and $\sim \pm 20\%$ for the *L'* band spectra. For the 381 d spectrum, no contemporary photometry was available and so no flux correction was attempted; the fluxing error in this case could

be as much as 50%. The *IJK*-band spectra are shown in Fig. 8, while the detailed evolution of the Pa α 1.875 μm line is shown separately in Fig. 9. The *L'*-band spectra for epochs 200 d and 266 d are shown in Fig. 10. IR line identification is discussed in Section 4.

The NIR spectroscopic coverage is among the most complete ever achieved for a supernova at late times. Indeed, SN 2002hh is the first supernova beyond the Local Group for which *L*-band spectra have been acquired. The temporal coverage of the Pa α line (Fig. 9) is also unsurpassed for a supernova at late times. The strong atmospheric absorption in this region means that this line has seldom been observed in Type II SNe.

3 REDSHIFT AND EXTINCTION

3.1 Redshift

Strong, narrow Na I D 5890, 5896 \AA and K I 7699 \AA absorption was detected in the early-time spectra. In Fig. 11 we show this spectral region at high resolution on day 8 obtained with Keck/ESI. This reveals two sets of Na I D lines corresponding to velocities of $-20 \pm 10 \text{ km s}^{-1}$ and $+110 \pm 10 \text{ km s}^{-1}$. The K I line has components at $-15 \pm 15 \text{ km s}^{-1}$ and $+113 \pm 10 \text{ km s}^{-1}$. The Galactic coordinates of SN 2002hh are $l = 95.68^\circ$ and $b = +11.67^\circ$. We suggest that the blueshifted component is due to absorption within the Milky Way, perhaps within the Perseus Arm. It is unlikely that the $+110/113 \text{ km s}^{-1}$ absorptions are local, given the kinematic distribution of the Milky Way (Martos et al. 2004) and the Galactic longitude of SN 2002hh.

Narrow emission lines of H α , H β (4861 \AA), [N II] (6548, 6584 \AA) and possibly [S II] (6717, 6731 \AA) are present in some of the spectra, showing redshift velocities consistent with the derived redshift of $+110 \text{ km s}^{-1}$. The narrow lines in the 6300–6800 \AA region from 4 d to 397 d are shown in detail in Fig. 14 in the next Section. During the earlier phase, narrow lines are present on days 4 and 44 at comparable intensity, fade by 162 d, and have vanished by 227 d. However, the lines are also completely absent at 8 d. A somewhat broader slit was used on the days when the narrow lines were apparent (see Table 5) and so we suspect that the cause is incomplete background subtraction. H II regions 420 and 421 (Bonnarel, Boulesteix & Marcelin 1986) lie within $3''.0$ of the supernova, and may be responsible for the narrow emission. By 397 d, narrow lines have re-appeared. They are unresolved at a resolution of 285 km s^{-1} and are again centred at about $+110 \pm 10 \text{ km s}^{-1}$. They are more than a factor of 10 weaker than at 44 d. Inspection of the 2D frames again suggests that the origin of the narrow lines is due to incomplete background subtraction. While a relatively narrow $1''.0$ slit was used at 397 d, the much weaker ejecta emission by this epoch is probably the reason that residual narrow lines from the background have become apparent. That the narrow emission lines show redshift velocities consistent with the $\sim +110 \text{ km s}^{-1}$ derived from the Na I D and K I absorptions may indicate a physical association between the H II regions and the line-of-sight absorbing material.

Figure 11. Interstellar absorption lines toward SN 2002hh at +8 days. The thick (upper) line is K I 7699 \AA and the thin (lower) line is the Na I D doublet. The spectra are plotted in velocity space relative to the rest frames of the K I and Na I D1 lines, respectively. The Na I D2 line can also be seen at the right. Each line has two components produced by absorption in, respectively, the Milky Way and NGC 6946. The lines are unresolved at a resolution of 75 km s^{-1} .

We adopt $+110 \pm 10 \text{ km s}^{-1}$ as the redshift of the SN centre-of-mass, although neither the narrow absorption lines nor narrow emission lines necessarily have any physical connection with the supernova. This value is larger than the redshift of the host galaxy ($+48 \pm 10 \text{ km s}^{-1}$); the difference is caused by the rotation of NGC 6946 (see Walsh et al. 2002).

3.2 Extinction

As mentioned in the Introduction, the extinction to SN 2002hh is very high. To estimate and correct for the extinction, we compared the spectra and light curves of SN 2002hh with those of SN 1999em. The justification for this was that the light curves of both supernovae indicate that both events were normal Type IIP. We therefore assumed that the two events were identical, and endeavoured to match their coeval optical spectra (epoch $\sim +7$ days) by adjusting the amount of dereddening for SN 2002hh. We adopted the Cardelli et al. (1989) extinction law, initially with $R_V = 3.1$. For the SN 1999em extinction we took $A_V = 0.31 \text{ mag}$ (Baron et al. 2000) and for the explosion epoch we adopted JD2451475.4 (1999 Oct. 23.9), which is the weighted mean of the estimates of Baron et al. (2000), Hamuy et al. (2001), Leonard et al. (2002a) and Elmhamdi et al. (2003). The SN 1999em spectrum was also scaled by a factor of 4 to allow for the difference in distance (cf. Leonard et al. 2003). However, we found that no value of A_V would provide a satisfactory match between the spectra. We therefore allowed both A_V and R_V to vary. From this, we found that satisfactory matches could be obtained with $A_V(\text{SN 2002hh}) = 5.2 \pm 0.2 \text{ mag}$ and $R_V = 1.9 \pm 0.2$.

Figure 12. Comparison of coeval spectra of SN 2002hh and SN 1999em taken at about +7 days post-explosion. The SN 2002hh spectrum has been dereddened according to the 2-component extinction model *viz.* $A_V = 3.3$ mag, $R_V = 3.1$ plus $A_V = 1.7$ mag, $R_V = 1.1$ (see text for details). The SN 1999em spectrum has been dereddened with $A_V = 0.31$ mag, $R_V = 3.1$, and scaled by $\times 4$ to correct for the difference in distance between the two SNe. The extinction law of Cardelli et al. (1989) was used in both cases. Also shown is a blackbody curve for a temperature of 13,400 K. The faint red spectrum near the bottom is the original un-dereddened spectrum of SN 2002hh plotted on the same scale. This illustrates the very large extinction correction that has been applied. In spite of this, the dereddened spectra of the two SNe appear remarkably similar.

Figure 13. Dereddened absolute magnitude optical and NIR light curves of SN 2002hh (filled squares) compared with those of the Type IIpec SN 1987A (lines) and the Type IIP SN 1999em (open squares – Leonard et al. 2002a; triangles – Hamuy et al. 2001, see text for details; circles – Elmhamdi et al. 2003). For clarity, the light curves have been displaced vertically by the amounts indicated at the RHS. See text for further details. Note that the early SN 2002hh IR points are J and K at +21 d (see also text).

As a check on the above extinction estimate, we examined the narrow Na I D and K I interstellar absorption lines (Fig. 11). At such a high extinction (see above), it is recognised (e.g., Munari & Zwitter 1997) that the equivalent width (EW) of Na I D is of little value since the lines are too close to saturation. That this is the case here is confirmed by the EW ratio of the Na I 5890 Å to 5896 Å lines, which is 1.2 for the Milky Way and 1.3 for NGC 6946 (toward SN 2002hh) — that is, both are close to the total saturation ratio of 1.1 and far from the unsaturated value of 2.0. However, the K I line is expected to remain unsaturated for much higher extinctions (Munari & Zwitter 1997). We obtain K I line EW values of 0.131 ± 0.021 Å and 0.146 ± 0.026 Å for the Milky Way and NGC 6946, respectively. From the EW vs. $E(B - V)$ curve of Munari & Zwitter (1997), we deduce corresponding $E(B - V)$ values of 0.50 and 0.57 mag. The former is reasonably consistent with the $E(B - V) = 0.34$ mag value from the far-IR maps of Schlegel et al. (1998). For $R_V \approx 3$, the latter is consistent with the $A_V = 1.2^{+1.3}_{-1.7}$ mag which Barlow et al. (2005) derive from the extinction profiles of Holwerda et al. (2005). However, Munari & Zwitter caution that the derived value of $E(B - V)$ may be an overestimate if the absorption line is formed by unresolved multiple components. Alternatively, the presence of a dense “dust pocket” might not be traced by the absorption lines, leading to an underestimate of $E(B - V)$.

Notwithstanding these comments, the total $E(B - V) = 1.07$ mag corresponds to only $A_V = 3.3 \pm 0.3$ mag ($R_V = 3.1$). Taken at face value, this suggests that the remaining $A_V = 1.9 \pm 0.2$ mag of the total 5.2 mag extinction was unrevealed by the K I lines. This additional extinction may be associated with the line-of-sight H II regions and so did not show the correlation with the K I absorption EW which occurs in H I regions.

To investigate this further, we dereddened the day +8 SN 2002hh spectrum using a 2-component extinction where the first component, due to the combined effect of the ISMs of the Milky Way and NGC 6946, was assigned $A_V = 3.3$ mag and $R_V = 3.1$. A second component was then added, with A_V and R_V as free parameters. A satisfactory match was obtained with $A_V = 1.7 \pm 0.2$ mag and $R_V = 1.1$ for the second component. The dereddened spectra of SNe 1999em and 2002hh are shown in Fig. 12. Also shown is the spectrum of a blackbody corresponding to $T = 13,400$ K and an expansion velocity of $6,800$ km s $^{-1}$, with the expansion beginning 7 days earlier. While the value obtained for R_V is small, such values have been invoked in the past in multi-component extinction models (see Wang et al. 2004 and references therein). It implies that the “dust pocket” grain size is small compared with the average value for the local ISM. Also, as already indicated, the EW-derived ISM extinction may be an overestimate. A smaller ISM extinction would allow a larger “dust pocket” extinction and hence a larger value for R_V , with the upper limit being the $R_V = 1.9$ obtained in the single-component case.

Wang (2005) has suggested that the anomalous reddening seen toward a number of Type Ia supernovae could be produced by *normal-sized* grains within a dusty circumstellar cloud. In this “light-echo” scenario, not only is light

scattered out of the beam, but also we see light that has been scattered into our line-of-sight. Thus, in addition to the scattering cross-section we also need to consider the (wavelength-dependent) albedo of the grains. Wang finds that a dust cloud of inner radius 10^{16} cm would produce a significant reduction in R_V . However, we suggest that survival of grains at such a small distance from most supernovae of any type is rather unlikely. In Section 5.4 below, we find that the evaporated dust-free cavity of SN 2002hh has a radius of $\sim 10^{17}$ cm (8750 A.U.). Dust at this large distance would have only a modest effect on R_V (see Fig. 4 of Wang 2005). We therefore remain persuaded that the most plausible explanation for the small-value R_V component is due to a line-of-sight dust pocket where the grain size is atypically small.

As noted in the Introduction, Pooley & Lewin (2002) derived a column density of $N_H = 10^{22}$ cm $^{-2}$ from their X-ray data. Adopting $A_V = 0.53 \times 10^{-21} [N(\text{HI}) + 2N(\text{H}_2)]$ (Bohlin, Savage & Drake 1978) we obtain $A_V = 5.3$ mag, in good agreement with the values derived from spectral matching and the K I interstellar lines.

In Fig. 13 we show the dereddened absolute magnitude optical and IR light curves of SN 2002hh and SN 1999em, as well as those of the peculiar Type II SN 1987A. To the data for SN 2002hh we have added the +21 d J and K points of Meikle et al. (2002), which, according to our 2-component extinction model, correspond to dereddened absolute magnitudes of $M(J) = -17.6$ and $M(K) = -18.2$. The SN 1999em optical magnitudes are from Hamuy et al. (2001), Leonard et al. (2002a) and Elmhamdi et al. (2003). The IR magnitudes of SN 1999em are instead from Fig. 1 of Hamuy et al. (2001): no tabulated data were presented there, nor were these subsequently published. The optical magnitudes for SN 1987A are from Hamuy et al. (1988) and Suntzeff et al. (1988), JHK magnitudes from Bouchet et al. (1989) and Bouchet & Danziger (1993), and L' magnitudes from Catchpole et al. (1988) and Whitelock et al. (1988). Dereddening of the SN 1999em and SN 2002hh light curves was by means of, respectively, the single-component and 2-component extinction laws described above. The adopted distances are 5.9 Mpc for SN 2002hh (see above) and 11.7 Mpc for SN 1999em (Leonard et al. 2003). For SN 1987A we used a distance of 51.4 kpc and an $A_V = 0.6$ mag (Romaniello et al. 2000, 2002). Its magnitudes were dereddened using the Cardelli et al. law with $R_V = 3.1$.

Since the A_V and R_V values used for dereddening the SNe 1999em and 2002hh light curves were obtained by matching their day +7 optical spectra, we checked that a match was also obtained between the VRI light curves of the two supernovae at around +7 d. In the R and I bands a good match (difference < 0.1 mag) was indeed found. However, in the V band, the SN 2002hh magnitude was about 0.3 mag fainter than that of SN 1999em, in spite of the good match obtained between the spectra in this wavelength range. We attribute this discrepancy to differences in the true effective wavelengths (used in the light curve dereddening) of the V band between the two SNe due to the large difference in extinction together with the intrinsically steep spectral slope. We find that by shifting the effective wavelength of the V

band for SN 2002hh to the blue by 200 Å a good match is obtained at +8 d. The same effective VRI wavelengths are used for dereddening the optical light curves at all epochs. This may explain, at least partly, why the light-curve match between SNe 1999em and 2002hh becomes poorer at later epochs.

The optical light curves of SNe 1999em and 2002hh are generally well-matched in both the photospheric and nebular phases. The early-time difference with respect to SN 1987A is not surprising given its rather different nature. Nevertheless, the radioactive tails of all three supernovae match reasonably well in the optical. In the NIR, the early-time difference between SN 1987A and SN 2002hh is similar to that seen in the optical. However, in contrast to the optical region, by 266 d the HK luminosities of SN 2002hh slightly exceed those of SN 1987A. Moreover the excesses increased by 314 d. In addition, the L' luminosity of SN 2002hh is significantly brighter than that of SN 1987A from as early as 137 d, and this excess also shows some sign of increasing with time. This “IR excess” is discussed below.

The NIR light curves of SNe 1999em and 2002hh, while consistent with having similar shapes, display what appears to be an approximately constant relative offset of 0.5–0.7 mag spanning 10 to 200 days, with SN 1999em being the fainter of the two. Given the good optical match between SNe 1999em and 2002hh at early times, and between all 3 supernovae during the radioactive tail, this large NIR mismatch between SN 1999em and 2002hh is puzzling. The occurrence of this mismatch both at early times and in the J band probably rules out emission from warm dust in SN 2002hh (see below) as the source of this difference. We have tried to match the light curves by leaving both R_V and A_V as free parameters, but no satisfactory match was found for the $VRIJHK$ photometry, not even with the two-component dust model: while the optical light curves agree, the IR light curves are always offset by the amount specified above. We therefore suspect that a spurious systematic offset is present in the SN 1999em NIR data, possibly related to the IR calibrations.

The above analysis confirms that the extinction toward SN 2002hh is high and that the bulk of it occurs within NGC 6946. There is some indication that the extinction within NGC 6946 comprises two components. One of these has an exceptionally small R_V and is not traced by the K I absorption lines. It may be due to a localised dust cloud associated with line-of-sight H II regions.

3.3 Optical/IR luminosity and the ^{56}Ni mass

As explained above, we derived the total extinction by assuming that SN 1999em and SN 2002hh were alike in the optical region at about 1 week post-explosion. The fact that the subsequently dereddened VRI absolute light curves also agree to as late as ~ 270 d tends to support the validity of this assumption. We also find good agreement with the late-time VRI tails of SN 1987A. From these matches we conclude that the mass of ^{56}Ni ejected by SN 2002hh was

Table 7. Nebular OIR flux and luminosity of SN 2002hh.

Epoch (days)	F_{OIR}^a (10^{-10} erg s $^{-1}$ cm $^{-2}$)	L_{OIR}^b (10^{41} erg s $^{-1}$)
200	0.442(0.053)	1.84(0.25)
266	0.215(0.034)	0.89(0.16)

^{a, b} Error given in brackets; see text.

similar, about $0.08 \pm 0.01 M_{\odot}$.

A more direct approach to estimating the mass of ^{56}Ni ejected is by determining the total late-time luminosity during the radioactive tail. In the earlier part of the nebular phase, Type II SNe become largely optically thin to UV/optical/IR (UVOIR) radiation, but remain optically thick to the high-energy gamma rays from the radioactive decay. Thus, in principle, the late-time UVOIR light curve can allow us to estimate the amount of ^{56}Ni produced in the SN explosion. The problem in attempting such an analysis for SN 2002hh is the enormous extinction correction required. One possible concern is that we have no useful data shortward of the V band which cuts off at about 4300 Å. However, given the late epochs considered, this may only result in a small underestimate. In SN 1987A at 203 d the luminosity peaked in the I band, while less than 2% of the total was emitted shortward of 4300 Å (Catchpole et al. 1988, Fig. 4). Thus, if the similarity of SN 2002hh to SN 1987A is maintained at these shorter wavelengths, we can safely ignore the lack of UB -band data. Nevertheless, even in the I band we estimate an extinction reducing the flux by a factor of 8 ± 1 .

We have estimated the ^{56}Ni mass in SN 2002hh using our late-time $VRIJHKL'$ photometric data obtained at 200 d and 266 d to derive optical/IR (OIR) luminosities. The optical and IR magnitudes (see Tables 2 and 4) were converted into fluxes at the effective wavelengths of the filters using the flux calibrations of Bessell (1979) and those of Bersanelli, Bouchet & Falomo (1991), respectively. Adopting the two-component extinction model ($A_{V1}=3.3 \pm 0.3$ mag, $R_{V1} = 3.1$; $A_{V2}=1.7 \pm 0.2$ mag, $R_{V2} = 1.1$; see above), the fluxes were then dereddened according to the Cardelli et al. (1989) extinction law. The total fluxes at the two epochs were then derived by fitting spline curves (Press et al. 1992) to the dereddened $VRIJHKL'$ fluxes and integrating over the wavelength range 4288–44993 Å using a trapezoidal rule (the range is fixed by the limits of the filter functions used in the photometric observations) (see Table 7, Col. 2). Finally, the OIR luminosities were derived from the total fluxes by adopting a distance of 5.9 ± 0.4 Mpc to the host galaxy (see Table 7, Col. 3). The reported uncertainties take into account the internal errors from the spline fit plus the uncertainties in both the distance and extinction values. As discussed below, a fraction of the IR luminosity may be due to an IR echo. At 200 d and 266 d the echo model described below suggests that around 10% of the late-time luminosity could have been due to an echo.

The mass of ^{56}Ni ejected from SN 2002hh is obtained from $M(^{56}\text{Ni}) = M(^{56}\text{Ni})_{87A} \times L_{02hh}/L_{87A} M_{\odot}$, where

$M(^{56}\text{Ni})_{87A}$ is the mass of ^{56}Ni produced by SN 1987A, L_{02hh} is the OIR luminosity of SN 2002hh and L_{87A} is the coeval UVOIR luminosity of SN 1987A. We adopt $M(^{56}\text{Ni})_{87A} = 0.073 \pm 0.012 M_{\odot}$, which is the weighted mean of values given by Arnett & Fu (1989) and by Bouchet, Danziger & Lucy (1991), and includes uncertainties in distance and extinction. Thus, for SN 2002hh we obtain an ejected ^{56}Ni mass of $0.08 \pm 0.02 M_{\odot}$ (where the given error includes the uncertainty in the distance and extinction of SN 2002hh plus the uncertainty in the ^{56}Ni mass of SN 1987A). Reducing this by 10% to allow for the IR echo contribution, we obtain $0.07 \pm 0.02 M_{\odot}$. To within the errors, this is the same value as obtained above from the similarity of the VRI light curves. The large uncertainty is primarily due to the high extinction correction.

Similar coeval luminosities for the [Fe II] 1.257 μm line are obtained in SNe 1987A and 2002hh although the SN 2002hh values are of low S/N (see Fig. 21 in Section 5). Assuming a similar ionisation degree and temperature for the two SNe and that most of the iron results from the decay of ^{56}Ni , this provides additional support for our conclusion that similar masses of ^{56}Ni were ejected by the two SNe.

4 SPECTROSCOPIC BEHAVIOUR

4.1 Overview

4.1.1 Photospheric phase

During the photospheric phase, the 4 d and 8 d dereddened optical spectra (Fig. 6, right) are characterized by a blue continuum with few discrete features. Broad, low-contrast P-Cygni-like $\text{H}\alpha$ is visible at 4 d, together with $\text{H}\beta$ 4861 Å, He I 5876 Å, and strong, narrow (interstellar) Na I D absorption (see Section 3.1). Narrow emission lines of $\text{H}\alpha$ and $\text{H}\beta$ are also present and are probably due to nearby H II regions (see Section 3.1). By 44 d, following the typical spectral evolution of Type IIP SNe, the broad $\text{H}\alpha$ and $\text{H}\beta$ P-Cygni emission had become much more prominent while the blue continuum had faded significantly. In addition, broad P-Cygni lines of O I 7773 Å and the Ca II triplet had appeared.

In the 8 d spectrum, features occur at about 4600 Å and 5500 Å. Similar features are also visible in near-coeval spectra of SN 1987A, SN 1999em and SN 1999gi (see Elmhamdi et al. 2003; Leonard et al. 2002b). For SN 1999em, Baron et al. (2000) suggest N II ~ 5679 Å (multiplet 3) as the origin of the second of these. Recently, Dessart & Hillier (2005) have presented a quantitative spectroscopic analysis of the photospheric phase of Type IIP SNe: from synthetic fits to early-time spectra they confirm the Baron et al. identification. They conclude that the 4600 Å and 5500 Å features in SNe 1987A, 1999em and 1999gi are due, respectively, to N II ~ 4623 Å (multiplet 5) and N II ~ 5679 Å (multiplet 3). We therefore propose that the 4600 Å and 5500 Å features in the 8 d spectrum of SN 2002hh are also due to the N II multiplets. As pointed out by Dessart & Hillier, this indicates an overabundance of nitrogen in the outer layers of the progenitor star prior to core collapse.

4.1.2 Nebular phase

In our investigation of the nebular-phase spectra (Figs. 7–10), we were guided by the spectroscopic studies of SN 1987A performed by Meikle et al. (1989; 1993) and Spyromilio et al. (1991). The optical and NIR spectra are dominated by broad emission lines of neutral or singly ionised species. In Tables 8 and 9 we list, for the optical and NIR regions respectively, the identifications of the stronger nebular-phase lines (uncorrected for redshift) together with their intensities. The evolution of the velocity widths for the most prominent single emission lines is described in Table 10. In the optical region, a weak flat continuum is present up to at least 262 d (see Fig. 7, right). However, by the time the SN is recovered on day 397 d, a strong blue continuum has developed. A strong, persistent IR continuum was also present in the nebular phase and this is discussed in the next section.

4.1.3 Individual Elements

Hydrogen and Helium

The late-time spectra (see Figs. 7, 8) are dominated by broad H α emission together with lines of the Paschen and Brackett series. H β is undetected. Given a typical intrinsic H β /H α intensity ratio plus the high extinction, this is unsurprising. Pf γ can be seen in the day 200 2.85–4.15 μm spectrum (see Fig. 10). Strong He I 1.083 μm and 2.058 μm are also present. Both He I features show P-Cygni-like troughs which persist right up to the last epoch. As the supernova evolved, the H lines gradually weakened with respect to other lines. The H/He line profiles and their evolution are discussed later.

Oxygen

We identify the strong 1.13 μm feature with the O I 1.129 μm Bowen resonance fluorescence line. Ly β photons pump the 1025 \AA triplet and the subsequent cascade feeds the O I 8446 \AA and 1.129 μm lines. An alternative identification is [S I] 1.131 μm (the other [S I] line at 1.082 μm would be blended with He I). However, the O I 1.129 μm identification is confirmed by the presence of the strong, narrow feature at ~ 8500 \AA (see Fig. 7) which we identify with the O I 8446 \AA line, blended with the Ca II IR triplet. The O I 1.129 μm line increased in prominence during the 137–314 d period with respect to Pa γ (see Table 9 for details). In addition, its width narrowed up to day 266. Its presence is important since, for the Bowen mechanism to operate, there must have been intimate mixing of hydrogen and oxygen. Other oxygen lines visible in our spectra include [O I] 6300, 6364 \AA and O I 7771 \AA (probably blended with K I 7676 \AA), although the different components are not resolved. The P-Cygni absorption may be affected by the uncorrected telluric absorption at ~ 7600 \AA .

Sodium

By 162 d, the broad He I 5876 \AA P-Cygni line had given way to a P-Cygni feature due to Na I D. The presence of

sodium emission is confirmed by Na I 2.206 μm emission, initially seen as a red wing to the Br γ line. In addition, the red wing of the O I 1.13 μm feature is probably due to the Na I 1.138 μm doublet.

Magnesium

We identify the strong 1.5 μm feature with Mg I 1.503 μm . This dominated the *H*-window to day 266, but faded quite rapidly thereafter. Its optical transition at 8807 \AA probably contributes to the red wing of the Ca II triplet.

Silicon

At all five epochs a broad feature in the 1.16–1.22 μm range is present. The same feature occurred in SN 1987A and was attributed to a blend of K I(multiplet 6), Mg I(6) and Si I(4) by Meikle et al. (1989). However, Fassia, Meikle & Spyromilio (2002) noted that, given this multiple origin, the constancy of the shape between days 112 and 1822 is remarkable and may argue against a blend of different species. The virtual absence of [Si I] 1.6068 μm emission in SN 2002hh suggests a significantly lower silicon abundance than was seen in SN 1987A (see section 5.2).

Calcium

The Ca II IR triplet is prominent in both the optical and IR spectra, probably blended with O I 8446 \AA , and possibly with [C I] 8727 \AA and Mg I 8807 \AA . We also identify the [Ca II] 7291, 7323 \AA feature. [Fe II] 7388, 7452 \AA possibly may be contributing to its red wing. The lack of prominent emission at 1.99 μm tends to rule out a significant contribution from Ca I 1.94, 1.98 μm .

Iron, Cobalt, Nickel

We identify [Fe II] 1.257 μm and possibly [Fe II] 1.644 μm in the NIR plus a weaker feature in the optical region due to [Fe II] 7155 \AA . [Fe II] 1.257 μm became increasingly prominent with time and by 381 d was quite significant despite the low S/N of the spectrum (partly due to atmospheric conditions; see note in Table 6). In the 1.4 – 1.8 μm window, as the Brackett lines faded, a prominent feature at ~ 1.643 μm emerged, probably due to [Fe II] 1.644 μm . While [Si I] 1.645 μm may also have been contributing, there is little sign of the other component of this doublet at 1.607 μm which should be 40% of the 1.645 μm intensity. We conclude that [Si I] 1.645 μm made at most a minor contribution. In Section 3.3 above, we have used the [Fe II] 1.257 μm line to estimate the mass of ejected ^{56}Ni .

There is little sign of [Co II] 1.547 μm emission. In SN 1987A during the period 255–377 days the intensity ratio of the features at 1.54 μm (a blend of [Fe II] 1.533 μm and [Co II] 1.547 μm) and 1.64 μm was typically 0.25. Thus, given the relatively low S/N of the 1.64 μm feature in SN 2002hh during this period, it is likely that the 1.54 μm feature is buried in the noise.

As Br γ and Br δ faded it is clear that by 266 sd another species was contributing to the feature at 1.94 μm . By

Table 8. Optical emission features observed on days 162 to 397 in SN 2002hh.

ID	Epoch (days)	λ_{peak} (Å)	Intensity (10^{-13} erg s $^{-1}$ cm $^{-2}$)
[O I] 6300, 6364 Å	162	6267	0.16
	227	6298	0.09
	250	6304	0.08
	262	–	–
	397	6300	0.03
H α 6563 Å ^a	162	6543	1.50
	227	6545	0.86
	250	6546	0.73
	262	–	–
	397	6554	0.18
[Ca II] 7291, 7323 Å	162	7303	1.00
	227	7298	0.43
	250	7303	0.54
	262	7305	0.39
	397	7298	0.17
O I 7771 Å + K I 7676 Å	162	7763	0.82
	227	7678	0.18
	250	7770	–
	262	7685	0.16
	397	7718	0.05
O I 8446 Å + Ca II 8498 Å	162	8505	0.77
	227	–	–
	250	8517	0.63
	262	8520	0.50
	397	8529	0.11
Ca II 8542 Å + Ca II 8662 Å	162	8676	2.44
	227	–	–
	250	8662	1.32
	262	8672	0.99
	397	8677	0.24

^a The H α 6563 Å intensity excludes, when present, interstellar nebular emission (see the 162 d and 397 d spectra).

the final epoch, this feature is the most prominent in this window. In SN 1987A Meikle et al. (1989, 1993) attributed this to a blend of Br δ , Ca I 1.94 μm and [Ni II] 1.94 μm (plus a small contribution from [Fe II] 1.95 μm). They found that at 377 d the [Ni II] line contributed 30% of the blend, increasing to 60% by 574 d. However, any Ca I 1.94 μm contribution should be accompanied by a comparably strong Ca I 1.98 μm feature. The lack of a strong emission feature at 1.98 μm in SN 2002hh tends to rule out a significant contribution of Ca I to the 1.94 μm blend during the 266–381 d period, although it may have made a more significant contribution at earlier epochs. We conclude that by 266 d the 1.94 μm feature is a blend of [Ni II] 1.94 μm and Br δ .

Carbon Monoxide

CO first-overtone emission is detected by 137 d. As time passes the longer-wavelength components fade faster as the cooling ejecta depopulates the higher vibrational levels (Spyromilio et al. 1989). The presence of CO emission is important as it may presage the condensation of dust in the ejecta (see Introduction). The CO temporal evolution in the period

137–381 d is discussed in detail in Section 5.2.1.

4.1.4 Nebular line-profile evolution

In Figs. 14 to 19 we show the evolution of the most prominent, isolated lines. In all these plots, the rest-frame wavelengths of the lines are indicated by vertical dotted lines. As the supernova evolved, the H lines gradually weakened with respect to other lines. Due to difficulty in disentangling contributions from other species, we were able to measure the velocity widths (FWHM) and shifts of just H α in the optical region, and of O I, Pa β , Mg I and Br γ in the IR region. The line widths and shifts are listed in Table 10.

During the nebular phase, line widths of around 3800–4600 km s $^{-1}$ (FWHM) are seen in the hydrogen lines. There is weak evidence of a modest decline in the widths of the other lines with time. During the earlier part of the nebular phase both the Balmer and Paschen lines tend to be asymmetric with enhanced red wings. The profiles of [O I] 6300, 6364 Å and Mg I 1.503 μm (see Figs. 15, 18) exhibit pronounced irregularities during the earlier part of the neb-

Table 9. IR emission features observed on days 137 to 381 in SN 2002hh.

ID	Epoch (days)	λ_{peak} (μm)	Intensity (10^{-13} erg s $^{-1}$ cm $^{-2}$)
Ca II triplet 0.85-0.87 μm	137	0.871	1.49
	200	0.867	3.74
	266	0.867	2.21
	314	–	–
	381	–	–
Pa δ 1.005 μm + ? ^(a)	137	1.003	0.92
	200	1.003	1.20
	266	–	–
	314	–	–
	381	–	–
Pa γ 1.094 μm + He I 1.083 μm	137	1.093	2.57
	200	1.092	2.29
	266	1.090	1.51
	314	1.095	0.51
	381	1.094	0.52
O I 1.129 μm	137	1.128	1.23
	200	1.127	1.67
	266	1.130	0.88
	314	1.128	0.66
	381	–	–
Pa β 1.282 μm	137	1.281	3.60
	200	1.279	2.66
	266	1.279	1.40
	314	1.281	0.73
	381	1.281	0.62
Mg I 1.503 μm	137	1.501	0.87
	200	1.505	0.68
	266	1.507	0.36
	314	1.506	0.16
	381	1.505	0.08
Pa α 1.875 μm	137	1.876	–
	200	1.875	7.75
	266	1.875	3.70
	314	1.878	1.10
	381	–	–
Br δ 1.945 μm	137	1.944	0.81
	200	1.944	0.76
	266	1.938	0.50
	314	1.945	0.34
	381	1.945	0.40
Br γ 2.166 μm	137	2.162	1.08
	200	2.162	0.86
	266	2.162	0.32
	314	2.164	0.20
	381	–	–
Pf γ 3.740 μm	200	3.750	0.29
Br α 4.051 μm	200	4.056	1.37

^a This feature is blended with an unidentified feature around 1.03 μm . The given intensity is for the whole double-peaked feature at peak emission.

Figure 14. Evolution of the H α emission-line profile during the 4-397 d period. The spectra have been dereddened and redshift-corrected, and have been displaced vertically for clarity. The vertical dotted line corresponds to the adopted redshift of 110 km s⁻¹ for the SN centre of mass (see text). Narrow emission lines of H α , [N II] $\lambda\lambda$ 6548, 6584 and [S II] $\lambda\lambda$ 6717, 6731 from the H II regions are also visible (see Section 3 for details).

Figure 15. As in Fig. 14, but showing the evolution of the O I $\lambda\lambda$ 6300, 6364 emission-line profile during the nebular phase.

ular phase. This may indicate clumping in the SN ejecta as was inferred for SN 1985F (Filippenko & Sargent 1989), SN 1987A, and SN 1993J (Matheson et al. 2000b, and references therein). In contrast, the lack of well defined small-scale structures in [Ca II] 7291, 7323 Å (see Fig. 16) suggests that calcium is more uniformly distributed in the SN ejecta. The [Ca II] feature does exhibit a persistent asymmetry with an extended red wing. However, a 3/2 intensity ratio is expected for the 7291,7323 Å lines of the doublet (see Spyromilio, Stathakis & Meurer 1993), which may explain most of the extended red wing. In addition, as inferred for SN 1987A (see Spyromilio et al. 1991), both [Fe

Figure 16. As in Fig. 14, but showing the evolution of the [Ca II] $\lambda\lambda$ 7291, 7323 emission-line profile during the nebular phase.

Figure 17. Evolution of the O I (1.129 μ m) and the Pa β (1.282 μ m) emission lines in SN 2002hh (days 137 to 381). All the spectra have been dereddened and shifted to the rest frame.

II] 7388,7452 Å and [Ni II] 7379,7413 Å may be contributing to the red wing.

The H α peak exhibits a blueshift (with respect to the adopted +110 km s⁻¹ centre-of-mass redshift) of -915 ± 30 km s⁻¹ at 162 d, declining to -430 ± 30 km s⁻¹ at 397 d (see Table 10 and Fig. 14). (An even larger blueshift, ~ -1700 km s⁻¹, is seen at the photospheric epoch of 44 d.). The Pa β line peak exhibits a blueshift of $\sim -200 \pm 100$ km s⁻¹ at 137 d, but by 200 d this has increased to -700 ± 100 km s⁻¹. A similar shift is seen at 266 d, after which the shift reverts to around -200 ± 100 km s⁻¹ again. Br γ shows an unchanging blueshift of about -550 ± 100 km s⁻¹ from 137 d to 266 d (see Fig. 19). The O I 1.129 μ m (Fig. 17) emission line shows an almost constant blueshift of $\sim -500 \pm 100$ km s⁻¹, except

Table 10. Emission-line velocity widths (FWHM) and shifts.

Optical line velocity widths, [shifts] ^a (km s ⁻¹)				
	Epoch (days)			
Feature	162	227	250	397
H α	4530, [-915]	4475, [-805]	4475, [-750]	4630, [-430]
Infrared line velocity widths, [shifts] (km s ⁻¹)				
	Epoch (days)			
Feature	137	200	266	314
O I	3565, [-530]	3295, [-530]	2750, [+50]	2470, [-400]
Pa β ^b	3830, [-235]	4115, [-700]	4285, [-700]	3865, [-235]
Mg I	3890, [-300]	3530, [+400]	2820, [+800]	1940, [+600]
Br γ	4350, [-555]	3840, [-555]	3915, [-555]	–

^a Associated uncertainties are ± 180 km s⁻¹ for the velocity widths, and ± 30 and ± 100 km s⁻¹ for the optical and IR line shifts, respectively.

^b Pa α is blueshifted by about -250 km s⁻¹.

Figure 18. As in Fig. 17 but showing the evolution of the Mg I 1.503 μ m emission line in SN 2002hh.

5 SPECTROSCOPIC COMPARISON OF SN 2002HH AND SN 1987A

We now compare near-coeval late-time optical and NIR spectra of SN 2002hh and SN 1987A during the period of 4.5 months to ~ 1 year (see Figs. 20–24). The excellent late-time spectroscopic coverage of SN 2002hh means that it is the first CCSN for which such a comparison is possible. This comparison can be justified at the outset since, as we have shown, the nebular-phase light curves of the two supernovae are quite similar and were powered by a similar amount of ⁵⁶Ni. Only at early times do the light curves differ significantly, primarily due to the different physical sizes of their progenitor stars (see Woosley 1988). In all the comparison figures the spectra have been corrected for redshift and extinction. The recession velocities are $+283$ and $+110$ km s⁻¹ for SN 1987A and SN 2002hh, respectively. The dereddening made use of the extinction law of Cardelli et al. (1989). For SN 1987A we adopted $A_V = 0.6$ mag and $R_V = 3.1$. For SN 2002hh, we used the two-component extinction model ($A_{V1} = 3.3$ mag, $R_{V1} = 3.1$; $A_{V2} = 1.7$ mag, $R_{V2} = 1.1$; see Section 3). In addition, the SN 1987A spectra have been scaled to the distance of SN 2002hh (5.9 Mpc).

Figure 19. As in Fig. 17 but showing the evolution of the Br γ 2.166 μ m emission line and the CO emission in SN 2002hh.

at 266 d when it shows a redshift of about $+50 \pm 100$ km s⁻¹. In contrast, Mg I 1.503 μ m (Fig. 18) shows an early blueshift of $\sim -300 \pm 100$ km s⁻¹, but from 200 d to 314 d it is redshifted by $\sim +600$ km s⁻¹.

The pattern of emission-line blueshifts is probably indicative of variations in relative abundancies and conditions across the ejecta. However, apart from Pa β , no lines show evidence of an *increasing* blueshift with time nor progressive attenuation of the red wing, suggesting that, up to 381 d, there was no significant dust condensation in the ejecta.

5.1 Optical spectra

In Figure 20 we compare optical spectra of SN 2002hh at epochs of 162 d, 250 d and 397 d with near-coeval spectra of SN 1987A. The SN 1987A spectra are from Spyromilio et al. (1991) and Stathakis (1996). The overall spectral form and evolution of the two SNe are rather similar, especially at 162 d and 250 d. At all three epochs the H α luminosity is similar between the two SNe. The Na I D P-Cygni feature is also similar in the two events. The most striking difference between the two SNe is that both [Ca II] 7291, 7323 Å and the Ca II IR triplet are much stronger in SN 1987A throughout the 162–397 d period. Moreover the strong Ca I 1.99 μ m feature in SN 1987A at 192 d is virtually absent in the SN 2002hh 200 d spectrum (see following section). We infer

Figure 20. Comparison of the optical spectra of SN 2002hh with near-coeval spectra of SN 1987A. The spectra have been corrected for redshift and extinction. The SN 1987A spectra have been scaled to the distance of SN 2002hh (5.9 Mpc) and displaced vertically for clarity. At the bottom we show the line identifications for SN 1987A as given in Spyromilio et al. (1991).

Figure 21. Comparison of the NIR spectra of SN 2002hh with near-coeval spectra of SN 1987A in the 0.8–1.4 μm region (which includes the *J* band). The spectra have been corrected for redshift and extinction. The SN 1987A spectra have been scaled to the distance of SN 2002hh (5.9 Mpc) and displaced vertically for clarity. At the bottom we show the line identifications for SN 1987A as given in Meikle et al. (1993).

Figure 23. As for Fig. 21, but for the *K* band (1.9–2.4 μm).

a significantly lower calcium abundance in SN 2002hh.

At 162 d and 397 d the SN 2002hh optical continuum is distinctly bluer than that of SN 1987A, while at 250 d they are about the same. At 162 d the flux levels toward the blue are similar, but by $1 \mu\text{m}$ the SN 1987A continuum flux exceeds that of SN 2002hh by more than a factor of 2. Comparison of the overlap of the red end of the 162 d optical spectrum with the blue end of the 137 d and 200 d infrared spectra of SN 2002hh suggests that some of the SN 2002hh/SN 1987A red discrepancy ($\sim \times 1.35$) is due to error in the linear flux correction function (see Section 2.3) for the 162 d SN 2002hh optical spectrum. At least some of the remaining discrepancy may be due to error in the SN 1987A fluxing. Unfortunately, we are unable to apply an overlap test here since there is a $0.12 \mu\text{m}$ gap between the SN 1987A optical and IR spectra.

In the 397 d optical spectrum of SN 2002hh, the continuum flux toward the red agrees well with that of SN 1987A at 371 d. However, as we move to the blue we see a growing excess in the SN 2002hh continuum relative to that of SN 1987A. We were unable to check the spectral fluxing of SN 2002hh against photometry for the 397 d optical or 381 d IR spectra, but nevertheless we find fair flux agreement in the small optical/IR overlap region around $0.94 \mu\text{m}$. This gives us confidence that the fluxing toward the red end of the SN 2002hh optical spectrum is good. However, it is possible that at least some of the blue discrepancy could be due to fluxing error which increases toward shorter wavelengths (see Section 2.3). Another possibility is the presence of uncorrected background contamination, as Milne & Wells (2003) concluded was the case for the Type Ia SN 1989B. A third explanation is that in SN 2002hh a small fraction of the peak luminosity is being scattered by circumstellar or interstellar dust. Thus, as the supernova flux fades between 162 d and 397 d, the relative contribution of the scattered light increases. Dust-echo enhancement of late-time optical spectra has been reported for the Type Ia SNe 1991T and 1998bu (Patat 2005 and references therein). Spectral modelling of the blue excess may distinguish between these possibilities for SN 2002hh. However, we are much less persuaded that the blue continuum is due to ejecta-CSM interaction since no signs of this are seen in the contemporary spectral lines.

5.2 Near-IR spectra

In Figures 21 to 24, we compare $\sim 0.8\text{--}4.2 \mu\text{m}$ spectra of SN 2002hh at 200 d, 266 d and 314 d with near-coeval spectra of SN 1987A taken from Meikle et al. (1989). At the bottom of each figure we show the line identifications for SN 1987A as given in Meikle et al. (1993). The fluxing for SN 1987A has been revised to match the IR photometry of Bouchet & Danziger (1993), Catchpole et al. (1987, 1988) and Whitelock et al. (1988). In particular, the L' -band spectra of SN 1987A at 192 d and 255 d have been scaled by factors of 1.31 and 1.46, respectively. In addition, the SN 1987A fluxes have been scaled to 5.9 Mpc, the distance of SN 2002hh. All the SNe 1987A and 2002hh spectra have been dereddened as described earlier.

As in the optical region, the spectral form and evolution

of the two SNe are very similar. The similarity of the form and fluxes of the spectra in the J and H bands is particularly impressive especially when one considers that the only corrections have been to the extinction and the difference in distance.

J-band spectra

The $\text{Pa}\gamma$ $1.094 \mu\text{m}$ -He I $1.083 \mu\text{m}$ blend is stronger in SN 1987A, especially by 314 d, and yet the He I absorption remains similar in the two SNe (although this could simply be due to saturation). The $\text{Pa}\beta$ $1.282 \mu\text{m}$ and O I $1.129 \mu\text{m}$ emission peaks are at about the same level in both events throughout the 200–314 d period. The [Fe II] $1.257 \mu\text{m}$ is about the same in both SNe up to 266 d, but at 314 d it is about twice as strong in SN 2002hh compared with SN 1987A. The Si I $1.20 \mu\text{m}$ emission is somewhat stronger in SN 1987A, but this difference fades with time. Some of the $\text{Pa}\gamma$ $1.094 \mu\text{m}$ -He I $1.083 \mu\text{m}$ blend difference may be due to the additional presence of [Si I] $1.099 \mu\text{m}$ at a stronger intensity in SN 1987A due to a higher abundance of silicon in this event. However, it seems unlikely that this can provide the whole explanation for the difference.

H-band spectra

The overall appearance of the H -band spectra is similar between the two SNe. The most striking and persistent difference is the factor of 2.5 greater luminosity of Mg I $1.503 \mu\text{m}$ in SN 2002hh. Redward of the Mg I line some other differences are seen between the two events. SN 1987A shows a persistent emission feature at $1.61 \mu\text{m}$ which is virtually absent in SN 2002hh. Meikle et al. (1989) ascribed the $1.61 \mu\text{m}$ emission to [Si I] $1.6068 \mu\text{m}$. The weakness of the corresponding emission in SN 2002hh suggests a lower silicon abundance in this SN. Interestingly, the $1.64 \mu\text{m}$ feature is comparable to, or slightly stronger than in SN 1987A during the 200–314 d period. Meikle et al. (1989) attribute this feature to a blend of [Fe II] $1.644 \mu\text{m}$, [Si I] $1.645 \mu\text{m}$ and Br12. However, the weakness of the [Si I] $1.6068 \mu\text{m}$ component in SN 2002hh suggests that the $1.64 \mu\text{m}$ feature is predominantly due to iron and hydrogen in this SN.

K-band spectra

The two SNe show very similar features from 200 d to 314 d, although no comparison can be made shortward of about $1.97 \mu\text{m}$ where the SN 1987A data terminate. The peak-base intensity of Br γ $2.166 \mu\text{m}$ is similar at 200 d, at 266 d it is stronger in SN 1987A, but by 314 d it is stronger in SN 2002hh. The He I $2.058 \mu\text{m}$ feature is of comparable strength at ~ 200 d in both SNe, but is stronger in SN 2002hh thereafter. The Na I $2.206 \mu\text{m}$ line, which shows up in both SNe on the red wing of the Br γ line at ~ 200 d, is increasingly prominent in SN 2002hh at later epochs. The CO first overtone is about a factor of 3 stronger in SN 1987A at 192 d than in SN 2002hh. However, the SN 1987A CO intensity fades more rapidly than in SN 2002hh so that by 314 d the situation is reversed. Indeed, by 381 d the SN 2002hh CO emission appears to be about twice as strong as in SN 1987A (see below). There is little sign of the unidentified $2.265 \mu\text{m}$ feature in SN 2002hh (see below). In addition, the strong

Figure 25. Comparison of the first-overtone CO profile of SN 2002hh at 137 d with that of SN 1987A at 110 d. The SN 1987A spectrum has been scaled to the distance of SN 2002hh, and has been displaced vertically so that the underlying continuum matches that of SN 2002hh (see text). The spectra have been corrected for redshift and extinction.

Figure 26. As for Fig. 25 but for SN 2002hh at 200 d and SN 1987A at 192 d.

Ca I 1.99 μm feature in SN 1987A at 192 d is virtually absent in the SN 2002hh 200 d spectrum. A striking difference between the two SNe is that SN 2002hh shows a much stronger underlying continuum. At 200 d, the excess continuum amounts to $\sim 1.4 \times 10^{-16} \text{ erg s}^{-1} \text{ cm}^{-2} \text{ \AA}^{-1}$, falling to about half this value at 266 d and maintaining this level until 314 d. The (SN 2002hh):(SN 1987A) continuum ratio rises from 1.6 to 3.6 between 200 d and 314 d. The continuum is discussed below.

L-band spectra

In spite of the lower S/N of the SN 2002hh spectra, we can see that Br α and Pf γ have strengths similar to those in

Figure 27. As for Fig. 25 but for SN 2002hh at 266 d and SN 1987A at 255 d.

Figure 28. As for Fig. 25 but for SN 2002hh at 381 d and SN 1987A at 377 d.

SN 1987A at 200 d. By 266 d Br α is still of roughly comparable strength in the two SNe, but there is no longer any sign of Pf γ in SN 2002hh. As in the *K* band, a striking aspect of the *L*-band spectrum is the much stronger continuum in SN 2002hh. The (SN 2002hh):(SN 1987A) continuum ratios in the *L* band are similar to those seen in the *K* band (1.8 at 200 d and 3.6 at 266 d). The continuum is discussed below.

5.2.1 Carbon monoxide

In Figures 25–28 we compare the CO first overtone emission spectra of SNe 1987A and 2002hh. The SN 1987A spectra have been scaled to the distance of SN 2002hh. In addition, in order to effect a better comparison between the two supernovae, the SN 1987A spectra have been displaced vertically so that the underlying continuum (judged from the spectrum to the blue of the CO emission) matches that of

SN 2002hh. The excess continuum in SN 2002hh is discussed below. Both spectra in each figure have been corrected for extinction and redshift.

In Fig. 25 we compare the 137 d spectrum of SN 2002hh with the 110 d spectrum of SN 1987A. In both cases CO emission is barely visible. In Fig. 26 we compare the 200 d spectrum of SN 2002hh with the 192 d spectrum of SN 1987A. First-overtone emission is clearly present in both spectra, but is significantly weaker in SN 2002hh. The unidentified 2.265 μm feature prominent in SN 1987A is completely absent in SN 2002hh (see below). While the relative weakness of the SN 2002hh CO emission persists to 266 d (Fig. 27), the supernovae exhibit a similar relative decline in the P branch ($\sim 2.37 \mu\text{m}$). Local thermodynamic equilibrium (LTE) modelling of the CO emission profile in SN 1987A (e.g., Spyromilio et al. 1988) showed that by 255 d the decline in the P branch ($\sim 2.37 \mu\text{m}$) flux implies that the temperature of the CO emitting region had fallen below 2000 K. We conclude that similar cooling took place in SN 2002hh. This is important as it suggests that some regions of the ejecta may cool sufficiently for dust condensation to take place. A quasi-periodic structure is produced by the R-branch bandheads of the 0–2, 1–3, 2–4 (etc.) vibrational transitions. The visibility of this structure in the 266 d SN 2002hh spectrum is similar to that of SN 1987A at 255 d, implying a similar CO velocity, 1800–2000 km s^{-1} .

In Figure 28, we compare the CO spectrum of SN 1987A at 377 d with that of SN 2002hh at 381 d. In spite of the very low S/N of the latter, it seems that by this epoch the R-branch intensity of SN 2002hh was about twice as strong as in SN 1987A.

5.3 The unidentified 2.265 μm feature

An emission feature at 2.265 μm is present in the spectra of SN 1987A from as early as 192 d to at least 2 years post-explosion. Spyromilio, Leibundgut & Gilmozzi (2001) also claim detection of this feature in the Type IIP SN 1999em at ~ 170 d, albeit at a much lower S/N. However, in other CCSNe *K*-band spectra the feature is at best marginally present [SN 1996ad (105 d), Spyromilio & Leibundgut 1996; SN 1998dl (~ 150 d), Spyromilio et al. 2001] or absent [SN 1998S (109 d), Fassia et al. 2001; SN 1999gi (126 d), SN 2000ew (97 d), Gerardy et al. 2002]. It might be inferred from this that the 2.265 μm feature is actually quite ubiquitous, but does not strongly appear until after ~ 150 d. However, our SN 2002hh observations (see Figs. 25–28) show that the feature was certainly absent up to 200 d and, perhaps, even up to 266 d. While the origin of this feature has been debated for many years (Spyromilio et al. 1988; Meikle et al. 1993; Liu & Dalgarno 1995; Spyromilio & Leibundgut 1996; Gearhart, Wheeler & Swartz 1999; Gerardy et al. 2000, 2002; Spyromilio et al. 2001), we must conclude that as yet there is no consensus as to its true identity nor why it seems to exhibit such a large range of intensities from one supernova event to another.

5.4 The late-time near-IR continuum

As already mentioned, one of the most notable differences between the late-time coeval NIR spectra of SN 1987A and SN 2002hh is the much stronger *KL* continuum in the latter event. This was illustrated for epochs 200 d and 266 d, for which both *K* and *L*-band spectra were available. Inspection of Figs. 23 and 24 shows that this excess in SN 2002hh probably persisted to beyond 314 d. We would like to understand the origin of this continuum, and in particular, why it is so much stronger than in SN 1987A.

In SN 1987A, Meikle et al. (1993) found that the late-time *JHK* continuum could be well represented by a $\lambda^{-2.5}$ law between 192 and 574 days. They found that this continuum was several times stronger than would be expected from optically thin, ionised hydrogen, as well as having a steeper spectrum than that of pure free-free emission. They suggested that the *JHK* continuum was due to a mixture of emission from optically thick and optically thin gas, comprising many contributing species and subject to spatial variations in temperature and ionisation. Different behaviour was seen in the *L*-band continuum. While the $\lambda^{-2.5}$ law provided a fair representation of the 192 d continuum to about 3.65 μm , at longer wavelengths the slope flattened. Moreover, by 349 d, the break in slope had moved back to $\sim 3.3 \mu\text{m}$. Meikle et al. found that between 192 d and 349 d the *L*-band continuum faded at the same rate as did the CO first overtone emission in the *K* band. They therefore suggested that the excess *L*-band continuum was caused by a blend of unidentified molecular emission bands.

Wooden (1989; see also Wooden et al. 1993 and Wooden 1997) hypothesized that at 60 d and 260 d, part of the 3–12 μm continuum of SN 1987A was due to warm dust in the circumstellar environment, heated by the early-time luminosity — an IR echo. She derived dust temperatures of ~ 1300 –1600 K at 60 d, falling to ~ 560 –700 K at 260 d, and suggested that the dust lay in the circumstellar ring (Wooden 1997). However, as Meikle et al. (1993) point out, the Wooden dust model does not account for much of the *L*-band continuum which appears to be in *excess* of the Wooden dust-model spectra. Nevertheless, even if we accept the Meikle et al. “blended molecular bands” hypothesis for SN 1987A, it is not clear that this solution can be extended to the significantly larger continuum excess in SN 2002hh. Two points argue against doing so. One is that there is convincing evidence that the excess is at least as strong in the *K* window, where strong, blended, and unidentified molecular emission is perhaps less likely. The other point is that, if we attribute all of the SN 2002hh continuum to molecular emission, then why is the CO emission so much *weaker* than in SN 1987A, at least for epochs 200 d and 266 d? We are therefore persuaded to examine the possibility that at least some of the excess continuum in SN 2002hh is due to warm dust.

Comparison of the SN 2002hh 1–4 μm spectra with blackbody functions shows that much of the excess continuum in the *K* and *L* windows could be reproduced with blackbodies at 1100–1300 K and having an expansion velocity of $\sim 1700 \text{ km s}^{-1}$. Such temperatures and velocities may

Figure 29. Infrared spectra of SN 2002hh compared with IR-echo model spectra for three epochs, illustrating that much of the KL excess could be due to an IR echo (see text for details of the model). No L -band spectrum was available for 314 d, so we show the corresponding L' photometry point instead.

Figure 30. The temporal evolution of the extinction-corrected colour $(K - L')_0$ for core-collapse supernovae, including SN 2002hh (filled squares). The epoch gives the approximate number of days since outburst. Pozzo et al. (2004) suggested that colours lying above the dashed line at $(K - L')_0 = 1.6$ indicate a contribution to the IR emission from hot dust. The $(K - L')_0$ colour of SN 2002hh is redder than that of SN 1987A by about 0.5 mag, although the temporal trend is similar. However, even the latest SN 2002hh point lies only slightly above the $K - L' = 1.6$ line and so provides little (if any) support for dust condensation.

be consistent with an origin in newly condensing dust or in an IR echo. However, the presence of the KL spectral excess as early as 200 d plus the rather high blackbody temperature tend to argue against the condensing dust hypothesis. In addition, the 200 d CO emission is a factor of 3 weaker in SN 2002hh than in SN 1987A, further reducing the prospect that sufficiently cold dust-forming conditions might have occurred around this epoch. The alternative possibility is that much of the excess could have been due to an IR echo from pre-existing dust in the progenitor CSM. We have therefore constructed an IR-echo model and have used this to explore the parameters of a dusty CSM that could produce an echo of about the right spectral shape and intensity to account for the excess.

The IR-echo model follows those of Bode & Evans, (1980), Dwek (1983) and Graham & Meikle (1986). The input UV-optical luminosity is a parameterised version of the peak and plateau parts of the SN 1999em $UBVRI$ light curve (Elmhamdi et al. 2003) scaled to the Cepheid distance of 11.7 Mpc (Leonard et al. 2003). To allow for radiation shortward of the U band, we assumed that the supernova spectrum could be roughly described by a blackbody at 12,000 K during the peak, and 5,500 K during the plateau. Therefore, we scaled the adopted light curve by factors of ~ 1.9 in the peak and 1.05 in the plateau. At wavelengths longer than the I band the fractions of the total blackbody radiation are about 5% at 12,000 K and 30% at 5500 K. However, at these wavelengths the absorptivity of the dust grains (size $\sim 0.1 \mu\text{m}$) is likely to fall quite rapidly. Therefore, to simplify the IR-echo calculation, we ignored the IR contribution to the bolometric luminosity. We also ignored the radioactive tail since this is (a) much fainter than the earlier phases ($< 10\%$ of the peak flux), and (b) dominated by infrared radiation. Thus, the bolometric light curve used for the model is $47.0 \times 10^{41} e^{-t(d)/18.7} \text{ erg s}^{-1}$ to 24 days, and $11.1 \times 10^{41} e^{-t(d)/171} \text{ erg s}^{-1}$ for 24–118 days. A grain UV-optical absorptivity of 1 was assumed. The dust grain size was $0.05 \mu\text{m}$, the grain material density was 3 g cm^{-3} , and the pre-explosion grain number density at 6700 A.U. was $9 \times 10^{-9} \text{ cm}^{-3}$ with an r^{-2} (steady wind) dependence. The resulting optical depth to the input UV-optical luminosity was $\tau = 0.05$. A dust grain emissivity proportional λ^{-2} was assumed for the IR emission. The evaporated dust-free cavity was $R_v = 8750 \text{ A.U.}$ This was obtained by scaling from the SN 1979C value (Dwek 1983) assuming $r_v \propto L_{peak}^{0.5}$ (Dwek 1985). The paraboloid corresponding to the peak SN luminosity lay beyond the dust-free cavity at all three epochs. The CSM outer radius was 133,000 A.U. and the distance of SN 2002hh was 5.9 Mpc. The derived vertex dust temperatures were 1195 K, 1075 K and 1025 K on days 200, 266 and 314, respectively. The total mass of dust is $1.6 \times 10^{-3} M_\odot$. Assuming a standard grain-to-gas ratio (by mass) of 0.006, the corresponding CSM mass was $0.26 M_\odot$, or $0.28 M_\odot$ if we include the gas in the dust-free cavity.

In Fig. 29 we compare the IR echo model spectra with the observed KL spectra for 200 d, 266 d and 314 d. In the last case, no L -band spectrum was available and so we show the corresponding L' photometric point instead. We conclude that much of the KL excess can be reproduced with a CSM mass of $\sim 0.3 M_\odot$. Only small optical depth (~ 0.05) is

required to reproduce the KL excess. In Section 3.2 we obtained $A_V = 1.9 \text{ mag}$, i.e., $\tau_V = 1.6$ for the “dust pocket.” We conclude that most of the dust-pocket extinction occurred well beyond the progenitor CSM.

Pozzo et al. (2004) suggested that if the $K-L'$ colour of a CCSN exceeds ~ 1.6 within a year after explosion it indicates the presence of circumstellar dust heated by the supernova’s early-time luminosity (i.e., an “IR echo”), although there may also be a contribution from newly condensed dust in the ejecta. In Fig. 30 we update Fig. 15 of Pozzo et al. where we plot the $K-L'$ evolution of SN 2002hh compared with other CCSNe. Even the latest SN 2002hh point lies only slightly above the $K-L' = 1.6$ line. We therefore conclude that the $K-L'$ analysis does not provide additional support for either hypothesis. As indicated in Section 4.1.4, the line-profile behaviour up to 381 d also yields no evidence for dust condensation in the ejecta.

The lack of evidence for dust condensation during the first year does not rule out the possibility of grain formation at later epochs. Dust formation happened only after the elapse of one year in SN 1987A, SN 1998S and SN 1999em.

6 CONCLUSIONS

We have presented optical/IR photometric and spectroscopic observations of SN 2002hh covering a period of ~ 400 days during the photospheric and nebular phases. We confirm it to be a normal Type IIP event. We show the first-ever L -band spectra for such an event. The only other supernova for which L -band spectra have been obtained was the peculiar (and very nearby) Type II SN 1987A.

SN 2002hh is one of the most highly extinguished supernovae ever investigated. By assuming a similar early-time spectroscopic behaviour to the well-studied “template” Type IIP SN 1999em, we first derived a total extinction of $A_V = 5.2 \text{ mag}$. This value was checked against the K I 7699 Å absorption line, from which we infer A_V values of 1.55 and 1.77 mag ($R_V = 3.1$) in the H I ISMs of the Milky Way and NGC 6946, respectively. This suggests that there is an additional $A_V = 1.7 \text{ mag}$ of extinction which is not traced by the K I absorption line. However, we find that a good match between coeval early-time spectra of SNe 1999em and 2002hh is obtainable using a 2-component extinction model for SN 2002hh, with $A_V = 3.3 \text{ mag}$ and $R_V = 3.1$ (Component 1), and $A_V = 1.7 \text{ mag}$ with $R_V = 1.1$ (Component 2). An R_V value as low as 0.7 has been invoked in the past in multi-component extinction models (see Wang et al. 2004 and references therein); it probably implies a distinct line-of-sight “dust pocket” where the mean dust grain size is smaller than in the H I ISM. We suggest that this dust pocket may be associated with the H II region and dust lane which lies close to the SN 2002hh line-of-sight. We do *not* associate most of the second extinction component with either newly condensed dust or the progenitor CSM (see below).

The early-time optical light curves of SNe 1999em and 2002hh are generally well-matched, as are the radioactive

tails of these two SNe and SN 1987A. This suggests a certain robustness in the adopted extinction in spite of it being derived using only one epoch of spectroscopic data. The late-time similarity of SN 2002hh to SN 1987A implies that $0.07 \pm 0.02 M_{\odot}$ of ^{56}Ni was ejected by SN 2002hh. This is confirmed by our derivation of the OIR luminosity at 200 d and 266 d and by the similar coeval luminosities of the [Fe II] 1.257 μm line in SNe 1987A and 2002hh. In the nebular phase, however, the *HKL'* luminosities of SN 2002hh exhibit a growing excess with respect to those of SN 1987A. We attribute much of this excess to an IR echo from a pre-existing, dusty CSM. The NIR light curves of SN 1999em are systematically fainter than those of SN 2002hh by about 0.6 mag. We suspect an error in the calibration of the SN 1999em magnitudes.

During the nebular phase, line widths (FWHM) of around 3800–4600 km s^{-1} are seen in the hydrogen lines. There is weak evidence of a modest decline in the widths of the other lines with time. During the earlier part of the nebular phase both the Balmer and Paschen lines tend to be asymmetric with enhanced red wings. The presence of strong He I 1.083 μm emission as early as 137 d (Fig. 8b) implies upward mixing of radioactive iron-group elements (Graham 1988, Fassia et al. 1998, Fassia & Meikle 1999). [O I] 1.129 μm is also prominent during the nebular phase, indicating microscopic mixing of hydrogen and oxygen. Further evidence of mixing is provided by the profiles of [O I] 6300, 6364 \AA and Mg I 1.503 μm which exhibit pronounced irregularities during the earlier part of the nebular phase. This suggests clumping in the SN ejecta as was inferred for SNe 1985F, 1987A, and 1993J. In contrast, the lack of well-defined small-scale structures in [Ca II] 7291, 7323 \AA points to a more uniform distribution in the SN ejecta.

Persistent blueshifts are seen in a number of prominent nebular-phase lines. The pattern of blueshifts is probably due to variations in relative abundancies and conditions across the ejecta. However, apart from Pa β , no lines show evidence of an *increasing* blueshift with time nor progressive attenuation of the red wing, suggesting that, up to 381 d, there was no significant dust condensation in the ejecta.

We have presented a detailed comparison of the late time optical and NIR spectra of SNe 1987A and 2002hh. While the overall impression is one of similarity between the spectra of the two events, there are notable differences. The Mg I 1.503 μm luminosity in SN 2002hh is much stronger while emission from silicon and calcium is much weaker. Yet, a number of pieces of evidence point to similar iron-group masses having been produced in the two events. The explosive nucleosynthesis models of Thielemann, Nomoto & Hashimoto (1996) suggest that the magnesium mass in particular is a sensitive indicator of progenitor mass, increasing by a factor of about 15 as we go from a progenitor mass of 13 M_{\odot} to 20 M_{\odot} . For this progenitor mass range, the same models also predict a silicon mass increase of a factor of 2 while the calcium abundance decreases slightly as the progenitor mass increases up to 15 M_{\odot} and then increases slowly thereafter. In contrast, due to the rising mass cut, the mass of ejected iron *falls* by a factor of about 2 over the same progenitor mass range. Clearly the overall abundance

trends in SN 1987A and SN 2002hh are not consistent with the explosion model predictions. It appears that during the burning to intermediate-mass elements, the nucleosynthesis did not progress as far as might have been expected given the mass of iron ejected.

Elmhamdi et al. 2003 (and references therein) made use of the [O I] 6300,6364 \AA doublet luminosity to place constraints on the progenitor mass of SN 1999em, by scaling from the [O I] luminosity and ^{56}Ni mass of SN 1987A. Following a similar procedure for SN 2002hh, at +397 d the coeval [O I] doublet luminosity is about a factor of 2.2 lower than in SN 1987A, while the ^{56}Ni masses are similar. We therefore deduce an oxygen mass of about one half of that found in SN 1987A (i.e., ~ 0.7 – $1.0 M_{\odot}$ in SN 2002hh). This suggests a massive progenitor with a main-sequence stellar mass of 16–18 M_{\odot} (Woosley & Weaver 1995), somewhat less than the 20 M_{\odot} of SN 1987A. Within the context of the Thielemann et al. models, this would be consistent with the observed lower silicon mass and possibly also with the lower calcium abundance in SN 2002hh. However, the apparent conflict with the strong Mg I 1.503 μm luminosity remains.

A striking difference between SN 1987A and SN 2002hh lies in the velocity shifts of some of the more prominent, isolated lines. While blueshifts of order -500 km s^{-1} were seen in SN 2002hh, *redshifts* of about the same size were seen in the same lines and phases in SN 1987A. These shifts were discussed by Spyromilio et al. (1990) and Meikle et al. (1993). It was concluded that asymmetry in the ejecta was the most likely explanation. As indicated above, we propose that the blueshifts in SN 2002hh have a similar origin.

As already mentioned, during the first year of SN 2002hh we find no line profile-based evidence of dust condensation in the ejecta. This is consistent with an SN 1987A-like behaviour, where the first sign of dust condensation was at about 1 year (Meikle et al. 1993) and substantial dust-induced line attenuation did not occur until about 500–530 days (Danziger et al. 1991). The clear presence of CO emission by 200 d indicates that conditions may eventually allow grain condensation. However, the CO emission was generally weaker than seen in SN 1987A and so the mass of condensing dust may be less. Nevertheless, Meikle et al. (2005a,b and in prep.) report mid-IR evidence for the condensation of $\sim 10^{-3} M_{\odot}$ of dust by day 590 — a very similar mass and condensation epoch to those of SN 1987A. Modelling of the CO first-overtone emission using the constraint of the ^{56}Ni mass derived from the bolometric light curve, might provide an additional constraint on the progenitor core mass as was done for SN 1998S by Fassia et al. (2001). However, such modelling is beyond the scope of this paper.

Based on the IR-echo interpretation of the late-time *KL* excess we deduce that the progenitor of SN 2002hh underwent a mass-loss of $\sim 0.3 M_{\odot}$. This is similar to the CSM mass derived for the Type IIL SN 1980K by Dwek (1983), also based on IR-echo analysis. While this may be less than that of SN 1987A (e.g. Sugerman et al. 2005), the strong and relatively early IR excess points to a substantial proportion lying within ~ 100 light-days of the supernova — much closer than for SN 1987A. Likewise, the strong radio luminosity of

SN 2002hh (Beswick et al. 2005) as early as 381 d points to recent substantial mass-loss. Indeed, the radio luminosities reported by Beswick et al. are very similar to those of SN 1980K from which Weiler et al. (1992) derived a CSM mass exceeding $0.34M_{\odot}$. Extrapolating our IR echo model to the earliest epoch of the *Spitzer Space Telescope* observations *viz.* 590 days, it predicts a flux of ~ 0.3 mJy at $5.8 \mu\text{m}$ and $8.0 \mu\text{m}$. This is less than 10% of the total fluxes quoted by Barlow et al., but it is closer to the *decline* in flux found by Meikle et al. (2005a,b and in prep) between days 590 and 994. Thus, if we attribute only the declining component of the flux to the supernova, a much smaller CSM mass is needed to account for it. This is consistent with the finding of Meikle et al (2005a,b and in prep.) that the total mid-IR emission could not have arisen from an IR-echo within a dusty CSM ejected by the progenitor (see Introduction). It is, however, less consistent with the extremely massive (10–15 M_{\odot}) CSM claimed by Barlow et al. (2005). Furthermore, a mass loss of 10–15 M_{\odot} is about 100 times larger than the value recently estimated by Chevalier, Fransson & Nymark by modelling the radio data of Chandra et al. (2003) and Stockdale et al. (2004).

Given that the progenitor was probably massive and that the light curves exhibit a significant plateau phase, we conclude that the progenitor of SN 2002hh was a red supergiant as expected for normal type IIP SNe (Popov 1993; Li et al. 2006, and references therein). There is also evidence that a substantial, dusty wind was emitted by the progenitor star and that the mass outflow was ongoing almost up to the epoch of explosion. However, in spite of the progenitor differences between SN 2002hh and SN 1987A, much of their nebular spectroscopic behaviour was remarkably similar.

ACKNOWLEDGMENTS

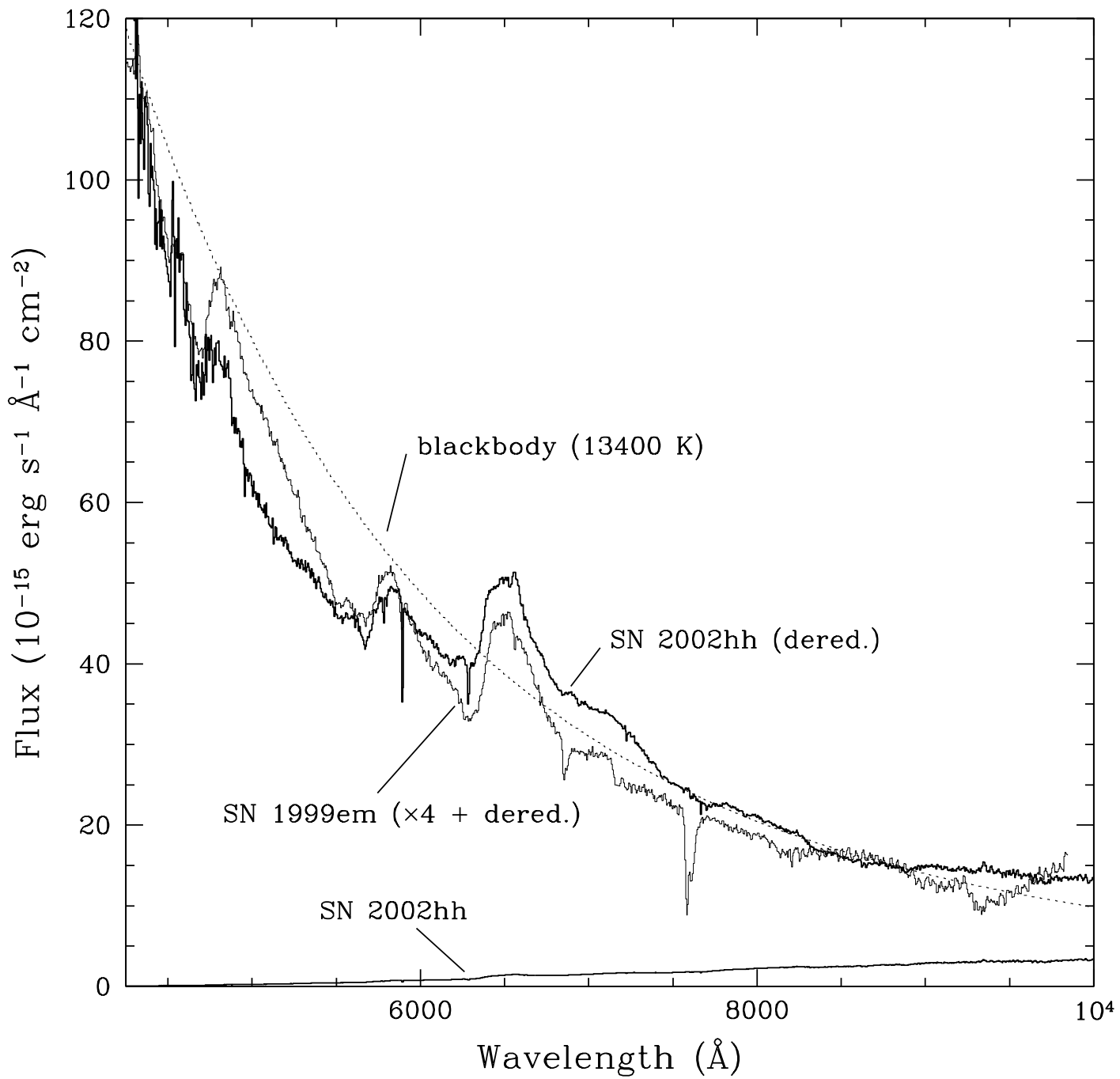
We would like to thank R. Stathakis for having provided us with the SN 1987A optical spectra in digitized format. We are also grateful to M. Gustafsson, P. Jakobsson, J. Melinder and G. Øye for observing and reducing the NOT spectrum of SN 2002hh; and to R. Chornock, S. Jha, M. Papenkova, B. Swift and D. Weisz for help with the Lick and Keck/ESI SN 2002hh spectroscopy. This work is based on observations collected at the William Herschel Telescope (WHT, La Palma), the Nordic Optical Telescope (NOT, La Palma), the Infrared Telescope Facility (IRTF, Hawaii), the Keck Telescope (Hawaii), and the Shane Telescope (Lick Observatory, CA). The WHT is operated on the island of La Palma by the Isaac Newton Group (ING) in the Spanish Observatorio del Roque de los Muchachos of the Instituto de Astrofísica de Canarias. The NOT is operated on the island of La Palma jointly by Denmark, Finland, Iceland, Norway, and Sweden, in the Spanish Observatorio del Roque de los Muchachos of the Instituto de Astrofísica de Canarias. IRTF is operated on behalf of NASA by the University of Hawaii. The W. M. Keck Observatory is operated as a scientific partnership among the California Institute of Technology, the University of California, and NASA; the Observatory was made possible by the generous financial support of the W. M. Keck Foundation. Lick Observatory is operated by the Univer-

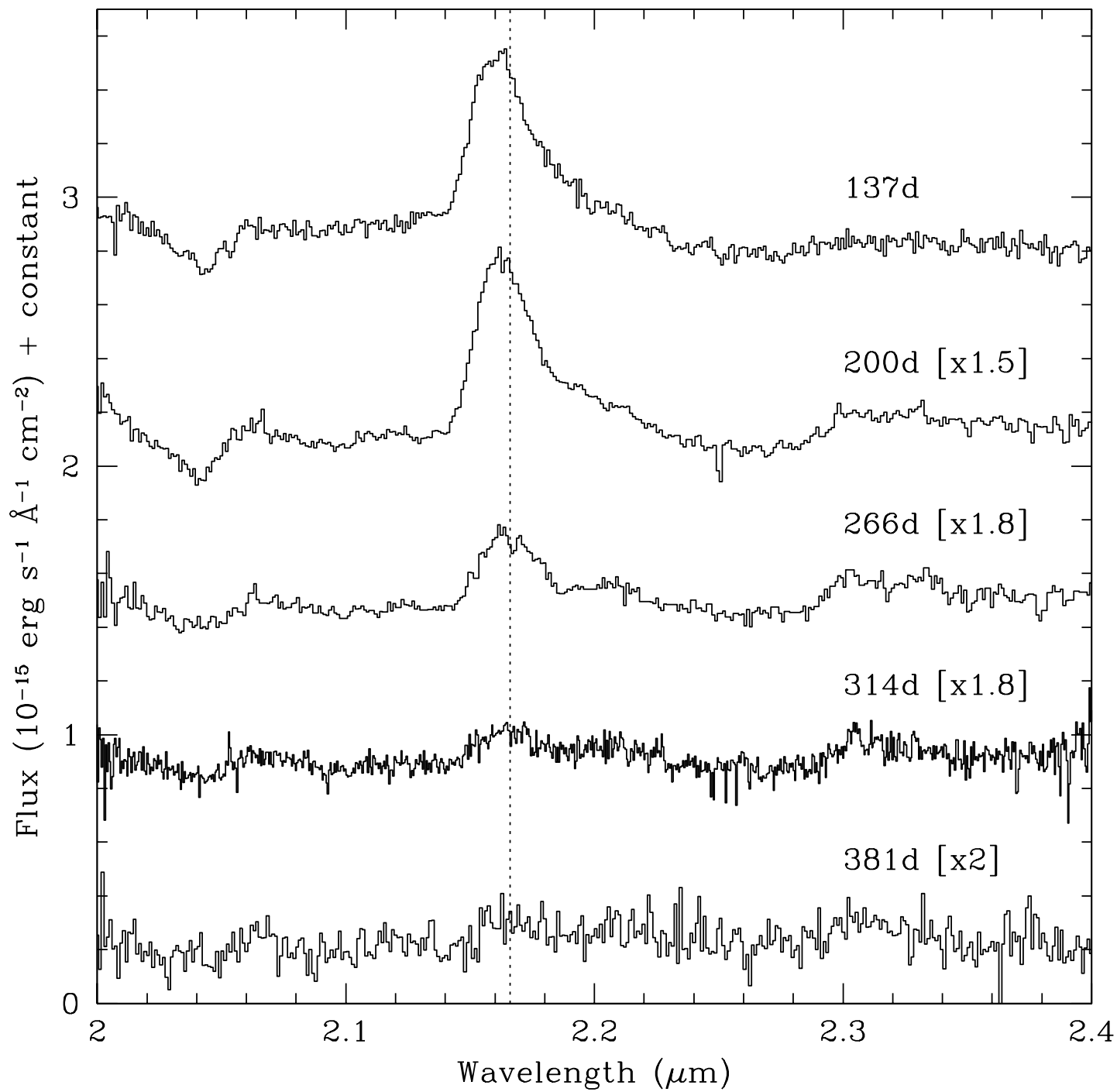
sity of California. KAIT was made possible by generous donations from Sun Microsystems, Inc., the Hewlett-Packard Company, AutoScope Corporation, Lick Observatory, the National Science Foundation (NSF), the University of California, and the Sylvia & Jim Katzman Foundation. MP is supported through PPARC grant PPA/G/S/2001/00512. AVF's group at UC Berkeley is supported by NSF grant AST-0307894.

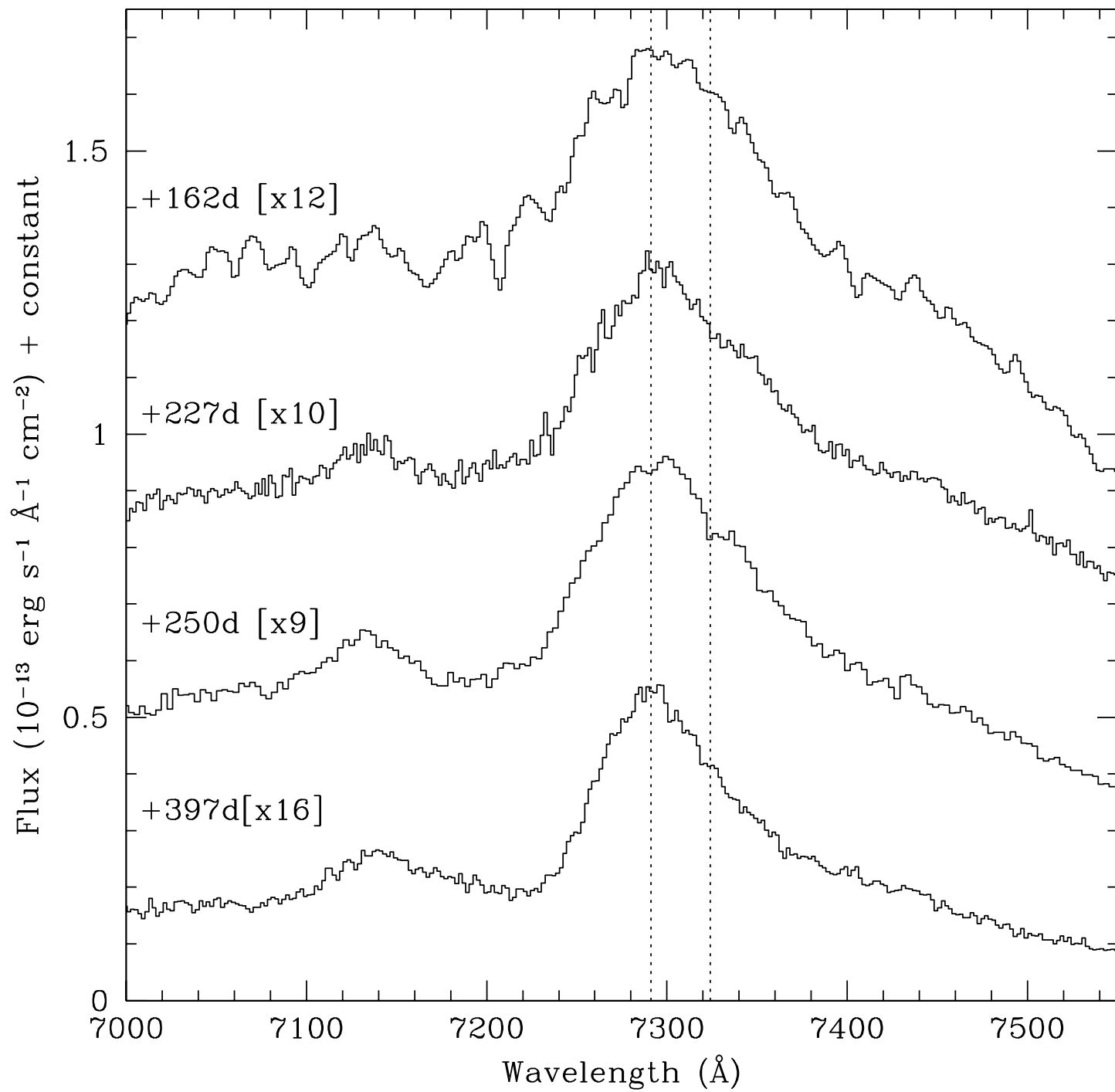
REFERENCES

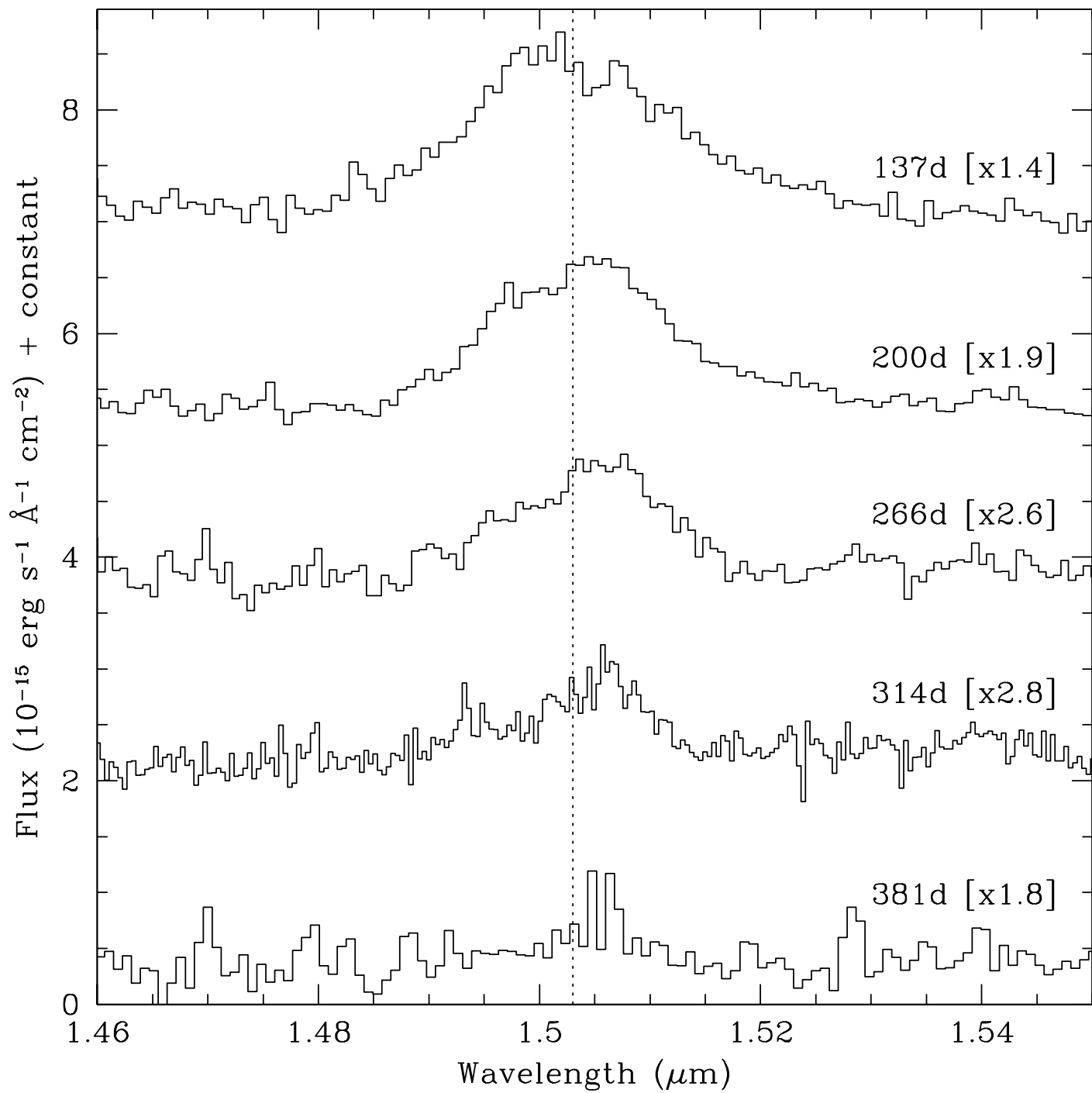
- Arnett W.D., Fu A., 1989, ApJ, 340, 396
 Barlow M., Fabbri J., Meixner M., Sugerman B., 2004, IAU Circ. 8400
 Barlow M.J., et al., 2005, ApJ, 627, L113
 Baron E., et al., 2000, ApJ, 545, 444
 Bersanelli M., Bouchet P., Falomo R., 1991, A&A, 252, 854
 Bessell M.S., 1979, PASP, 91, 589
 Bessell M.S., 1999, PASP, 111, 1426
 Beswick R.J., Fenech D., Thrall H., Argo M.K., Muxlow T.W.B., Pedlar A., 2005, IAU Circ. 8572
 Bode M.F., Evans A., 1980, MNRAS, 193, 21
 Bohlin R.C., Savage B.D., Drake J.F., 1978, ApJ, 224, 132
 Bonnarel F., Boulesteix J., Marcelin M., 1986, A&A, 66, 149
 Bouchet P., Danziger I.J., 1993, A&A, 273, 45
 Bouchet P., Danziger I.J., Lucy L.B., 1991, AJ, 102, 1135
 Bouchet P., Slezak E., Le Bertre T., Moneti A., Manfroid J., 1989, A&AS, 80, 379
 Cardelli J.A., Clayton G.C., Mathis J.S., 1989, ApJ, 345, 245
 Catchpole R.M. et al., 1987, MNRAS, 229, 15
 Catchpole R.M. et al., 1988, MNRAS, 231, 75
 Cernuschi F., Marsicano F., Codina S., 1967, Ann. d'Astr., 30, 1039
 Chandra P., Ray A., Bhatnagar S., 2003, IAU Circ. 8041
 Chevalier R.A., Fransson C., Nymark T.K., 2005, ApJ, in press (astro-ph/0509468).
 Danziger I.J., Lucy L.B., Bouchet P., Gouiffes C., 1991, in *Supernovae*, ed. S.E. Woosley (New York: Springer-Verlag), 69
 Dessart L., Hillier D.J., 2005, A&A, 437, 667
 Draper P.W., Gray N., Berry D.S., 2002, Starlink User Note 214.10
 Dunne L., Eales S., Ivison R., Morgan H., Edmunds M., 2003, Nat, 424, 285
 Dwek E., 1983, ApJ, 274, 175
 Dwek E., 1985, ApJ, 297, 719
 Dwek E., 1998, ApJ, 501, 643
 Elmhamdi A. et al., 2003, MNRAS, 338, 939
 Fassia A., Meikle W.P.S., 1999, MNRAS, 302, 314
 Fassia A., Meikle W.P.S., Geballe T.R., Walton N.A., Pollacco D.L., Rutten R.G.M., Tinney C., 1998, MNRAS, 299, 150
 Fassia A. et al. 2001, MNRAS, 325, 907
 Fassia A., Meikle W.P.S., Spyromilio J., 2002, MNRAS, 332, 296
 Filippenko A.V., 1982, PASP, 94, 715
 Filippenko A.V., 2005, in *The Fate of the Most Massive Stars*, ed. R. Humphreys & K. Stanek (San Francisco: ASP), 33
 Filippenko A.V., Foley R.J., Swift B., 2002, IAU Circ. 8007
 Filippenko A. V., Li W.D., Treffers R.R., Modjaz M., 2001, in *Small Telescope Astronomy on Global Scales*, ed. W.-P. Chen, C. Lemme, and B. Paczyński (San Francisco: ASP), 121
 Filippenko A.V. & Sargent W.L.W., 1989, ApJ, 345, L43
 Gearhart R.A., Wheeler J.C., Swartz D.A., 1999, ApJ, 510, 944
 Gehrz R., 1989, in *Interstellar Dust*, ed. L.J. Allamandola & A.G.G.M. Tielens (Dordrecht: Kluwer), 445
 Gerardy C.L., Fesen R.A., Höflich P., Wheeler J.C., 2000, AJ, 119, 2968

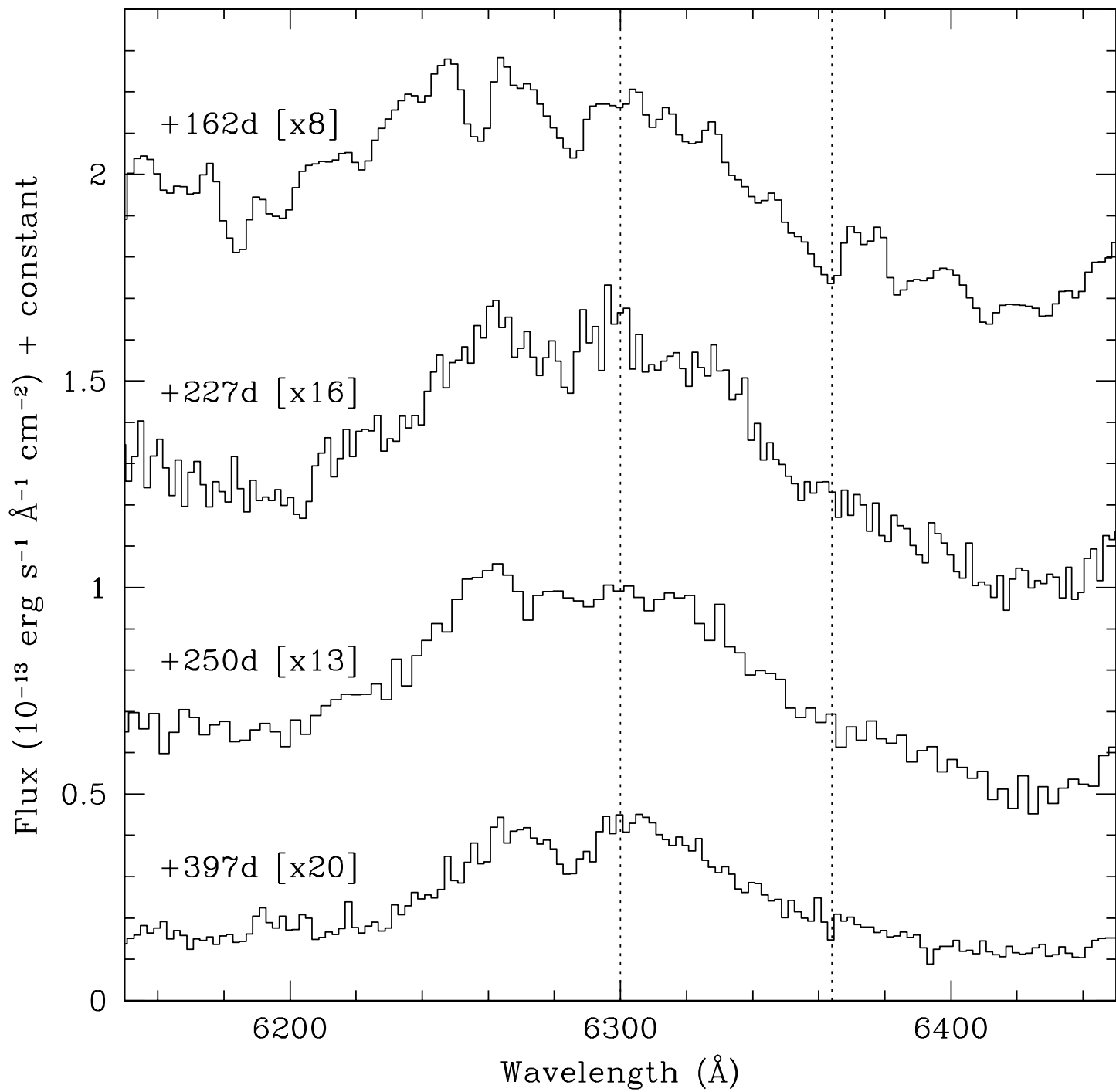
- Gerardy C.L., Fesen R.A., Nomoto K., Maeda K., Höflich P., Wheeler C., 2002, *PASJ*, 54, 905
- Graham J.R., 1988, *ApJ*, 335, L53
- Graham J.R., Meikle W.P.S., 1986, *MNRAS*, 221, 789
- Hamuy M., Suntzeff N.B., Gonzales R., Martin G., 1988, *AJ*, 95, 63
- Hamuy et al., 2001, *ApJ*, 558, 615
- Holwerda B.W., Gonzalez R.A., Allen R.J., van der Kruit P.C., 2005, *AJ*, 129, 1396
- Horne K., 1986, *PASP*, 98, 609
- Hoyle F., Wickramasinghe N.C., 1970, *Nat*, 226, 62
- Karachentsev I.D., Sharina M.E., Huchtmeier W.K., 2000, *A&A*, 362, 544
- Kotak R., Meikle W.P.S., Adamson A., Leggett S.K., 2004, *MNRAS*, 354, L13
- Krause O., Birkmann S.M., Rieke G.H., Lemke D., Klaas U., Hines D.C., Gordon K.D., 2004, *Nat*, 432, 596
- Leonard D.C. et al., 2002a, *PASP*, 114, 35
- Leonard D.C. et al., 2002b, *AJ*, 124, 2490
- Leonard D.C., Kanbur S.M., Ngeow C.C., Tanvir N.R., 2003, *ApJ*, 594, 247
- Li W., 2002, *IAU Circ.* 8005
- Li W. et al. 2000, in *Cosmic Explosions*, ed. S.S. Holt and W.W. Zhang (New York: AIP), 103
- Li W. et al., 2001, *PASP*, 113, 1178
- Li W., Van Dyk S.D., Filippenko A.V., Cuillandre J.-C., 2005, *PASP*, 117, 121
- Li W., Van Dyk S.D., Filippenko A.V., Cuillandre J.-C., Jha S., Bloom J.S., Riess A.G., Livio M., 2006, *ApJ*, in press (astro-ph/0507394).
- Liu W., Dalgarno A., 1995, *ApJ*, 454, 472
- Lucy L.B., Danziger I.J., Gouiffes C., Bouchet P., 1991, in *Supernovae*, ed. S.E. Woosley (New York: Springer-Verlag), 82
- Martos M., Hernandez X., Yáñez M., Moreno E., Pichardo B., 2004, *MNRAS*, 350, L47
- Matheson T. et al., 2000a, *AJ*, 120, 1487
- Matheson T., Filippenko A.V., Ho L.C., Barth A.J., Leonard D.C., 2000b, *AJ*, 120, 1499
- Mattila S., Meikle W.P.S., 2001, *MNRAS*, 324, 325
- Meikle W.P.S., Allen D.A., Spyromilio J., Varani G.-F., 1989, *MNRAS*, 238, 193
- Meikle W.P.S., Spyromilio J., Allen D.A., Varani G.-F., Cumming R.J., 1993, *MNRAS*, 261, 535
- Meikle P., Mattila S., Smartt S., MacDonald E., Clewley L., 2002, *IAU Circ.* 8024
- Meikle P., Fassia A., Geballe T.R., Lundqvist P., Chugai N., Farrah D., Sollerman J., 2003, in *From Twilight to Highlight: The Physics of Supernovae*, ed. W. Hillebrandt & B. Leibundgut (Berlin: Springer-Verlag), 229
- Meikle W.P.S., 2005a, Invited talk given at the National Astronomy Meeting, Birmingham, 2005 April 4-8
- Meikle W.P.S., 2005b, Invited talk given at the 206th American Astronomical Society Meeting, Minneapolis, 2005 May 29 - June 2, 28.09
- Miller S., Tennyson J., Lepp S., Dalgarno A., 1992, *Nat*, 355, 420
- Miller J. S., Stone R.P.S., 1993, *Lick Obs. Tech. Rep. No. 66* (Santa Cruz, CA: Lick Obs.)
- Milne P.A., Wells L.A., 2003, *AJ*, 125, 181
- Munari U., Zwitter T., 1997, *A&A*, 318, 269
- Nozawa T., Kozasa T., Umeda H., Maeda K., Nomoto K., 2003, *ApJ*, 598, 785
- Oke J.B. et al., 1995, *PASP*, 107, 375
- Patat F., 2005, *MNRAS*, 357, 1161
- Pooley D., Lewin W.H.G., 2002, *IAU Circ.* 8024
- Popov D.V., 1993, *ApJ*, 414, 712
- Pozzo M., Meikle W.P.S., Fassia A., Geballe T., Lundqvist P., Chugai N.N., Sollerman J., 2004, *MNRAS*, 352, 457
- Press W. H., Teukolsky S. A., Vetterling W. T., Flannery B. P., 1992, *Numerical Recipes*, 2nd edn. (Cambridge: Cambridge University Press)
- Rayner J.T., Toomey D.W., Onaka P.M., Denault A.J., Stahlberger W.E., Vacca W.D., Cushing M.C., Wang S., 2003, *PASP*, 115, 362
- Romaniello M., Salaris M., Cassisi S., Panagia N., 2000, *ApJ*, 530, 738
- Romaniello M., Panagia N., Scuderi S., Kirshner R.P., 2002, *AJ*, 123, 915
- Schlegel D.J., Finkbeiner D.P., Davis M., 1998, *ApJ*, 500, 525
- Sheinis A.I., Bolte M., Epps H.W., Kibrick R.I., Miller J.S., Radovan M.V., Bigelow B.C., Sutin B.M., 2002, *PASP*, 114, 851
- Shortridge K., 1991, FIGARO General Data Reduction and Analysis Starlink MUD, RAL, June 1991
- Spyromilio J., Leibundgut B., 1996, *MNRAS*, 283, L89
- Spyromilio J., Meikle W.P.S., Learner R.C.M., Allen D.A., 1988, *Nat*, 334, 327
- Spyromilio J., Meikle W.P.S., Learner R.C.M., Allen D.A., 1989, in 22nd ESLAB Symp. on Infrared Spectroscopy in Astronomy, ed. B.H. Kaldeich (Noordwijk: ESA Publications Division, ESTEC), 381
- Spyromilio J., Meikle W.P.S., Allen D.A., 1990, *MNRAS*, 242, 669
- Spyromilio J., Stathakis R.A., Cannon R.D., Waterman L., Couch W.J., Dopita M.A., 1991, *MNRAS*, 248, 465
- Spyromilio J., Stathakis R.A., Meurer G.R., 1993, *MNRAS*, 263, 530
- Spyromilio J., Leibundgut B., Gilmozzi R., 2001, *A&A*, 376, 188
- Stathakis R.A., 1996, PhD Thesis University of Sydney
- Stockdale C.J., et al., 2002, *IAU Circ.* 8018
- Stockdale C.J., Sramek R.A., Rupen M., Weiler K.W., Van Dyk S.D., Panagia N., 2004, <http://rsd-www.nrl.navy.mil/7213/weiler/kwdata/02hhdata.asc>
- Sugerman B., Barlow M., Fabbri J., Meixner M., 2005, in the 205th AAS Meeting, San Diego, CA, 9-13 Jan. 2005
- Suntzeff N.B., Hamuy M., Martin G., Gomez A., Gonzales R., 1988, *AJ*, 96, 1864
- Thielemann F.-K., Nomoto K., Hashimoto M.-A., 1996, *ApJ*, 460, 408
- Tielens A.G.G.M., 1990, in *Submillimetre Astronomy*, ed. G.D. Watt & A.S. Webster (Dordrecht: Kluwer), 13
- Todini P., Ferrara A., 2001, *MNRAS*, 325, 726
- Varani G.-F., Meikle W.P.S., Spyromilio J., Allen D.A., 1990, *MNRAS*, 245, 570
- Walsh W., Beck R., Thuma G., Weiss A., Wielebinski R., Dumke M., 2002, *A&A*, 388, 7
- Wang L., 2005, *ApJ*, 635, L33
- Wang J., Hall P.B., Ge J., Li A., Schneider D.P., 2004, *ApJ*, 609, 589
- Weiler K.W., van Dyk S.D., Panagia N., Sramek R.A., 1992, *ApJ*, 398, 248
- Whitelock P.A. et al., 1988, *MNRAS*, 234, 5
- Wooden D.H., 1989, PhD Thesis, Univ. California, Santa Cruz
- Wooden D.H., Rank D.M., Bregman J.D., Witteborn F.C., Tielens A.G.G.M., Cohen M., Pinto P.A., Axelrod T.S., 1993, *ApJS*, 88, 477
- Wooden D.H., 1997, in *Infrared Space Interferometry: Astrophysics & the Study of Earth-Like Planets*, ed. C. Eiroa, et al. (Dordrecht: Kluwer), 133
- Woosley S.E., 1988, *ApJ*, 330, 218
- Woosley S.E., Weaver T.A., 1995, *ApJS*, 101, 181

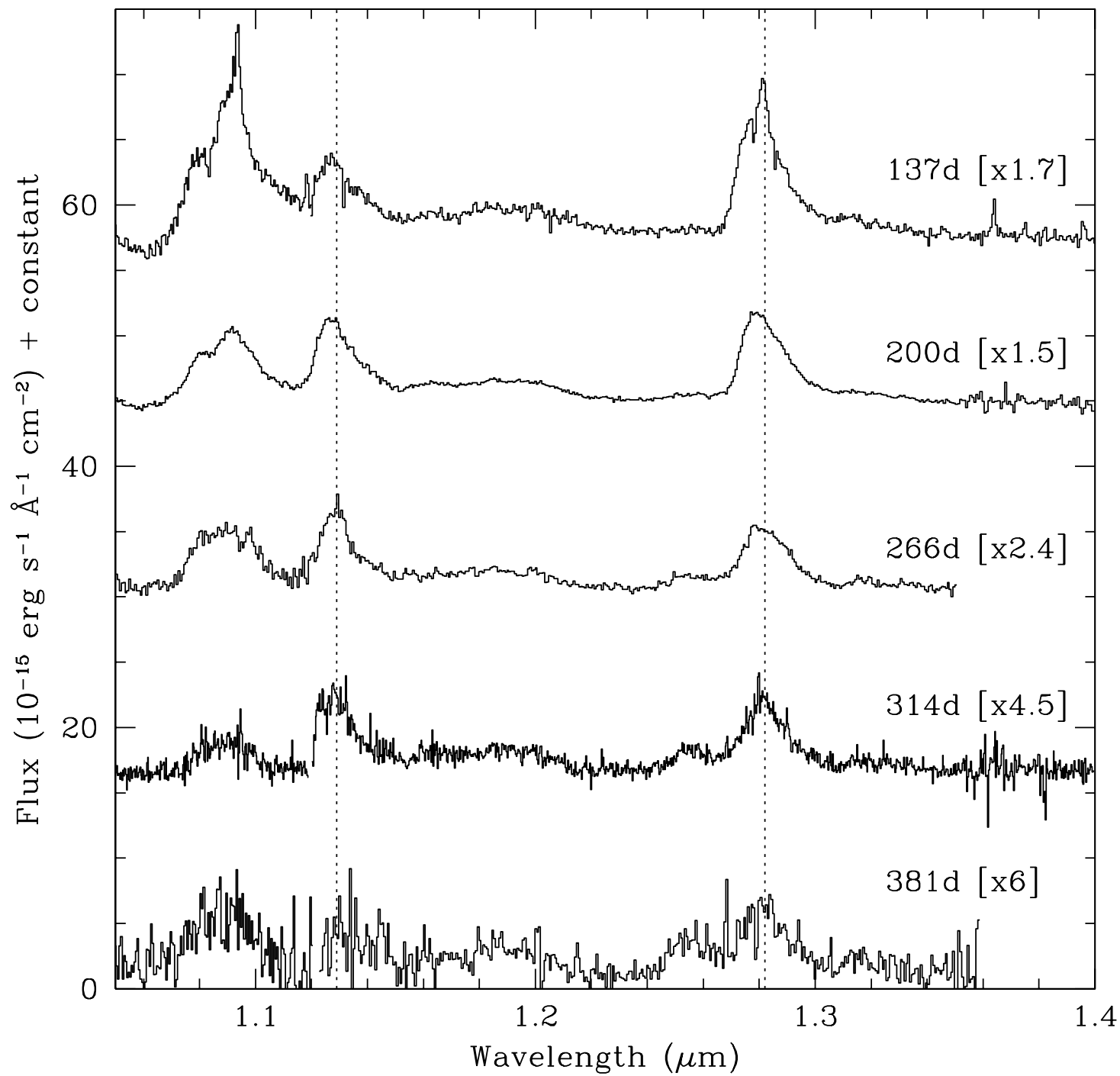


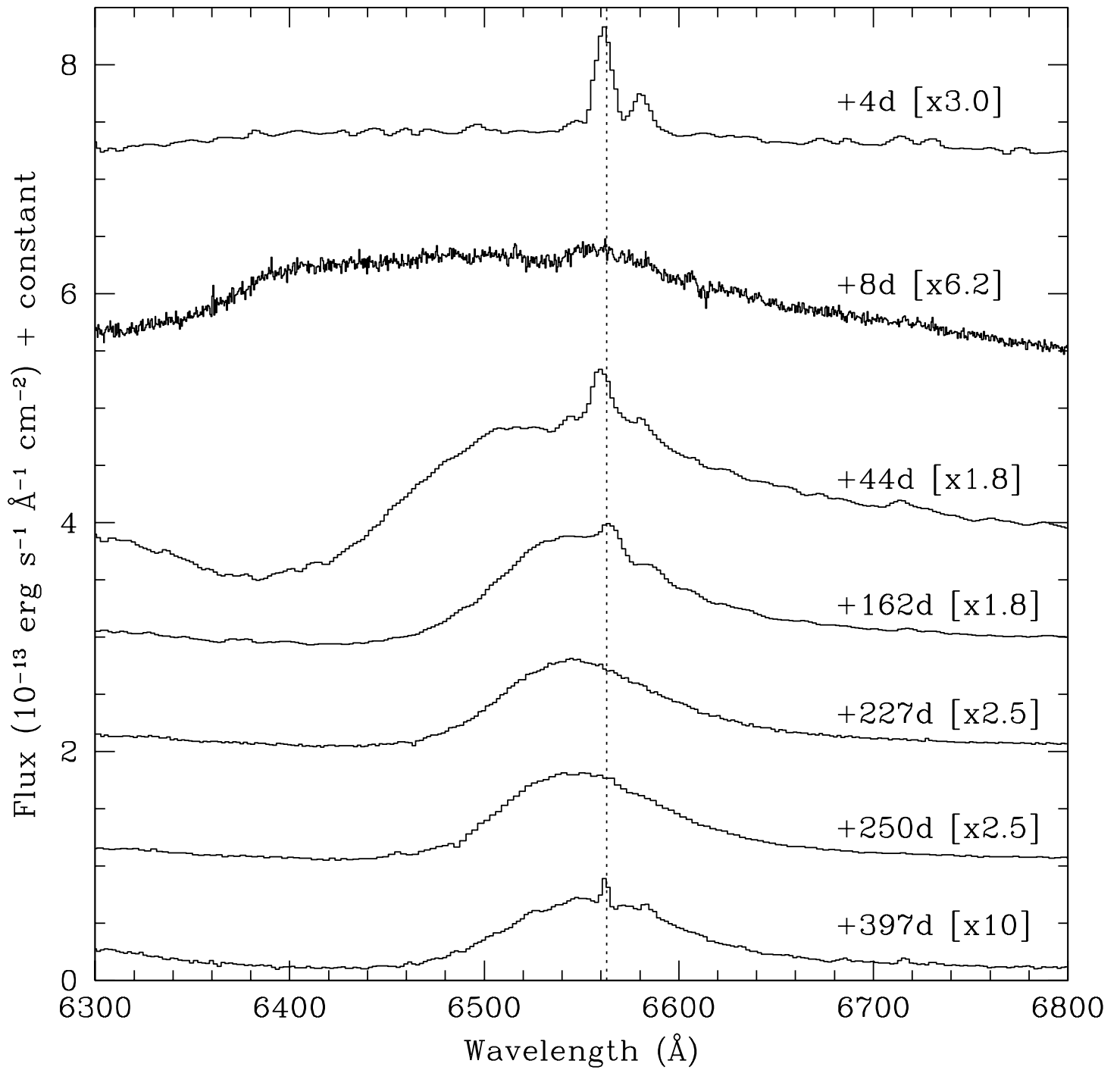


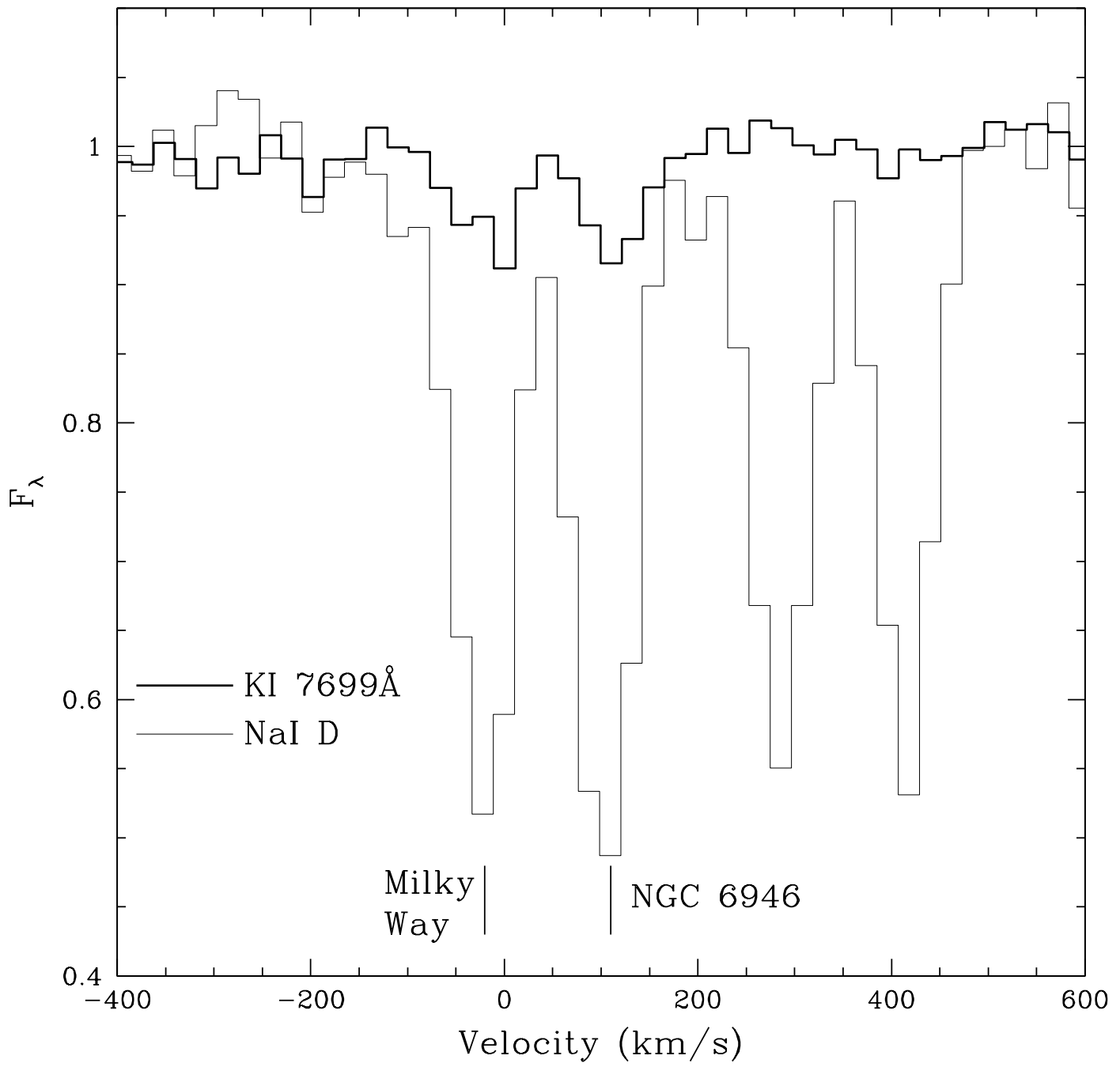


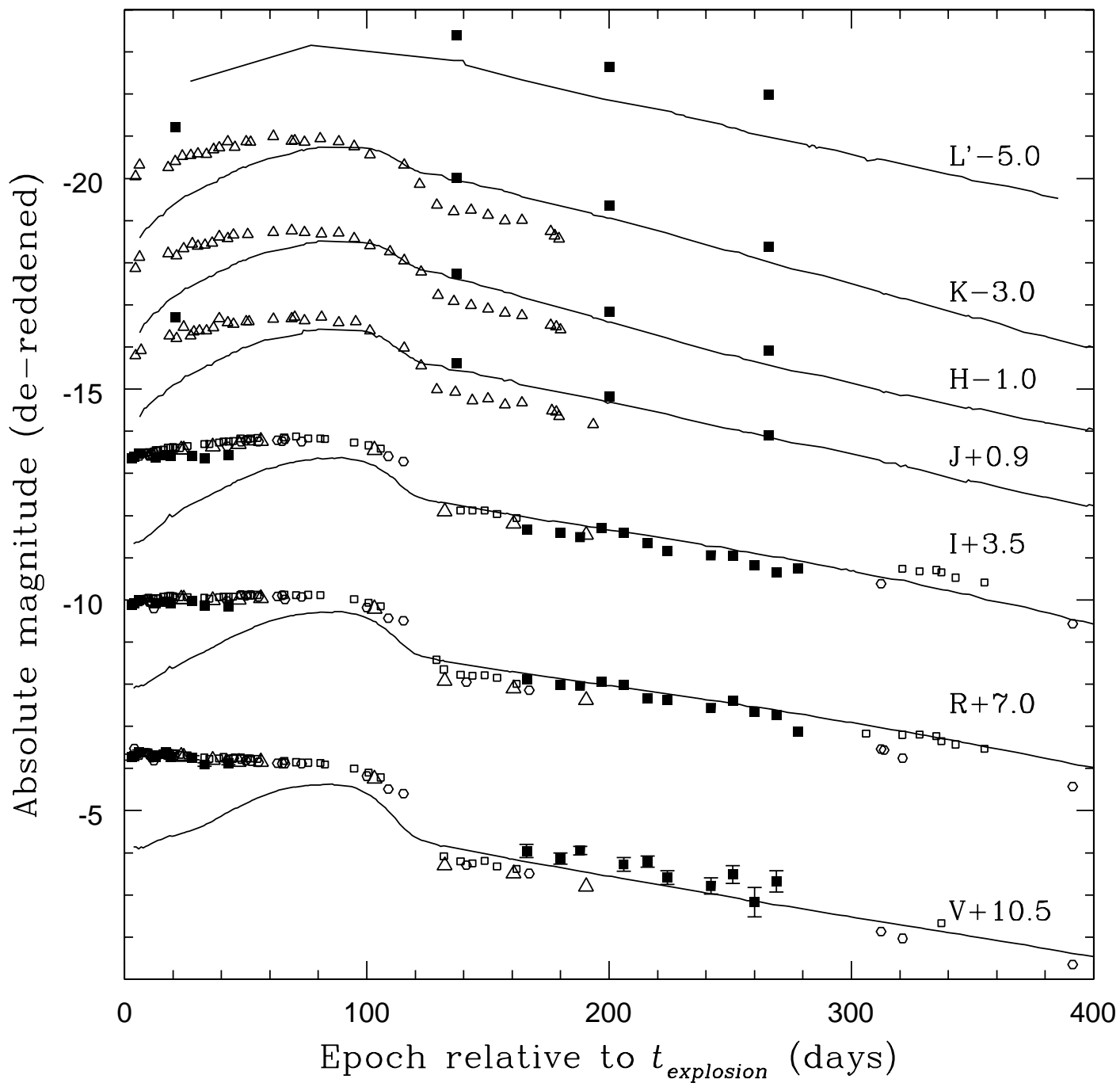


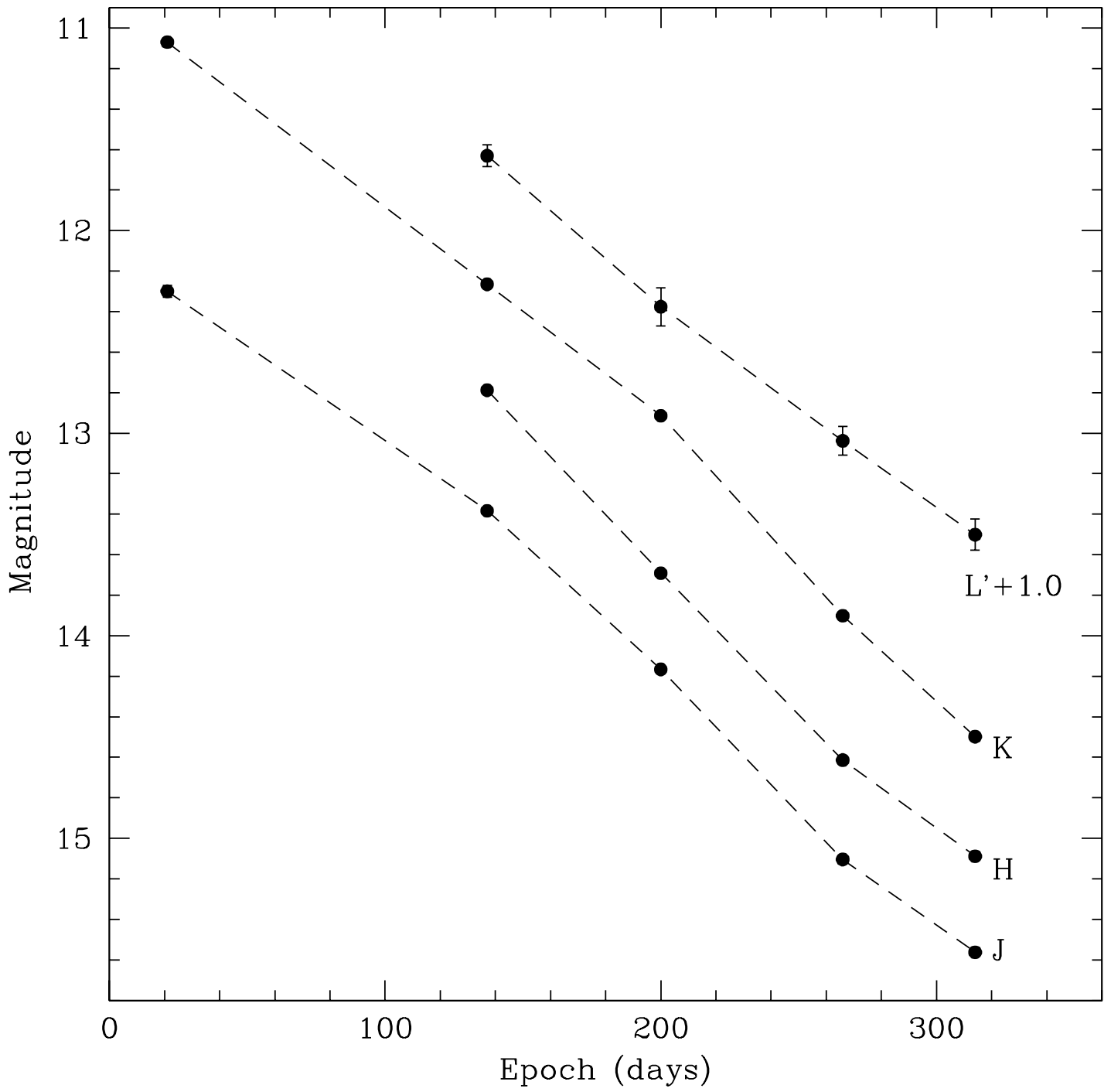


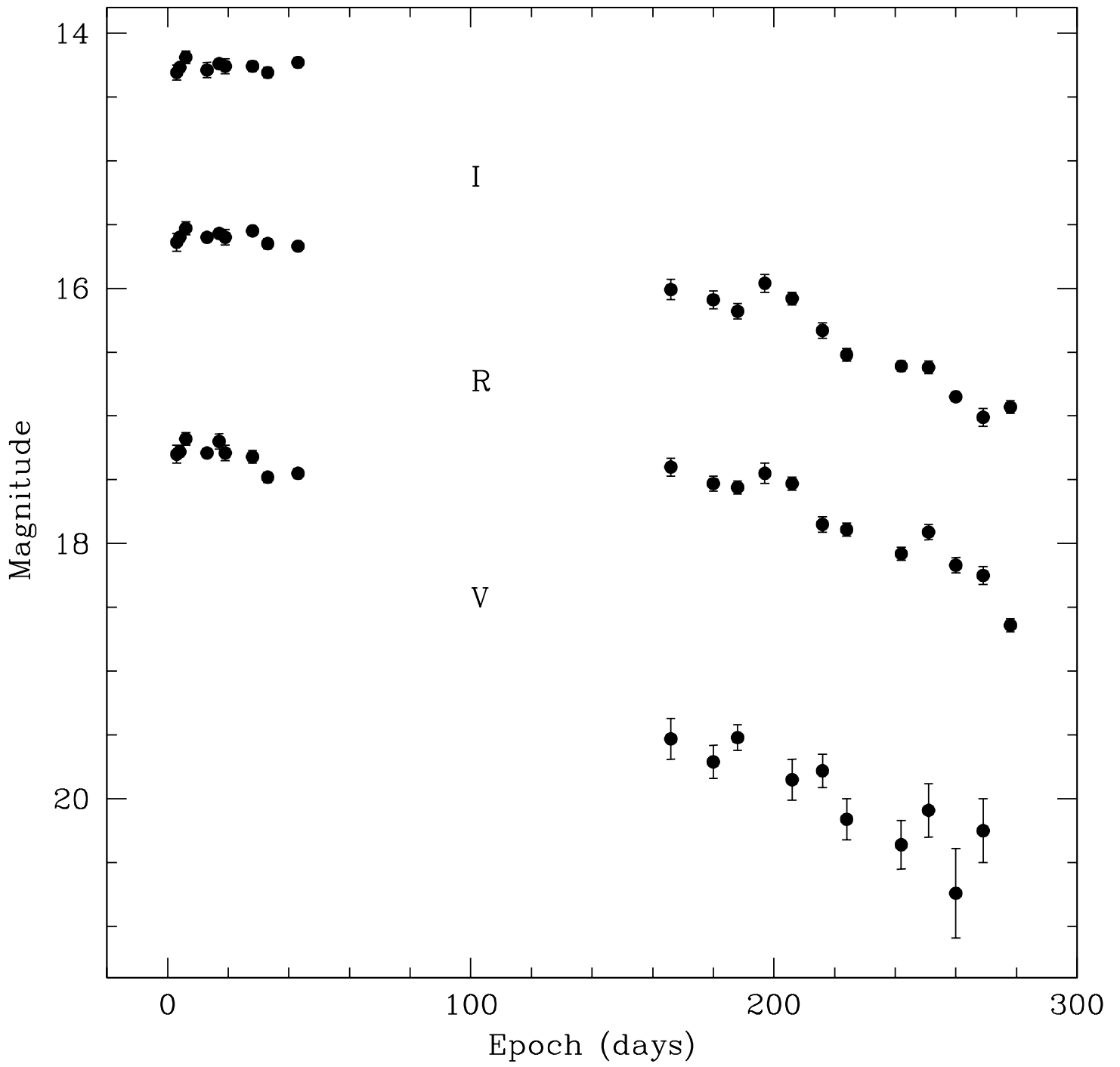


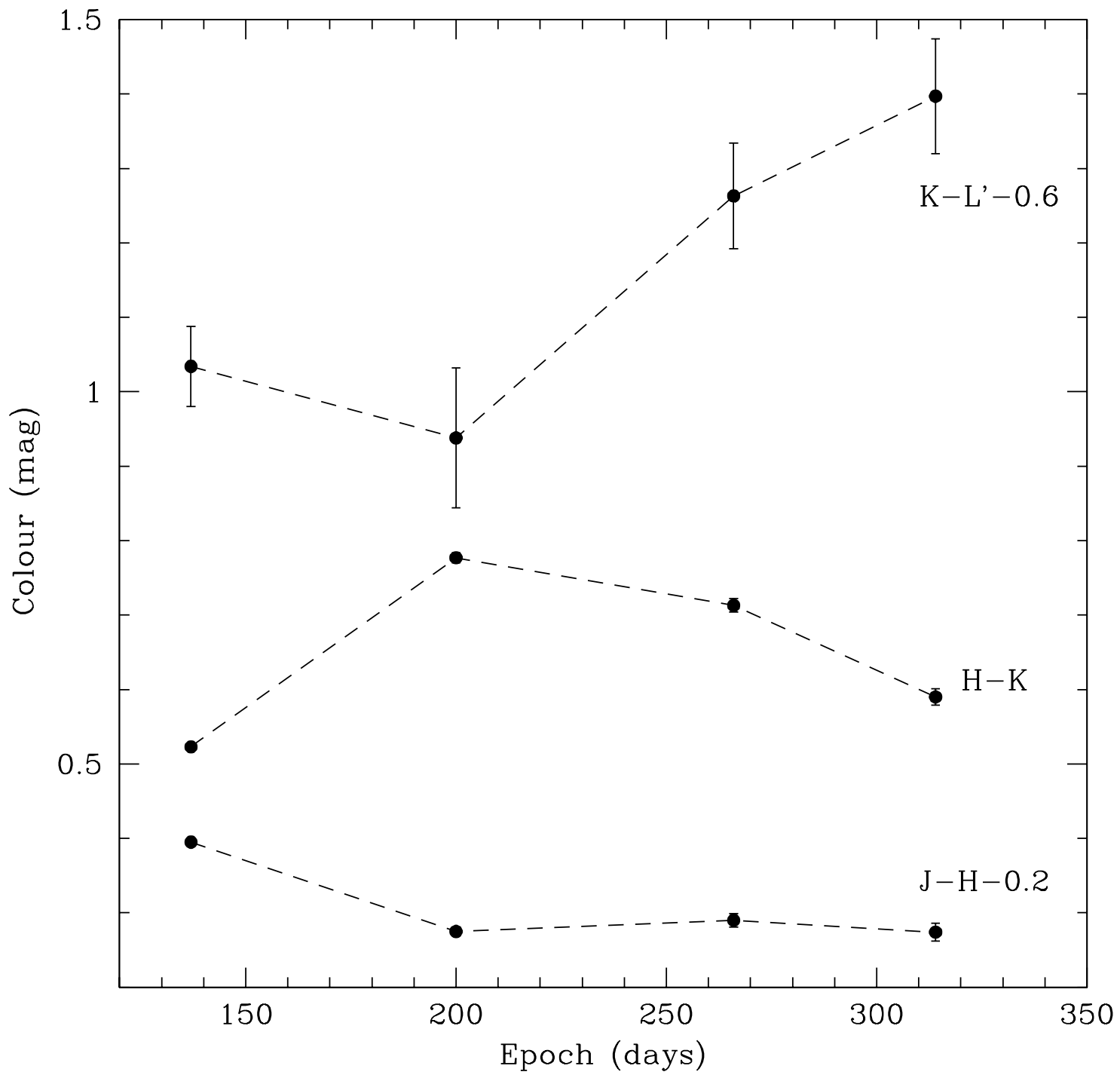


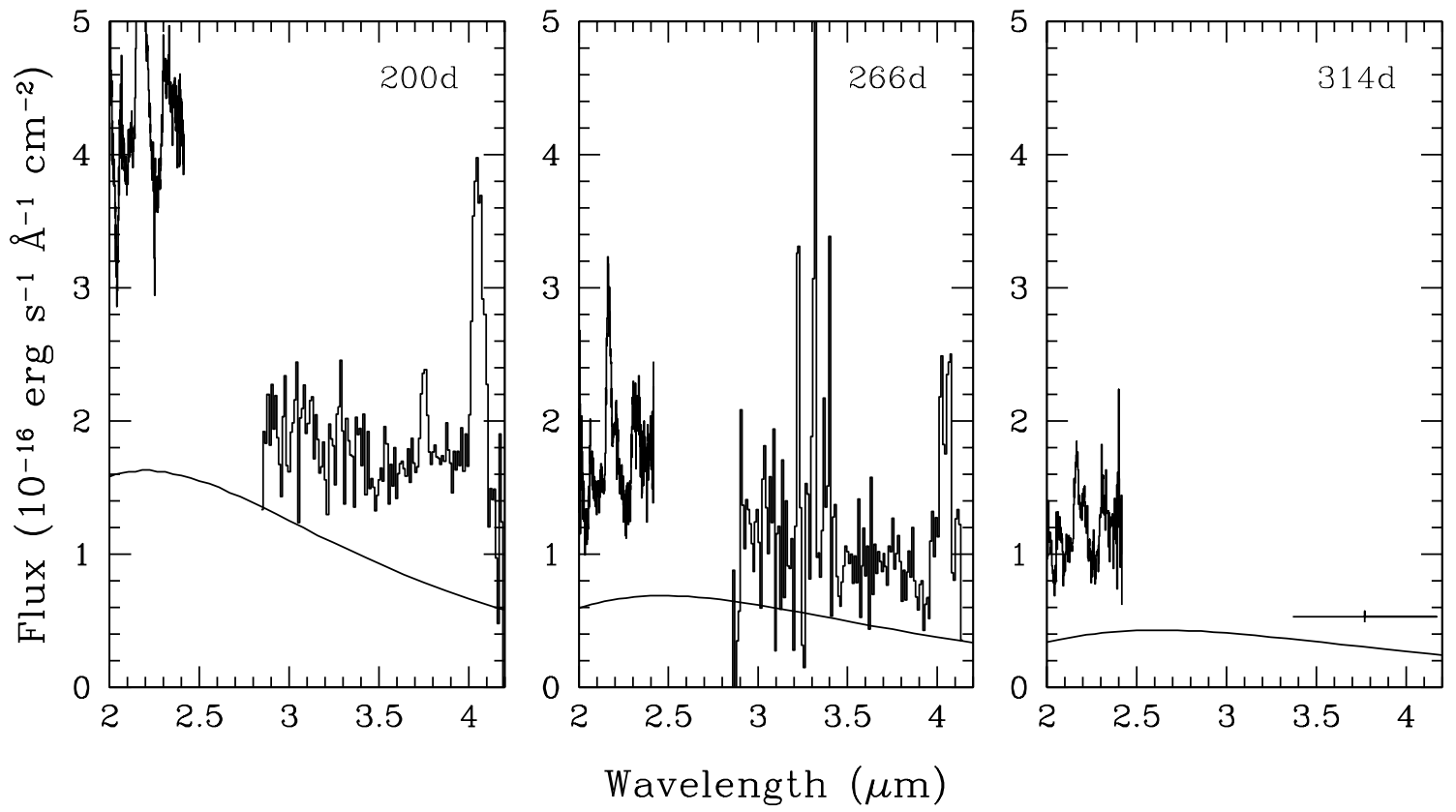


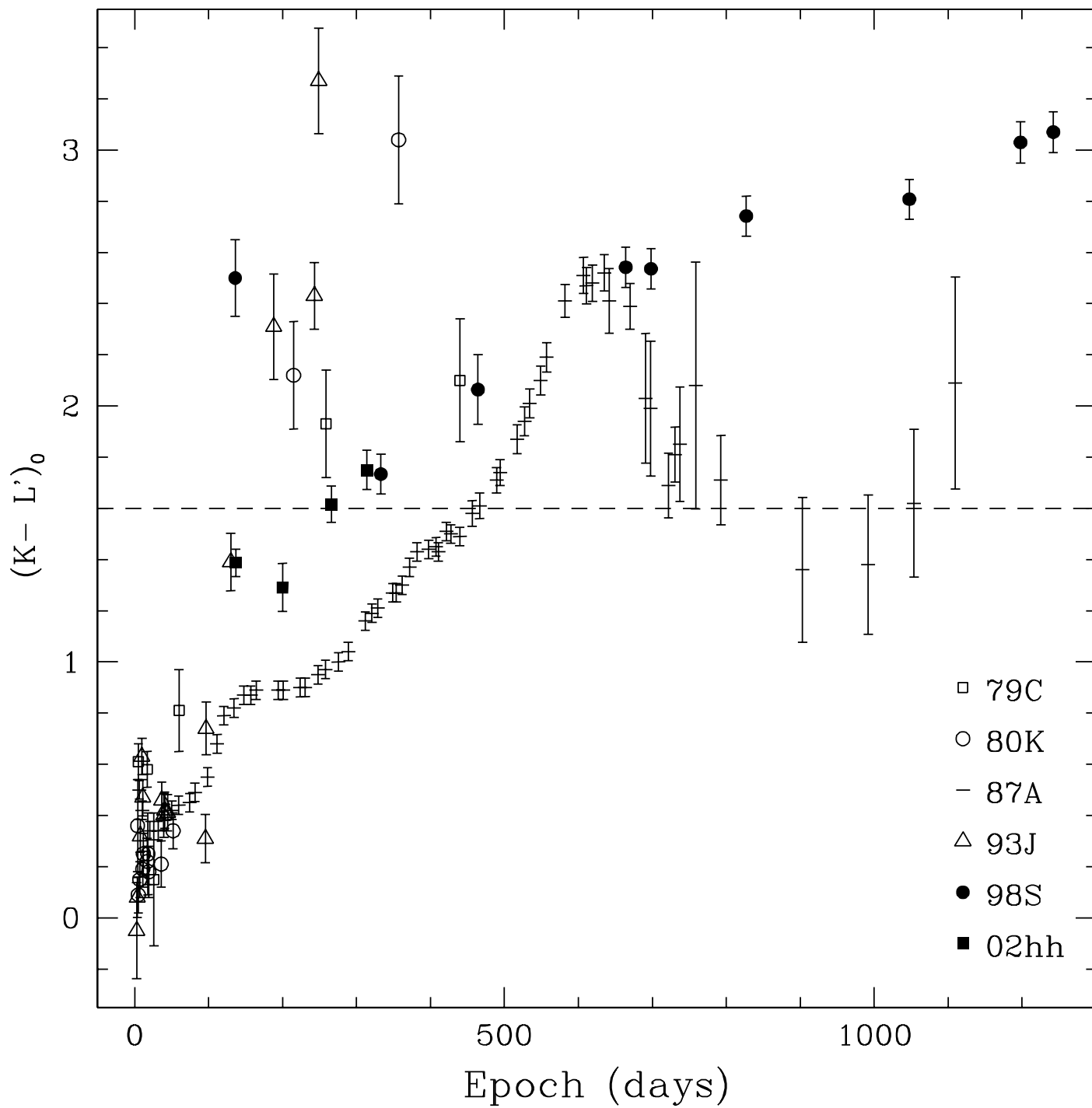


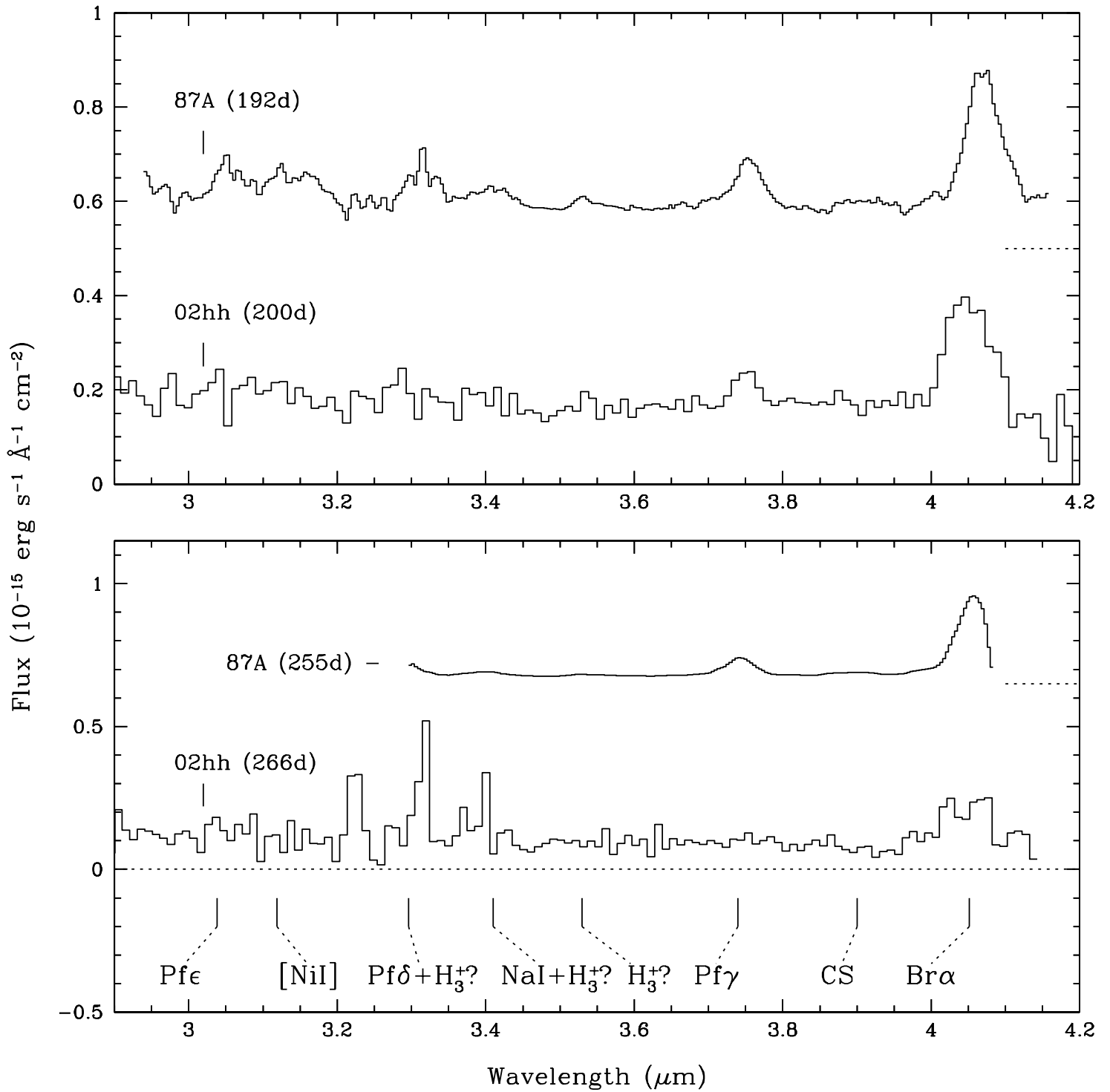


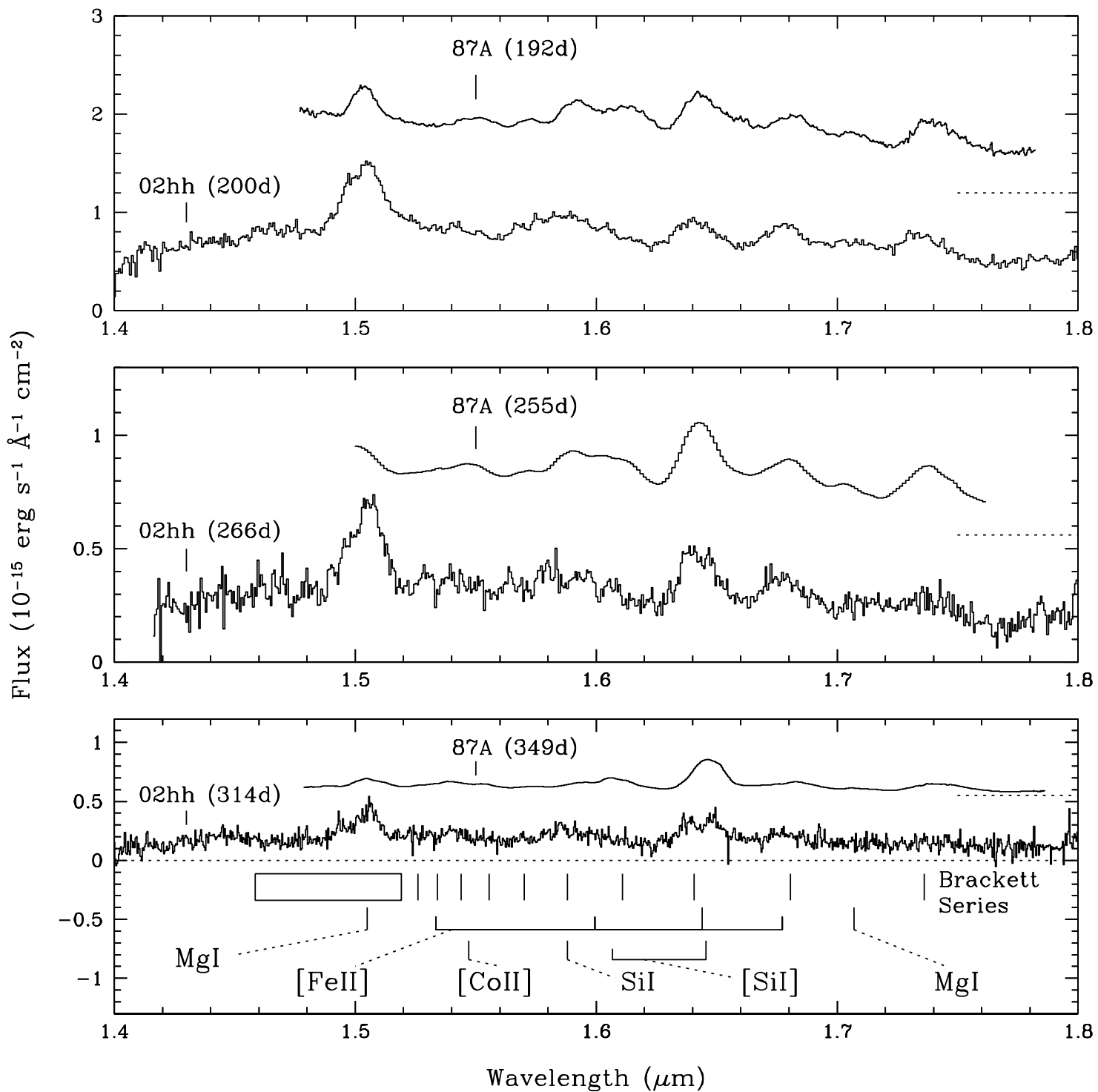


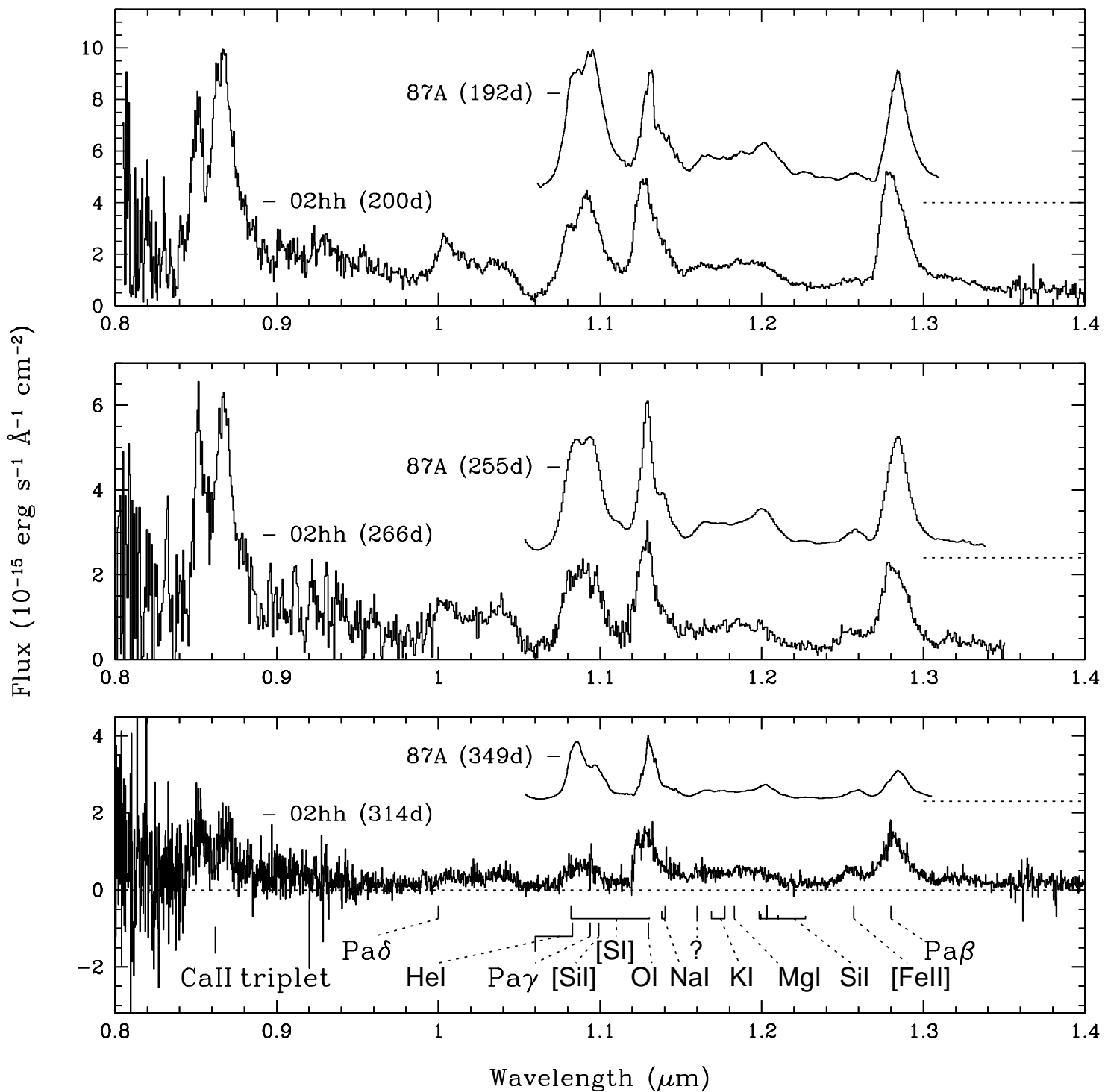


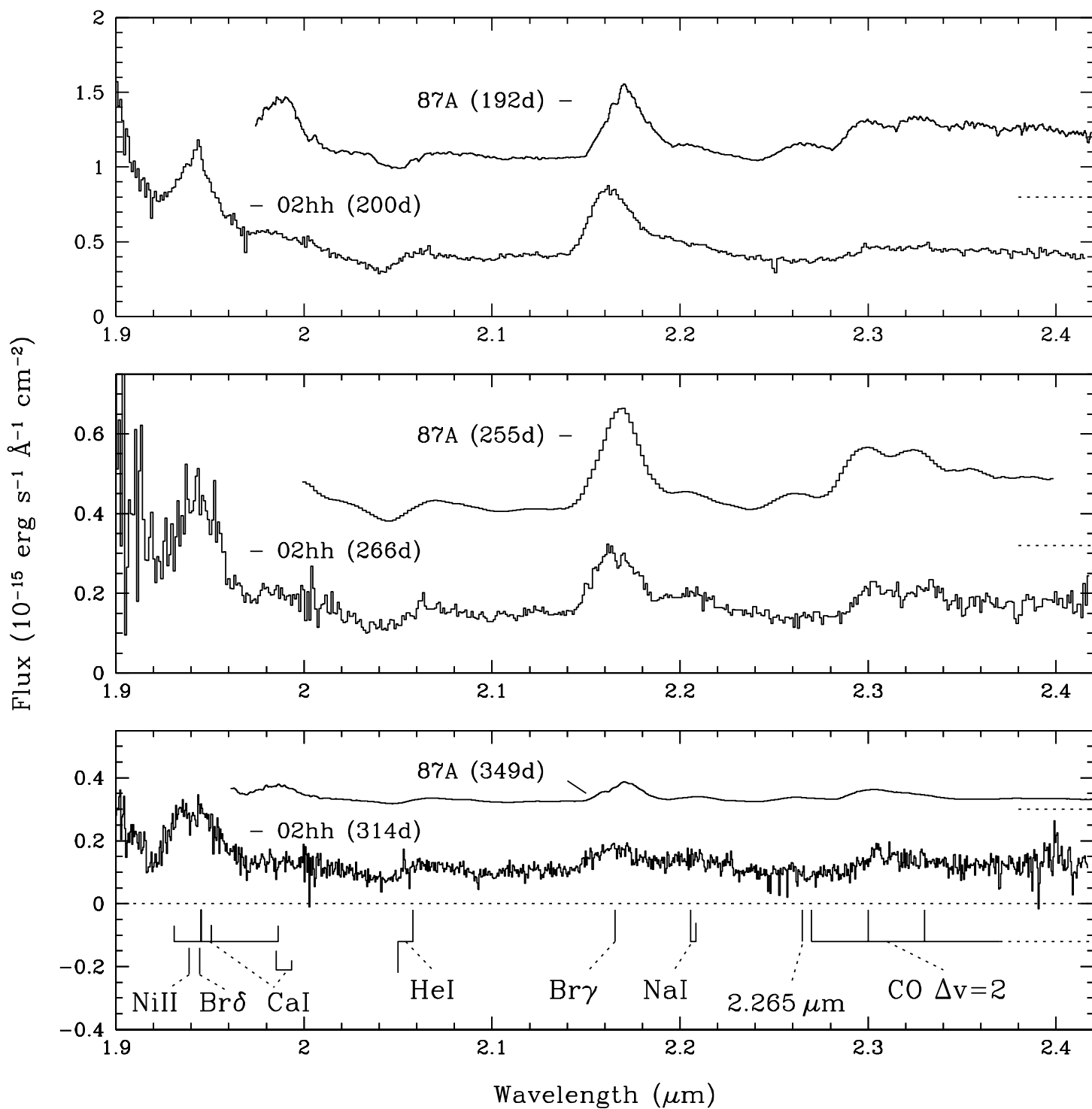


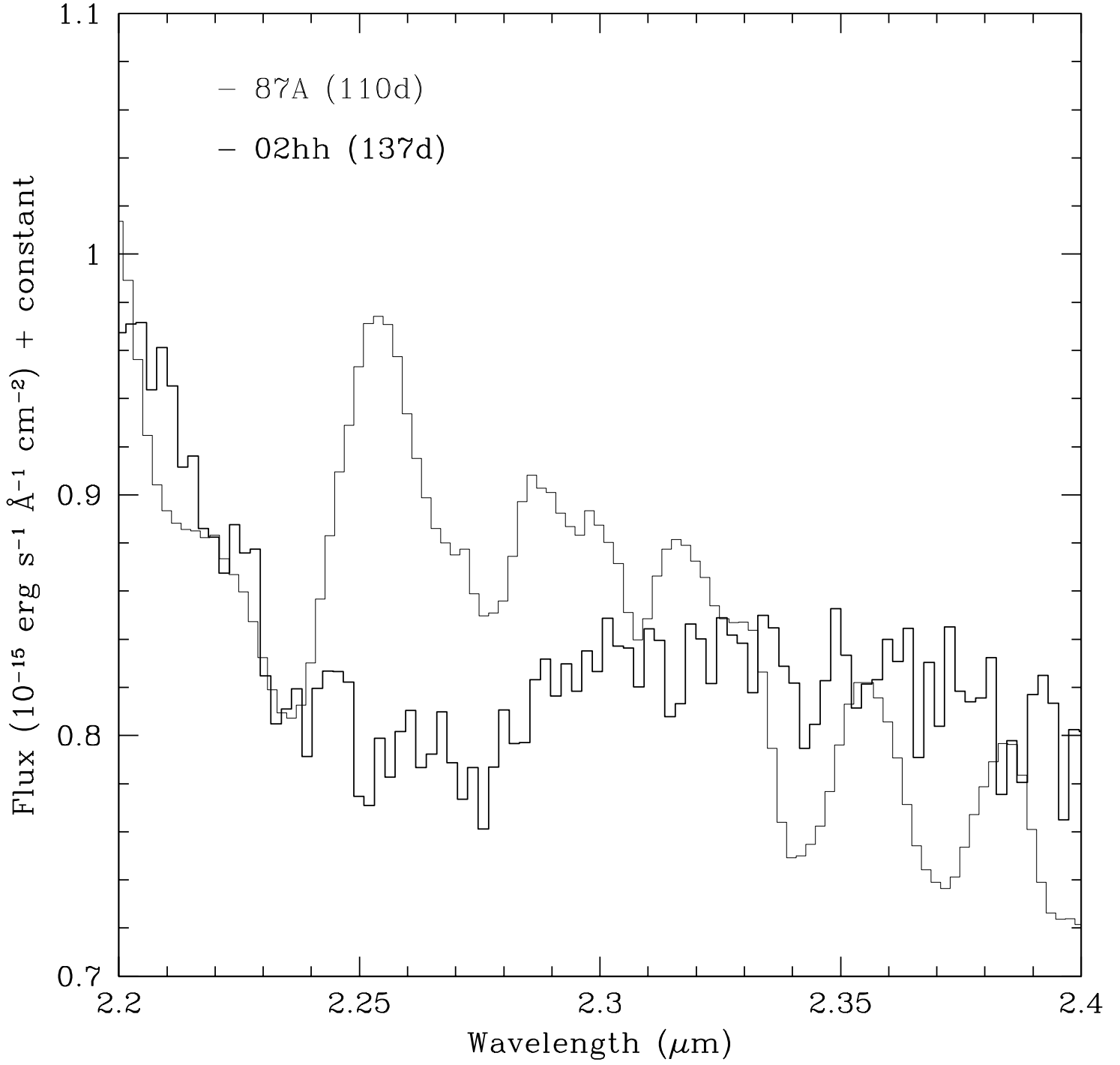


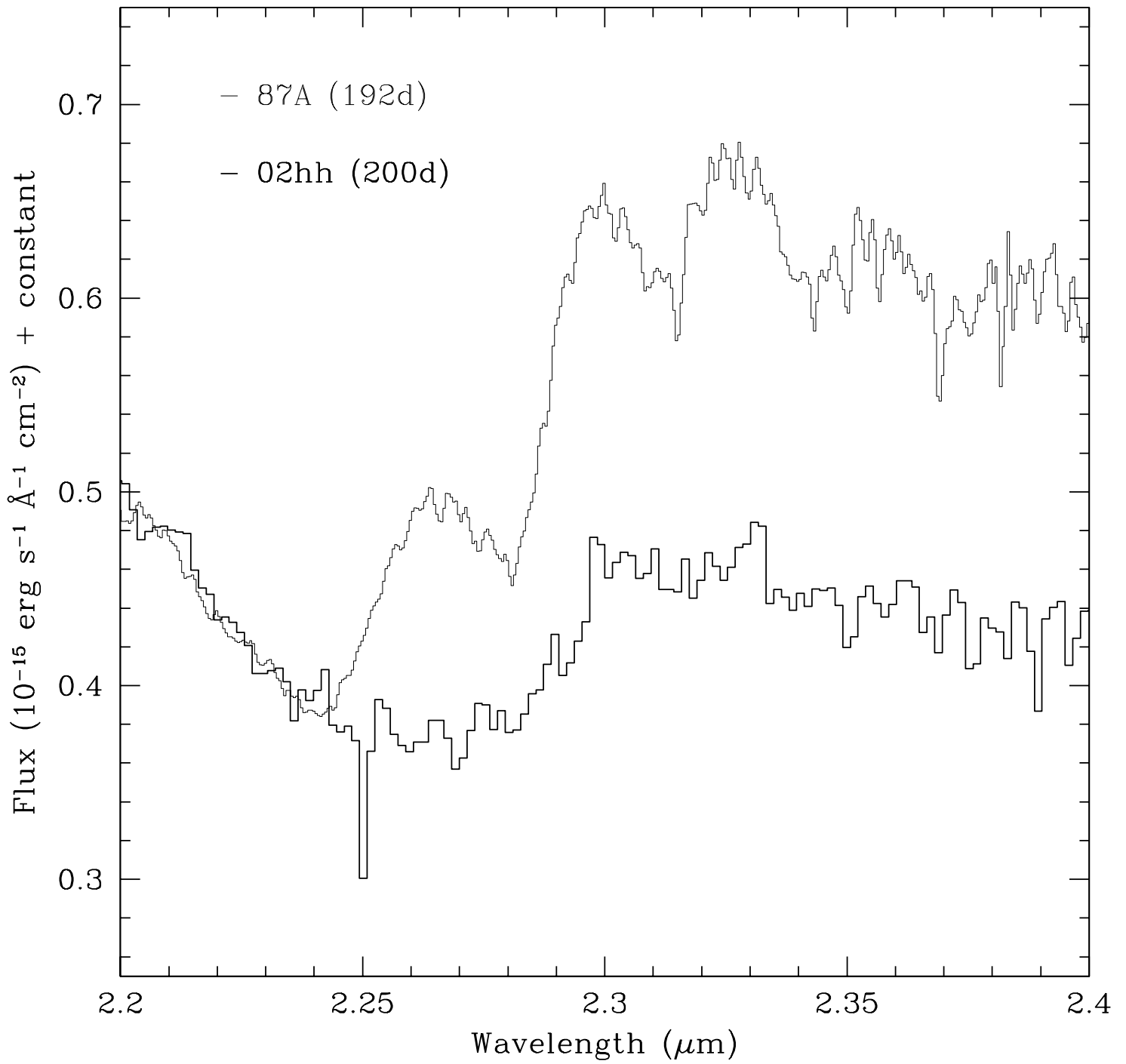


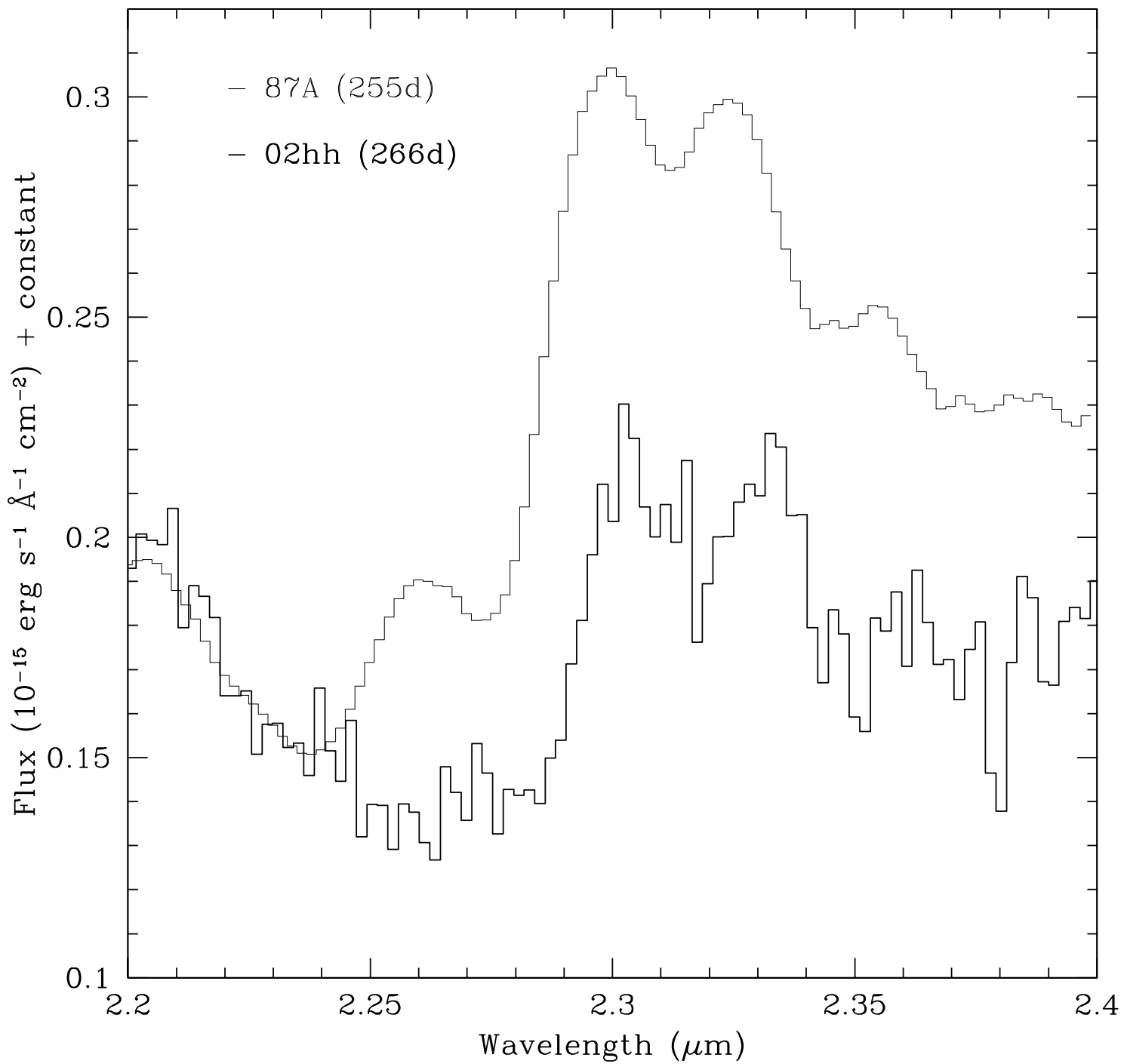


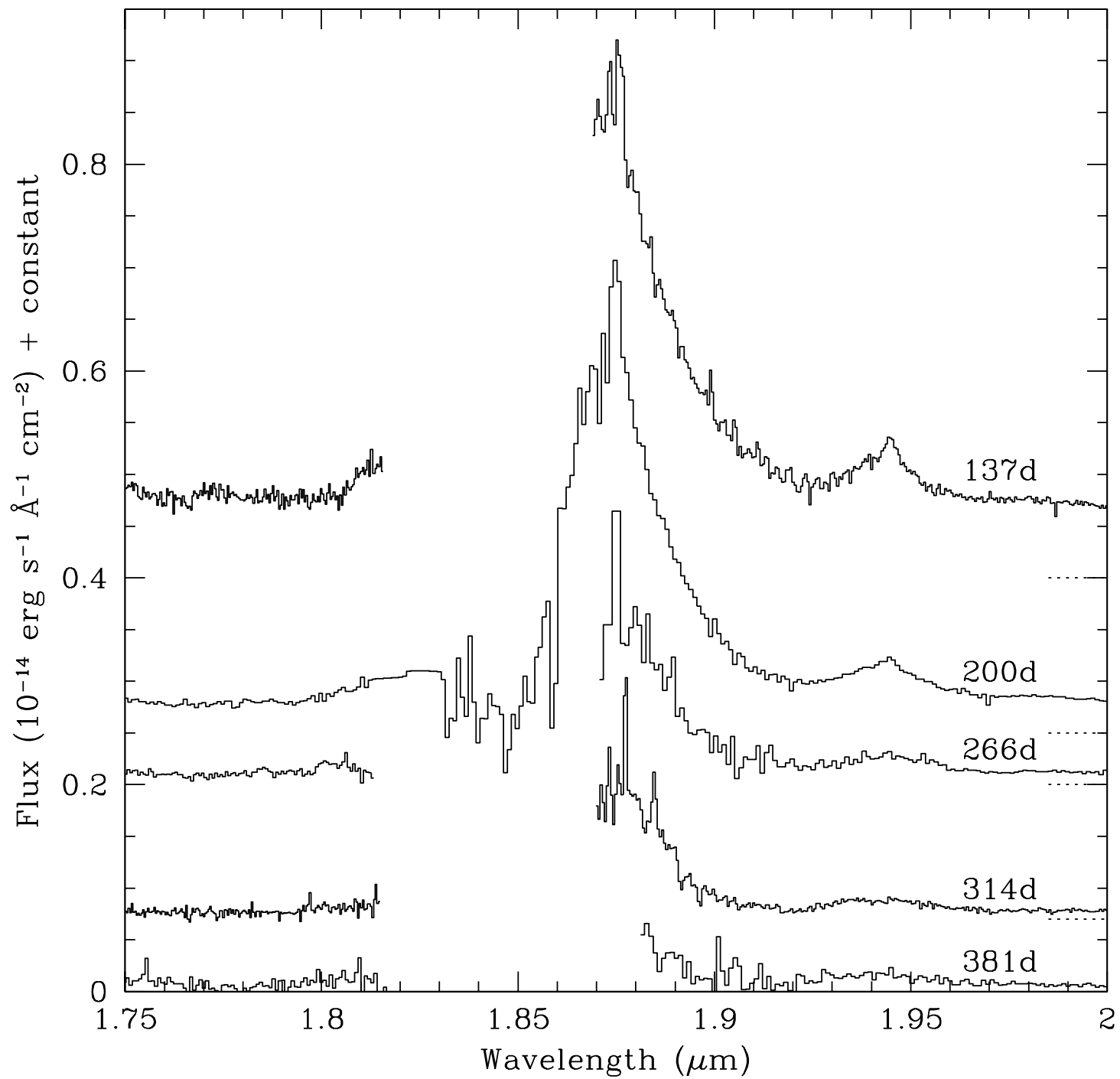


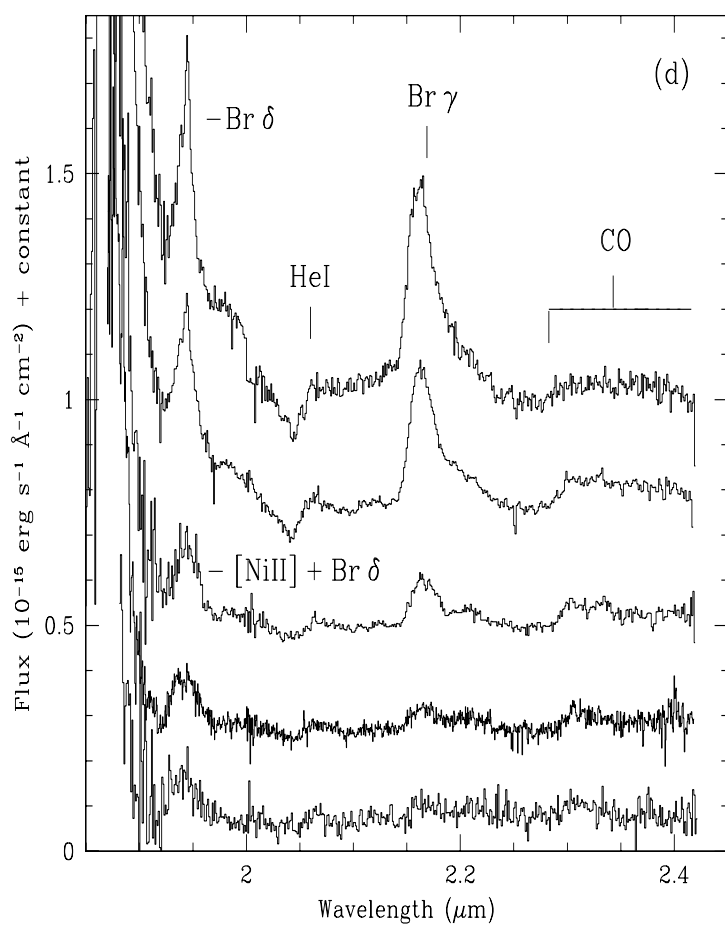
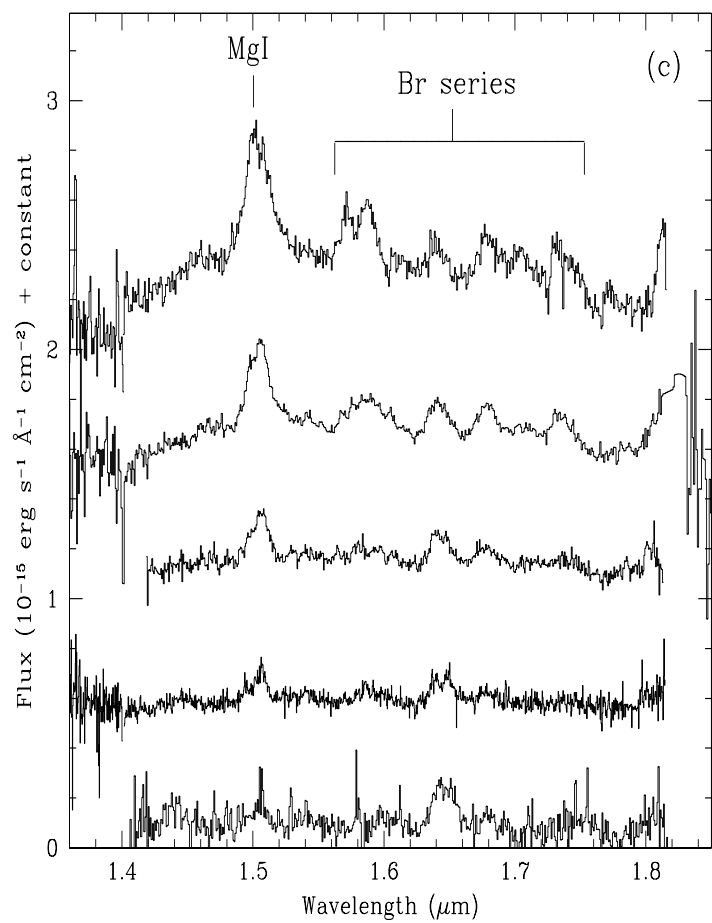
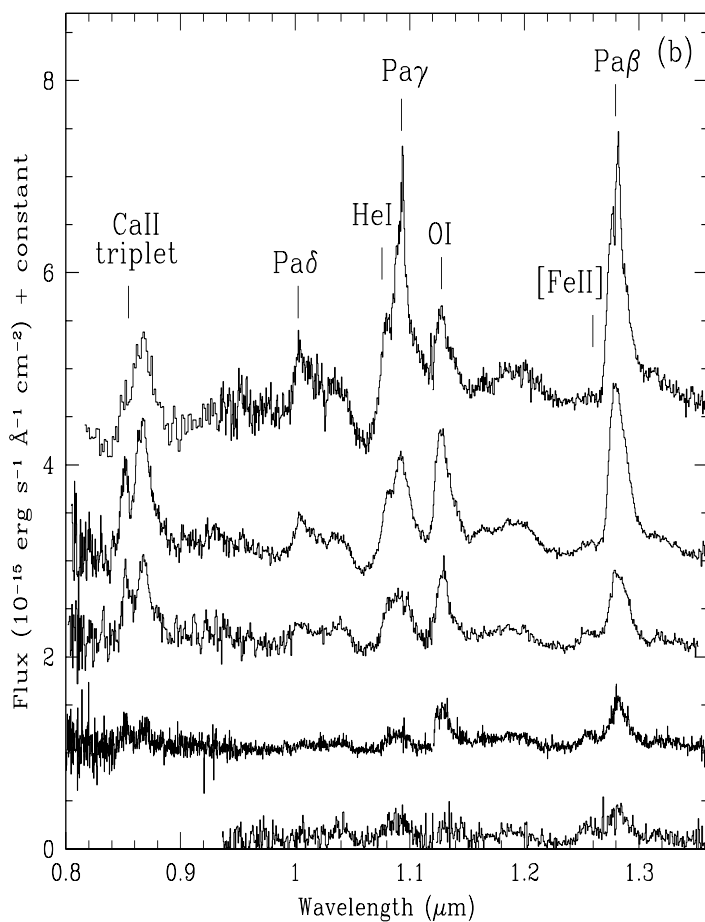
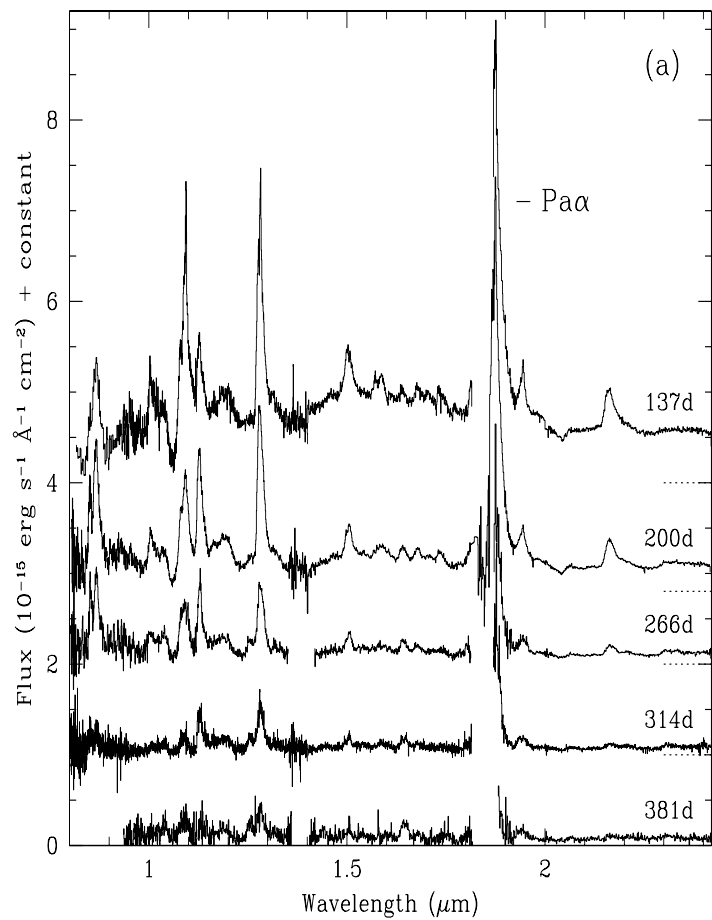


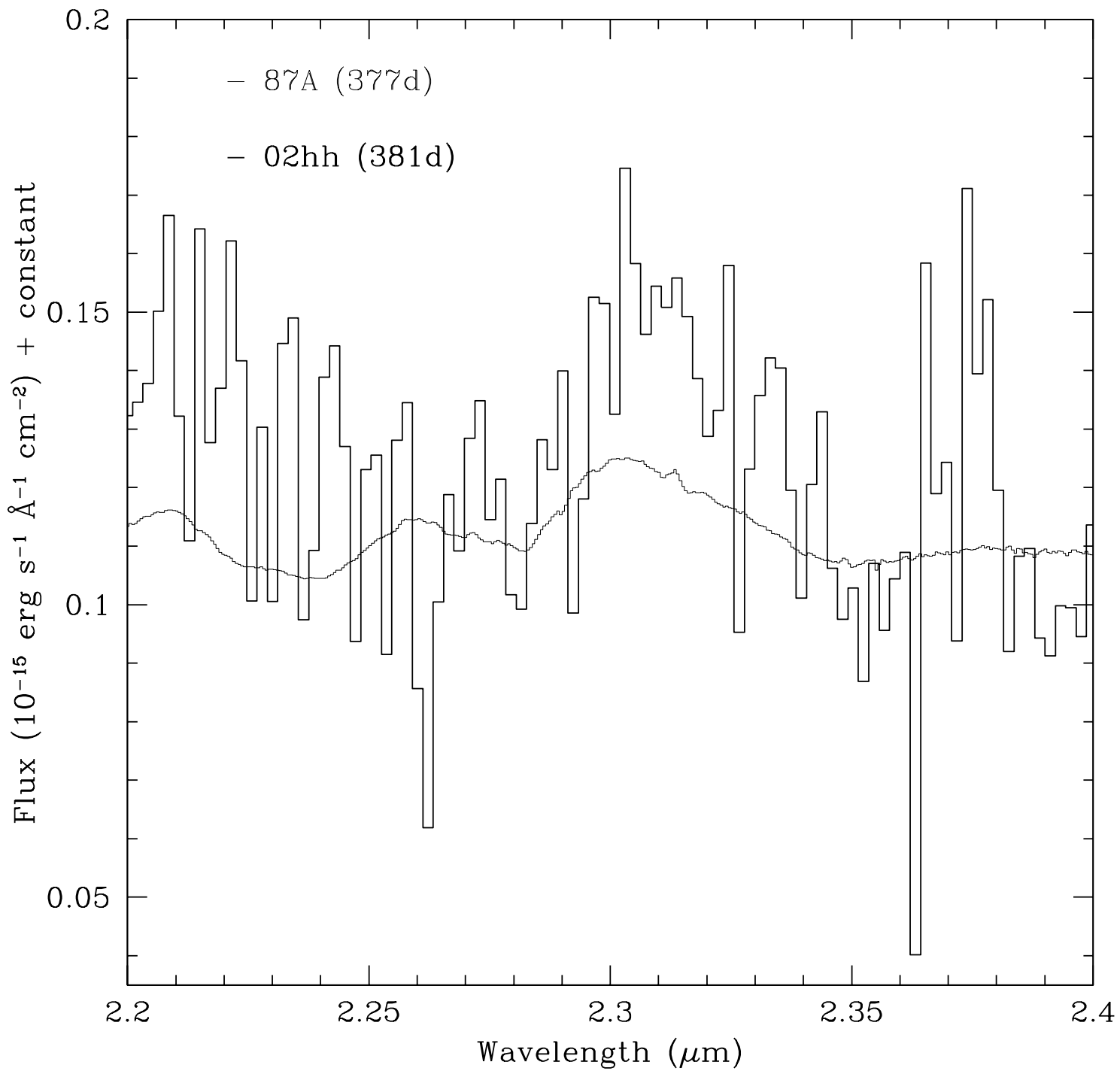


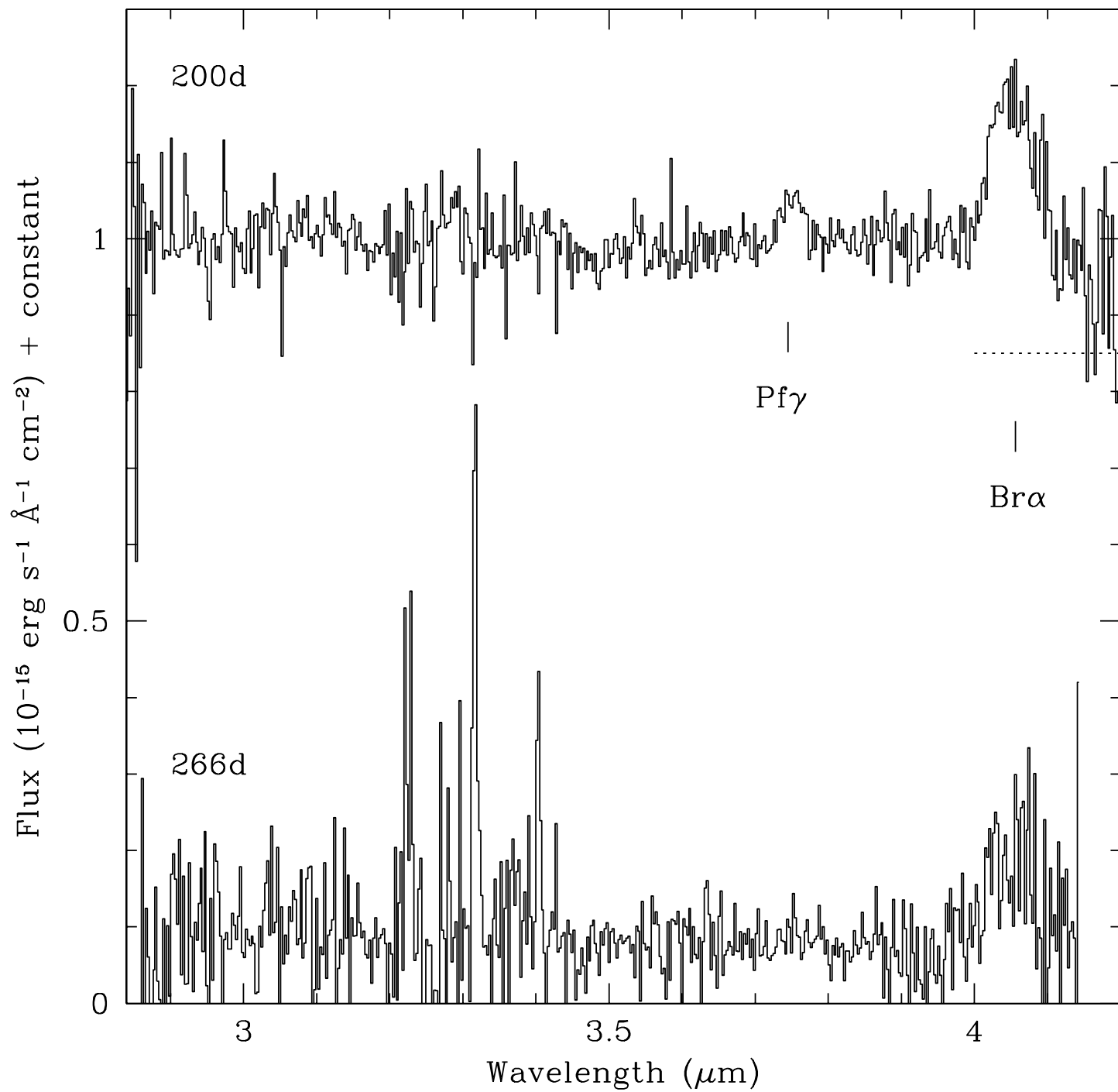


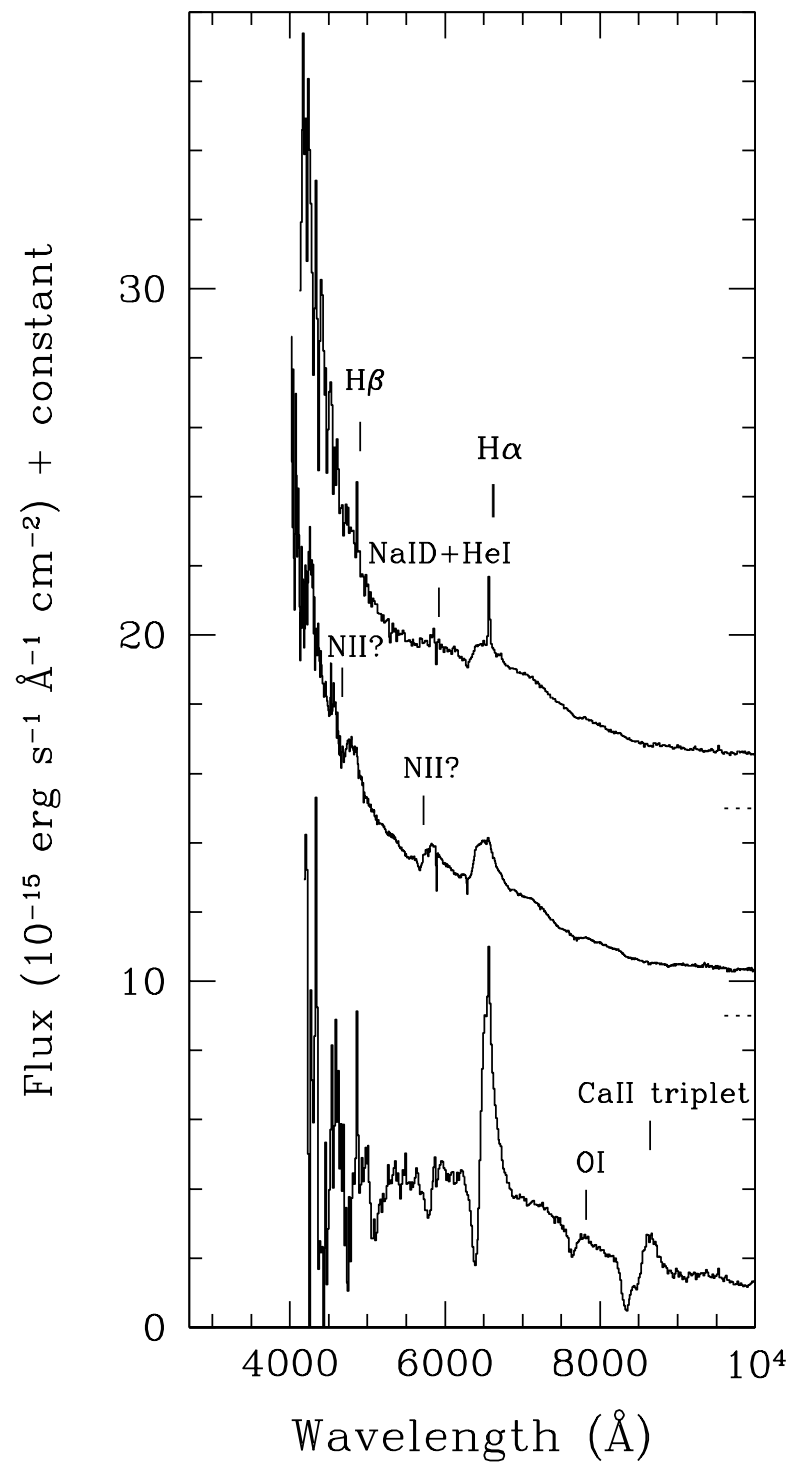
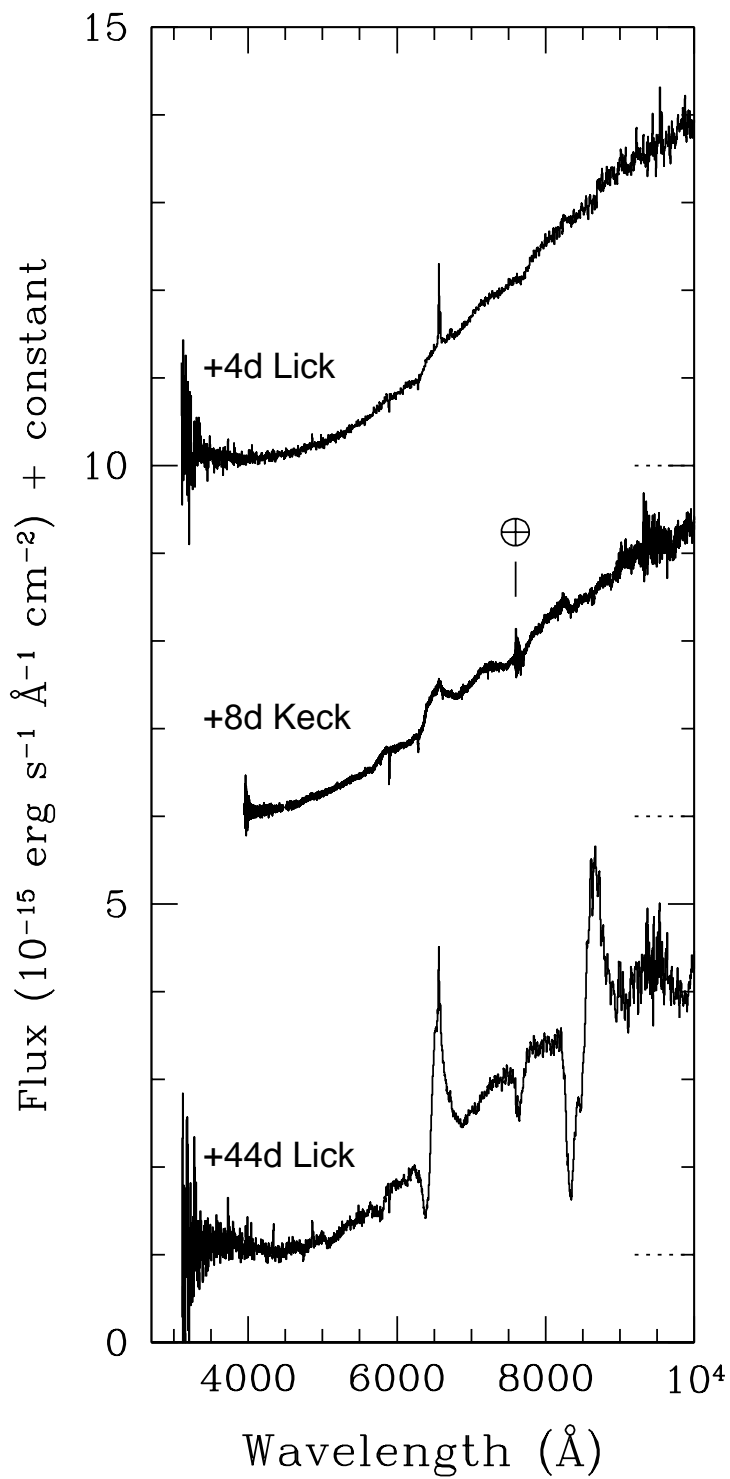


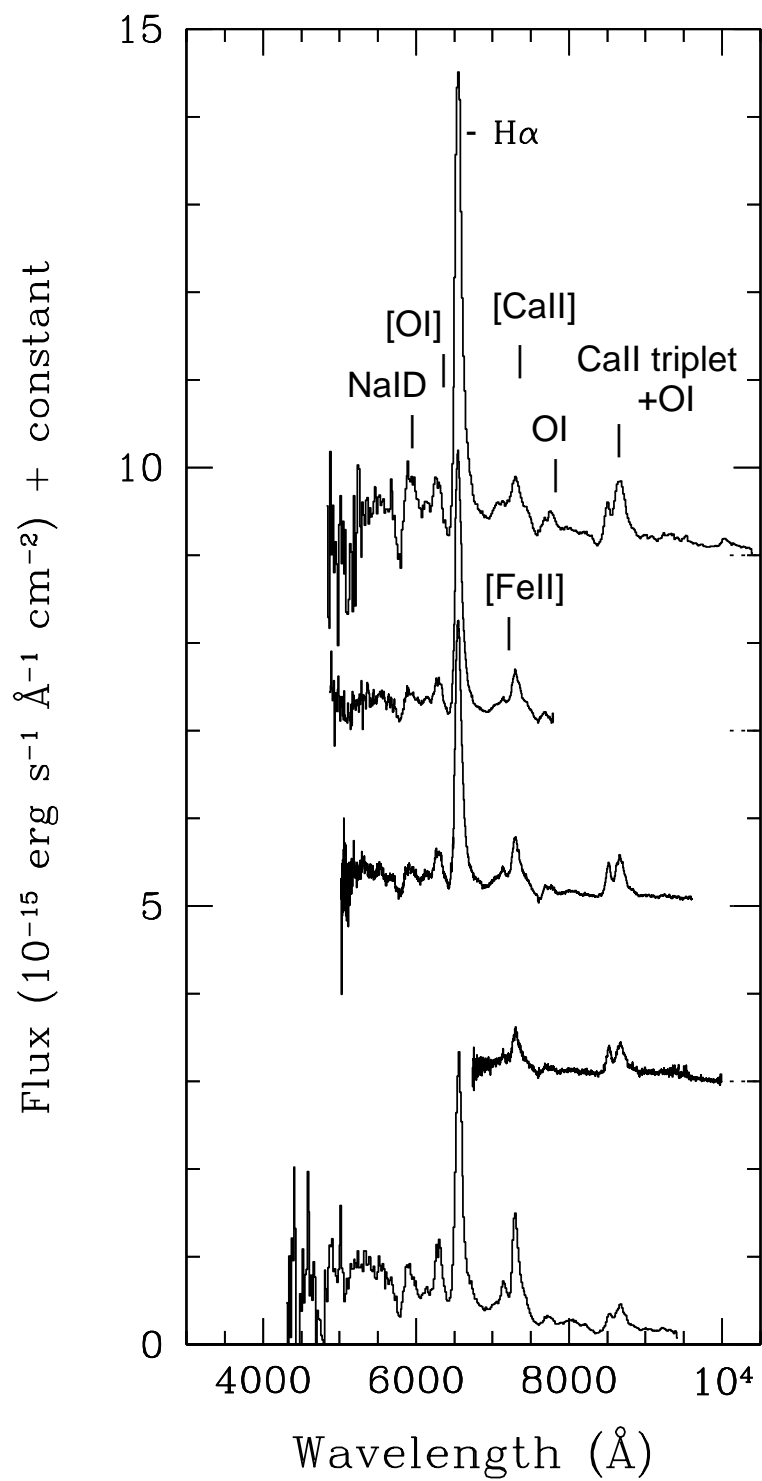
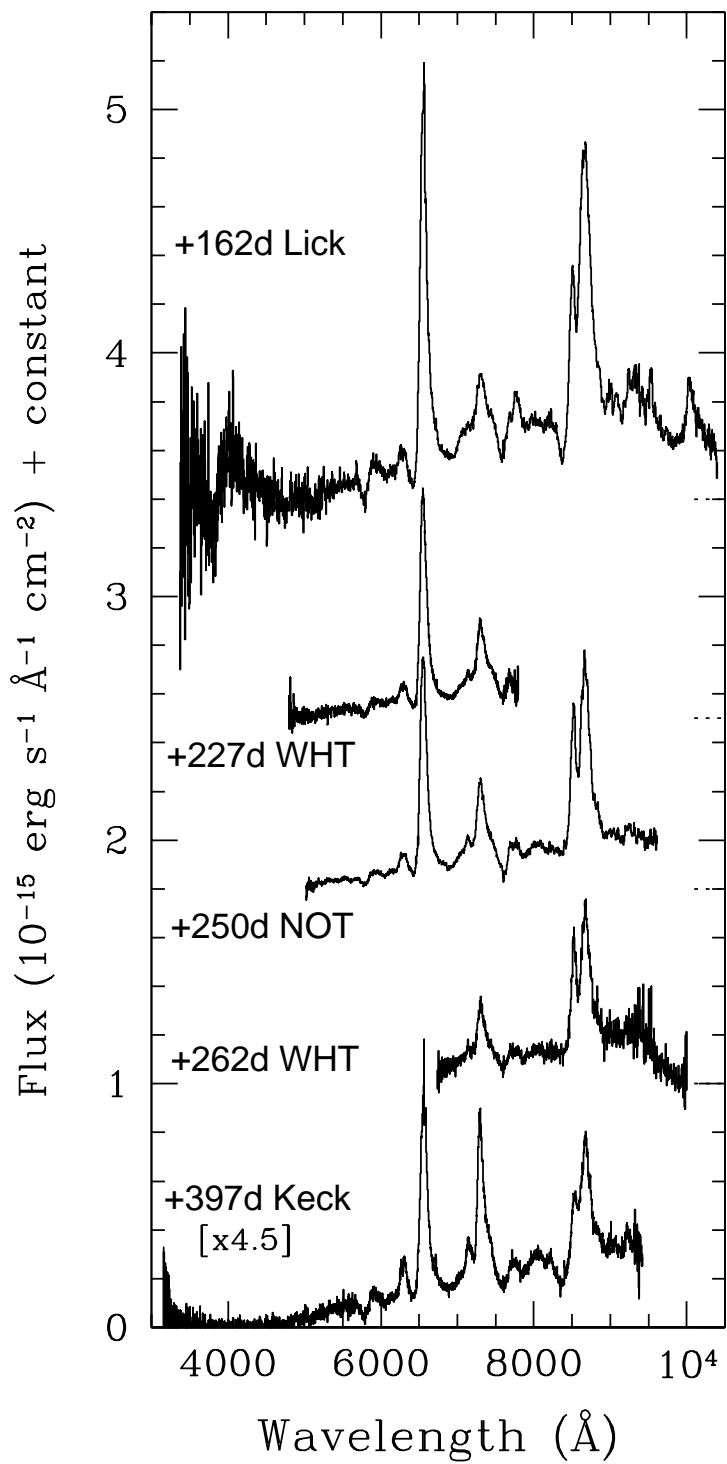


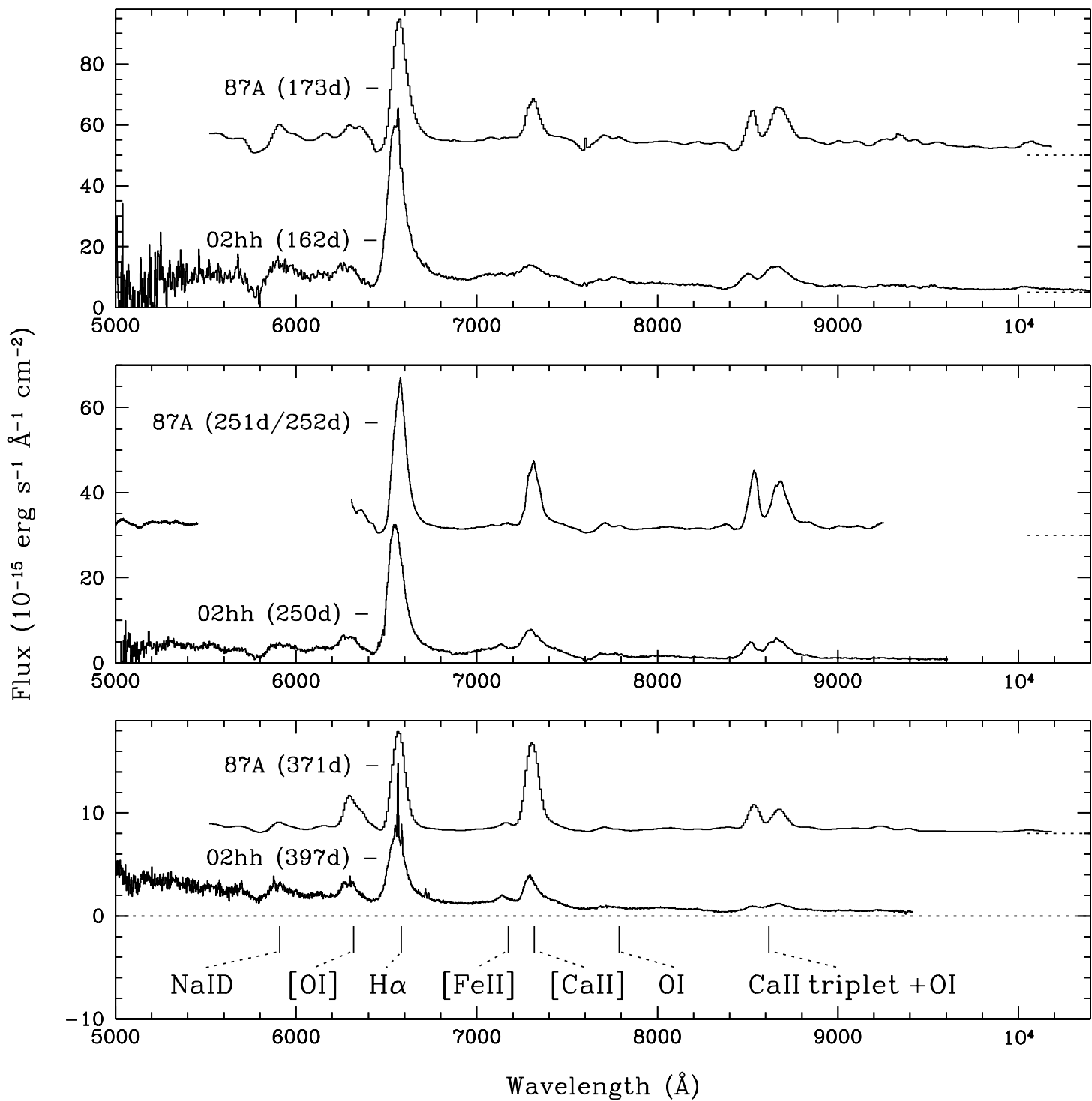


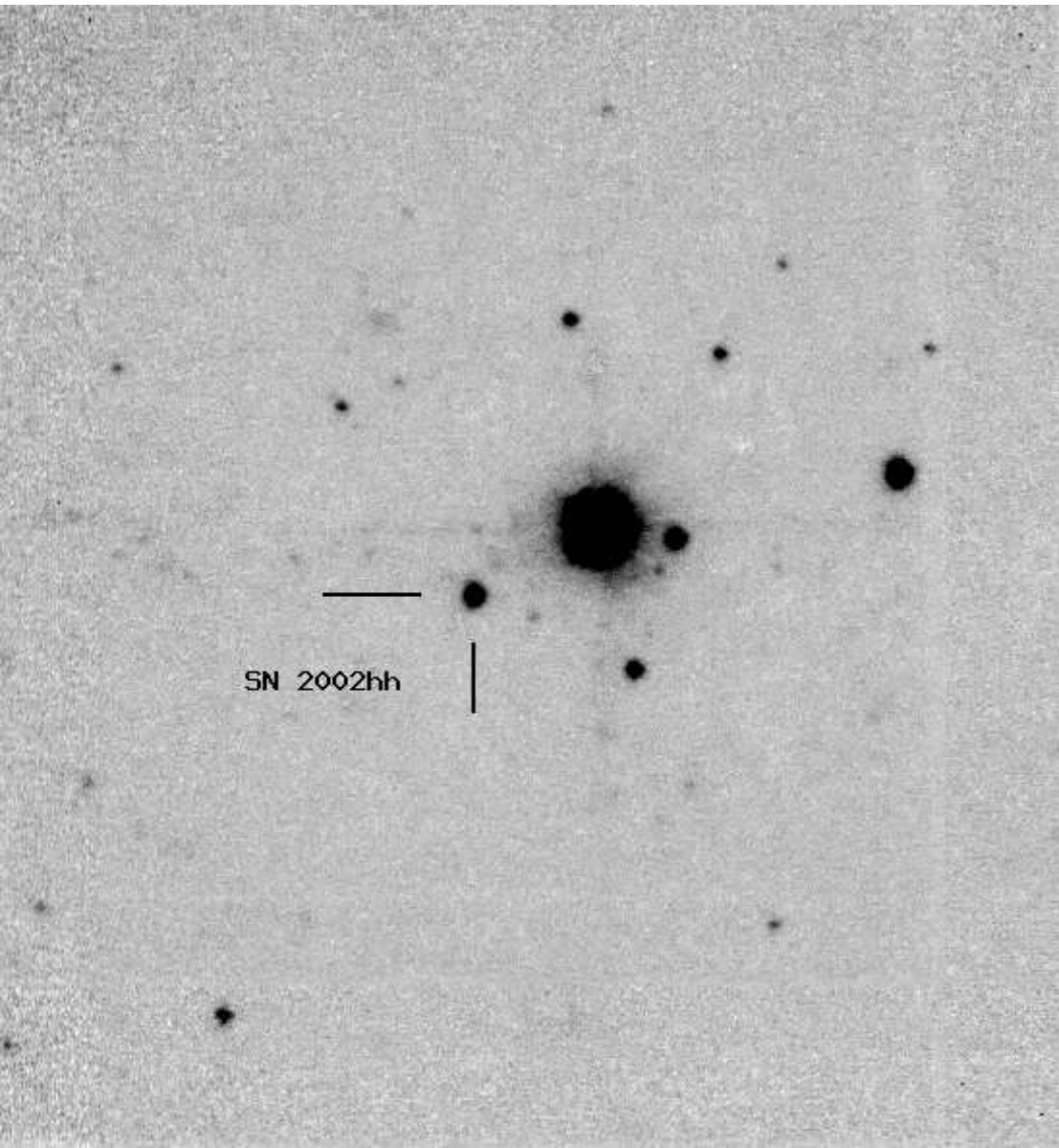












SN 2002hh

